UNIVERSITY OF
BIRMINGHAM

Contactless Heat-Assisted Single Point Incremental Forming

By

MOHAMMAD TALAL M. ALMADANI

A thesis submitted to The University of Birmingham for the degree of

DOCTOR OF PHILOSOPHY

Department of Mechanical Engineering
School of Engineering
University of Birmingham
October 2023

ABSTRACT

This thesis introduces a novel technique called Hot Air Contactless Single Point Incremental Forming (HASPIF) as an alternative to conventional single incremental point forming methods. HASPIF utilises hot compressed air to deform polymer sheets without physical contact with a forming tool, thereby eliminating the need for a rigid tool and reducing costs.

A case study was conducted using a polycarbonate sheet to validate the concept, employing specific parameters such as nozzle speed, air temperature, air pressure, stepdown and initial distance. The results demonstrated accurate shaping of the polycarbonate sheet with minimal springback, although slight deviations and material build-up were observed at the starting point of the nozzle.

Finite element modeling (FEM) was used to analyse the influence of the contactless tool on the shaping process, encompassing computational fluid dynamics (CFD) and transient structural models to estimate the resulting shape and deformation of the polymer sheet. The FEM model not only forecasted the final part of geometries and dimensions but also provided insights into the normal strain progression, which aligned well with experimental data.

Furthermore, the thesis optimised the HASPIF process using a design of experiment (DOE) approach, evaluating five control factors and considering profile variation, thickness variation, and surface roughness as evaluation criteria. The study revealed that air temperature and feed rate had a significant influence on the deformation process, while air pressure and feed rate impacted thickness variation and surface roughness. A prediction model was developed to optimise process parameters, aligning well with predicted profile and thickness variations. However, surface roughness did not exhibit the same agreement due to the stepwise nature and inherent waviness of the contactless forming technique.

In conclusion, this study presents a promising approach for developing innovative contactless forming techniques using hot compressed air as a forming tool, offering advantages such as reduced tool wear and lubrication requirements compared to traditional methods.

ACKNOWLEDGEMENTS

I would like to express my gratitude to my family, supervisors, and the safety and technical staff at my university for their invaluable assistance in bringing my thesis to a reality. I sincerely appreciate my first supervisor, Professor Khamis Essa, as none of this would have been possible without him. His unwavering support and guidance throughout my doctoral research, both as a supervisor and mentor, played a crucial role in the success of my primary research and the necessary tasks involved.

I would like to thank my second supervisor, Professor Moataz M Attallah, for his supervision and guidance in my research papers and for providing the necessary laboratory support for my study. His involvement was instrumental in carrying out essential experiments and conducting valuable research work.

Furthermore, I would like to express my gratitude to Professor Duc Ttuong Pham for his assistance in orienting the beginning of my PhD work. His guidance and support in the early stages of my research were immensely helpful in setting the foundation for my doctoral journey. I am deeply grateful to Dr Hany Hassanin for his supervision, guidance in my research papers, and the provision of essential laboratory support.

I would also like to extend my appreciation to safety officers Andy Dunn and Katie Tyler for their assistance in guiding me through the orientation of my laboratory work. Their expertise and support in ensuring a safe and efficient working environment were invaluable, and I am grateful for their contributions to my research experience.

I would like to express my heartfelt appreciation to the members of my research group: Dr. Ahmet Guner, Dr Sherif Abdelkhalek, Dr Weining Li, Dr Prveen Bidare, Dr Yasser Aljohani,

Dr Ahmed Bahabri, Dr Ahmed Binobaid, Dr Michele de Lisi, Dr Abdullah Alqahtani, Dr Abdullah Mohammed, and Dr Chang Shu. Their cooperation and assistance throughout my PhD study have been invaluable. I am truly grateful for their support and collaborative efforts, which have significantly contributed to the success of my research.

I am deeply indebted to my family's unwavering support and affection, as their encouragement and love have been instrumental in my ability to achieve this remarkable feat. I express my heartfelt gratitude to my beloved family members: my mother Eman; my father Talal; my wife Ghadeer; my sons Talal and Jad; my brothers and sisters, and my dear grandmother Badeeah (May Allah bless her soul), who have consistently stood by my side through both challenging and joyous moments. It is truly impossible to articulate the profound significance you hold in my life. This dissertation is dedicated to each and every one of you.

TABLE OF CONTENTS

Page

LIST OF FIGURES

LIST OF TABLES

ABBREVIATIONS

AFM	Atomic Force Microscopes
ANOVA	Analysis of Variance
APDL	ANSYS Parametric Design Language
CA	Cellular Automata
CAD	Computer Aided Design
CFD	Computational Fluid Dynamics
CFRP	Carbon fiber reinforced polymer
CHASPIF	Convective Heat-Assisted Single-Point Incremental Forming
CPU	Central Processing Unit
CSPIF	Contactless single point incremental forming
CMMs	Coordinate Measuring Machines
CNC	Computerised Numerical Control
CPFEM	Crystal Plasticity Finite Element Method
CSPIF	Contactless Single Point Incremental Forming
DC	Direct Current
DOE	Design of Experiments
DRX	Dynamic Recrystallization
DSLR	Digital Single Lens Reflex

dWJ	Diameter of The Water Jet
EBSD	Electron Backscatter Diffraction
FEA	Finite Element Analysis
FEM	Finite Element Model
FLC	Forming Limit Curve
FLD	Forming Limit Diagram
FSSPIF	Friction Stir-Assisted Single Point Incremental Forming
GFRP	Glass-Fiber-Reinforced Polymers
HASPIF	Heat-Assisted Single Point Incremental Forming
HSB	High-Speed Bearing
hSO	WJ Distance
HTC	Heat Transfer Coefficient
ISF	Incremental Single Forming
k	Relative Jet Diameter
LASPIF	Laser Single Point Forming Process
LED	light-emitting diode
MAPDL	Mechanical Ansys Parametric Design Language
ORB	Oblique Roller Ball
PA	Polyamide
PC	Polycarbonate

PE	Polyethylene
PET	Polyethylene Terephthalate
PID	Proportional integral derivative
POM	Polyoxymethylene
PP	Polypropylene
PVC	Polyvinyl Chloride
pW	Water Pressure
Ra	Average Roughness
Rq	Root Mean Square Roughness
Rt	The total height discrepancy between the highest peak and lowest valley within the evaluation length
RVE	Representative Volume Element
Rz	Maximum Height of The Profile
SIMPLEC	Semi-Implicit Method for Pressure Linked Equations-Consistent
SPIF	Single Point Incremental Forming
SSR	Solid State Relay
TPIF	Two-Point Incremental Forming
TTS	Through-Thickness-Shear
UV	Ultraviolet
UVSPIF	Ultrasonic Vibration Single Point Incremental Forming

VRB	Vertical Roller Ball
WJ	Water Jet
WJISF	Water Jet Incremental Sheet Forming

NOMENCLATURE

t	Workpiece's ultimate thickness
t0	Workpiece's initial thickness
α	Wall angle
tf	The thickness of the workpiece
N	The number of points where the workpiece thickness was measured
xi	The thickness at a given point i
$\bar{x}$	The average thickness value for all points
i	A given point
$k^{-\varepsilon}$	The viscous turbulence model
k	The turbulent kinetic energy
ε	Turbulent dissipation rate
Gk	The kinetic energy of turbulence that is made by mean velocity gradients
Gb	The amount of kinetic energy that is added to turbulence because of buoyancy
YM	The amount that fluctuating dilatation in compressible turbulence adds to the overall rate of dissipation
C1, C2, and C3	Constants
σ_k	The turbulent Prandtl numbers for k
σ_ε	The turbulent Prandtl numbers for ε
Sk	Source term that was made by users

$S\varepsilon$	Source term that was made by users
$\varepsilon 11$	Strain components for direction 1
$\varepsilon 33$	Strain components for direction 3

LIST OF PUBLICATIONS

First author journal article publications:

Mohammad Almadani, Ahmet Guner, Hany Hassanin, and Khamis Essa, *Hot-Air Contactless Single-Point Incremental Forming*. Journal of Manufacturing and Materials Processing, 2023, 7, 179. http://doi.org/10.3390/jmmp7050179.

Mohammad Almadani, Ahmet Guner, Hany Hassanin, Michele De Lisi, and Khamis Essa, *Contactless Single Point Incremental Forming: Experimental and Numerical Simulation*. International Journal of Advanced Manufacturing Technology, (2023) 129:5167–5179. https://doi.org/10.1007/s00170-023-12401-1

Mohammad Almadani, Ahmet Guner, Hany Hassanin, and Khamis Essa, *Optimisation of A Novel Hot Air Contactless Single Incremental Point Forming of Polymers*. Under review by Journal of Manufacturing Processes

1 Chapter One: Introduction

1 Introduction

1.1 Background

Traditional sheet-forming techniques are typically created with sophisticated and costly tool system designs that are fixed to a restricted, defined geometry. These techniques are only economically practical for mass production. The global manufacturing industry faces the challenge of developing flexible and cost-effective forming technologies to manufacture sheet materials with complex geometries for rapid prototyping. In recent times, the development of manufacturing processes in most industries has accelerated. This is driven by the need to meet market requirements, save time in the manufacturing process, and reduce material waste. Additionally, there is a growing interest in flexible and low-cost manufacturing processes to address changing customer demands, shorten the time from design to market, tackle resource scarcity, and minimise the carbon footprint.

However, conventional forming processes are expensive and fail to address these challenges. Therefore, the search for new forming approaches has become necessary, particularly for industries that need to create prototypes as the initial step in their manufacturing process. Leszek discovered a new forming process that can overcome many obstacles encountered in sheet forming. This process is called single point incremental forming (SPIF) [1], as illustrated in **Figure 1-1** [2]. SPIF involves a rigid tool controlled by a CNC machine that incrementally deforms the sheet to its final shape by following a programmed path. The process relies on highly localised plastic deformation as the tool enters the sheet with incremental vertical translation. This technology is considered flexible and capable of producing complex 3D shapes without the need for specific dies, unlike other forming methods. As a result, the SPIF process is employed in the manufacturing and fabrication of spares for obsolete parts as well

as in the production of components for small-volume industries such as aeronautics.

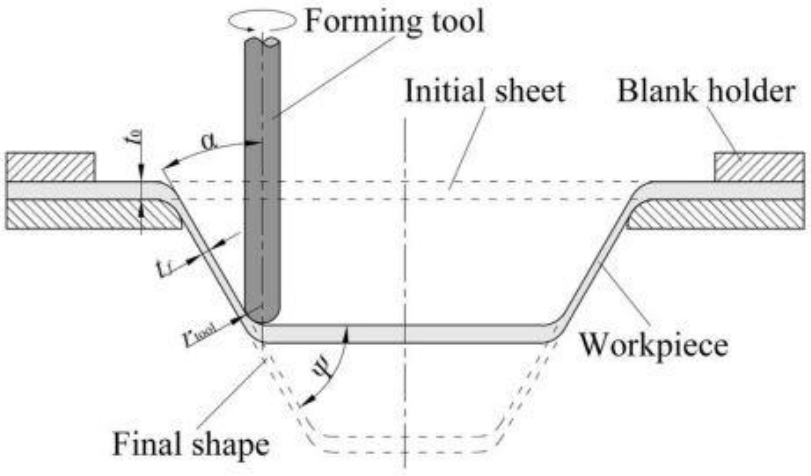

Figure 1-1 Traditional SPIF Setup [2].

The procedure has gained significant attention due to its notable adaptability and cost-effectiveness. SPIF has been extensively studied with metal materials, given their superior mechanical properties. Previous research by Radu [3] and Kim [4] demonstrated the high effectiveness of SPIF in deforming relatively hard materials at room temperature, including carbon steel, stainless steel, and aluminium. However, the die-less nature of the manufacturing process compromises the product's geometrical accuracy due to significant elastic springback, leading to diminished formability.

Conversely, there has been research conducted on the application of SPIF to polymer materials. Polymer materials offer advantages such as a higher strength-to-weight ratio and good corrosion resistance, which has motivated researchers to explore the deformation of polymeric materials using SPIF. Martins and colleagues [5] extended previous research by investigating the formability of five polymers at room temperature: polyoxymethylene (POM), polyethylene

(PE), polyamide (PA), polyvinyl chloride (PVC), and polycarbonate (PC). The results showed that PE and PA exhibited the best ductility factors, while POM had the lowest ductility factor. PVC exhibited the lowest springback factor, making it a favourable polymer for high-accuracy parts. It is important to note some of the applications that could be used by polymer sheets, as polymers prove to be a versatile option for a wide range of uses, such as optical and lighting systems, serving as a glass alternative. They are also utilised in medical packaging, automotive engineering, household items, electrical components, and safety products [6].

In contrast, Kulkarni and colleagues [7] conducted two experiments to investigate the effect of heat-assisted SPIF (HASPIF) on polymers, as seen in **Figure 1-2**. The first experiment aimed to determine the optimal temperature setting on the heat gun for forming. The second experiment involved forming a conical shape with varying wall angles.

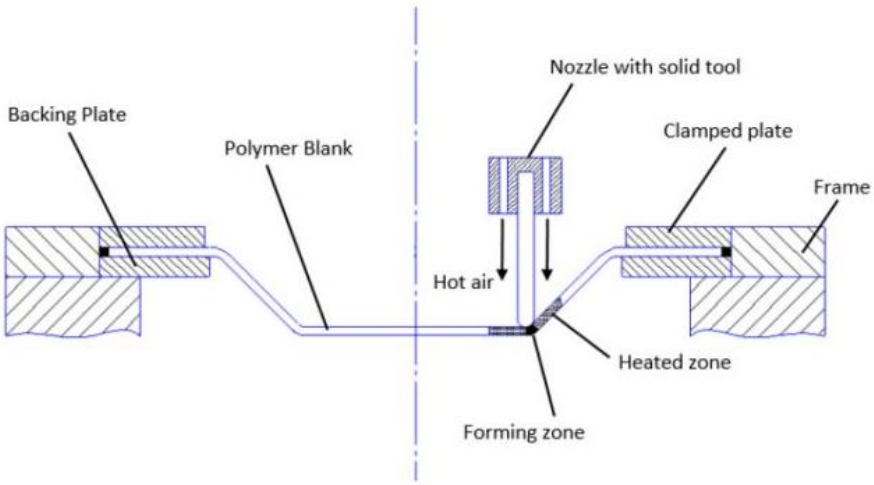

Figure 1-2 HASPIF Setup [7].

The results of these experiments demonstrated that heat-assisted SPIF using a heat gun improves the formability of polymer sheets by increasing the forming angle. However, the use of heat shifts the failure mode from circumferential cracking to wrinkling, possibly due to

reduced material strength when the solid tool comes into contact with it.

1.2 Motivation

Polymers constitute a significant portion of the raw materials used in industry. However, their processing techniques, which typically involve heating or rubbery conditions, are primarily suited for mass production due to high energy costs and substantial investments in equipment and tooling. Consequently, conventional polymer processing technologies are not well-suited for rapid product development and flexible small-batch production. This limitation hinders their ability to meet the growing demand for agile manufacturing in the market. Specifically, when it comes to sheet polymer components, there is currently no available technology that enables rapid prototyping in an efficient manner.

The need for novel solutions that can operate with low tooling and equipment costs has positioned SPIF as a strong competitor against the existing state-of-the-art techniques in sheet polymer production. SPIF has demonstrated the ability to deform polymer sheets at both room temperature and elevated temperatures, although it faces limitations due to the higher brittleness and lower melting points of the polymers. Developing a technique that can overcome these limitations and achieve a high deformation limit while ensuring product quality without failure modes has become crucial. One way to enhance the conventional SPIF system is by replacing the solid tool with a non-contact tool.

1.3 Aims and Objectives

The aim of this PhD project is to address the challenges associated with conventional SPIF and overcome them by developing a new contactless heat-assisted incremental sheet forming process utilising pressurised hot air. Utilising such a novel tool configuration will have several

crucial advantages, including the following: improved surface finish due to the absence of any contact between the forming tool and sheet surface; ability to deform low formability polymer materials (such as acrylics, fluorocarbons, polyamides, polycarbonates, polyesters, polyvinylchloride (PVC), and polyethylene); improved quality characteristics in terms of springback and geometrical accuracy; and eliminating the need to use a lubricant, which will eliminate sheet and tool wear. To attain the objective, the following objectives will be pursued:

1. Developing the conventional Single Point Incremental Forming (SPIF) process by integrating a novel contactless heat-assisted technique that utilises pressurised hot air. The proposed solution aims to mitigate or eliminate any potential defects or shortcomings that could occur because of tool contact.

2. Evaluate and validate the workability of the new mechanism by comparing the resultant shape with the CAD design in terms of geometric profile, thickness distribution, and surface roughness.

3. Developing a new numerical model to investigate the influence of the contactless tool on the deformation process. Two different models have been created and coupled. A computational fluid dynamics (CFD) model is developed to determine the pressure and temperature distribution of the air that impacts the sheet.

4. Evaluate the deformation of the polycarbonate sheet using a transient structural finite element model (FEM) that incorporates the results of the CFD model. This model is used to validate experimental results by analysing the sheet's deformation in terms of geometrical precision, thickness variation, and surface finish.

5. Optimising the characteristics of a novel non-conventional single incremental point in

polymer sheet formation using Design of Experiments (DOE) techniques. Evaluating the impact of air pressure, air temperature, feed rate, tool offset, and step-down size on profile variation, thickness variation, and surface roughness. Investigating the most effective process parameters and validating them with experimental results.

6. Conclude the doctoral dissertation and provide recommendations for future technological enhancements.

1.4 Organisation of the Thesis

This thesis is structured into six chapters, each of which is summarised as follows:

The first chapter provides a brief overview of the SPIF (Single Point Incremental Forming) methodology and describes the motivation behind this PhD research. In this chapter, the aims, objectives, and organisation of the thesis are outlined.

The second chapter describes the present limitations and constraints of this area of study and reports on the state-of-the-art in the field of research. The varieties and enhancements of tool design, numerical methods for tool path planning, various numerical modelling methods for typical features, and structural analysis under various process parameters are reviewed.

The third chapter introduces a novel sheet-forming process called Contactless Single Point Incremental Forming (CSPIF), which utilises hot compressed air as a deforming tool without physical contact between the forming tool and the polymer sheet. The mechanism of the novel process and the verification of its workability are performed by an experimental trail. This chapter aims to understand the development and evolution of forming force, geometric accuracy, thickness distribution, and surface roughness.

The fourth chapter reports the development and validation of numerical models to study the impact of the novel contactless tool on the deformation process. Two distinct models are created and coupled in order to estimate the deformation behaviour of polycarbonate sheets. A computational fluid dynamics (CFD) model is developed to determine the pressure and temperature distribution of the air impacting the sheet. A transient structural finite element model (FEM) is then coupled to analyse the sheet's deformation.

The fifth chapter demonstrates the optimisation of process parameters by using designs of experiments (DOE). This chapter aims to identify the significant process parameters and investigate their influence on the formability of the polycarbonate sheet. In this chapter, the effects of air pressure, air temperature, feed rate, tool offset, and step-down size on profile variation, thickness variation, and surface roughness are evaluated.

The sixth chapter presents the project's conclusion and recommendations for future research.

1.5 References

1. Leszak, E., Apparatus and Process for Incremental Dieless Forming, in http://www.freepatentsonline.com/3342051.html. 1967, Leszak, Edward: United States.

2. Zhu, H., H. Ou, and A. Popov, Incremental sheet forming of thermoplastics: a review. The International Journal of Advanced Manufacturing Technology, 2020. 111: p. 565-587.

3. Radu, M. and I. Cristea, Processing metal sheets by SPIF and analysis of parts quality. Materials and Manufacturing Processes, 2013. 28(3): p. 287-293.

4. Kim, Y. and J. Park, Effect of process parameters on formability in incremental forming of sheet metal. Journal of materials processing technology, 2002. 130: p. 42-46.

5. Martins, P.A.F., et al., Single point incremental forming of polymers. CIRP Annals, 2009. 58(1): p. 229-232.

6. Kyriacos, D. Chapter 17 – Polycarbonates. 2017.

7. Kulkarni, S., Heat Assisted Single Point Forming of Polymer Sheets. 2016.

2 Chapter Two: SPIF literature review

2 SPIF literature review

2.1 Introduction

As mentioned before, sheet material prototyping and small batch production can benefit from a new method called Incremental Single Forming (ISF). This technique has attracted much attention from researchers in both experimental and numerical fields. The following sections will discuss the main topics related to this technique based on the latest literature review. The current literature review focuses on the most recent experimental and numerical developments in the ISF technique.

The following sections will detail the extensive research conducted on this manufacturing method. The first section focuses on classifications of ISF processes and the benefits and drawbacks of forming processes. After that, we will investigate the various materials used in ISF. The third section contrasts the various SPIF process heating strategies. The fourth section will provide an overview of the most recent improvements in tool design. The following part will show the most current advances in lubrication and coating in the SPIF process, as well as their impact on the process and results. The next section will describe the numerical modeling methodologies used to simulate SPIF operations at the macroscale. The section that follows will concentrate on the formability and process parameters of the material. The following part will go through the most popular procedures used in ISF to study geometrical accuracy, strain, tool forces, thickness, and surface finish results. At the end of the chapter, there is a short review of the state of the art and the gaps that have been found in this chapter.

2.2 Incremental sheet forming development and classification

The ISF process is a metal shaping technique derived from conventional sheet forming

methods. It involves the use of a computer numerical control (CNC) system to gradually deform sheet materials [1]. According to Jeswiet and colleagues [2], the standard ISF can be categorised into two distinct types: single-point incremental forming (SPIF) and two-point incremental forming (TPIF).

2.2.1 Single point incremental forming (SPIF)

Single Point Incremental Forming (SPIF) is a type of Incremental Sheet Forming (ISF) that does not require a die, providing maximum flexibility in forming sheet metal. As illustrated in **Figure 2-1**, the workpiece is firmly clamped at the edges without any supporting dies underneath and is shaped using a single deforming tool to create complex forms.

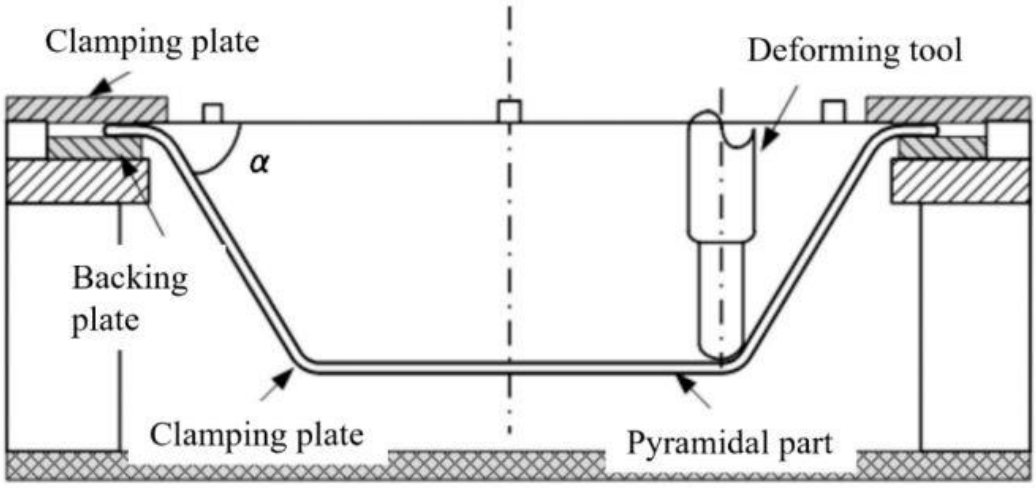

Figure 2-1 SPIF Process Mechanism [3].

SPIF demonstrates a significant improvement in formability because the die-less forming process allows for maximum flexibility in the movements of the forming tool. The procedure is adaptable to both metal alloys and polymer sheets. The tool path can be generated from computer-aided design (CAD), making it suitable for complex forming shapes. In this regard, research studies [4-6] have examined the enhancement in formability and geometric precision

for metal sheets such as aluminium, magnesium, and copper. Other studies have focused on deforming titanium by SPIF [7-9]. Several studies [10-13] have also utilised the forming process on various polymers, including polyvinyl chloride (PVC), polypropylene (PP), polyoxymethylene, polyethylene (PE), polyamide (PA), polycarbonate (PC), and polyethylene terephthalate (PET). These studies have modified the tool route and design to improve shaping while minimising the possibility of fracture. **Figure 2-2** illustrates the most common SPIF forming designs [2]. Panjwani and colleagues [14] and Sousa and colleagues [15] state that SPIF's formability extends to both axisymmetric and non-axisymmetric forming structures with a high level of geometric accuracy.

Figure 2-2 SPIF generating shapes [2].

Although SPIF can successfully deform sheet materials, it cannot entirely prevent material defects from occurring in the process and has limitations in formability. Due to the direct contact of the solid tool with the surface, high surface friction occurs during deformation.

Previous studies have explored various approaches to mitigate the impact of the solid tool on the surface finish of the product.

In terms of tool design, Lu and colleagues [16] developed the oblique roller ball (ORB) tool to reduce the tool's effect on the final surface finish. They examined the deformation behavior of both tools on four different types of aluminium sheet materials and found that the ORB tool improved surface finish quality and formability, although it did not eliminate the issues entirely. Heat assistance has also been employed to enhance formability. Al-Obaidi and colleagues [17] investigated electric-assisted SPIF on superior strength steel sheets. Their study involved localised heating of the workpiece, which resulted in a reduction in forming force and improved formability.

Another technique utilised is the use of lubricants to reduce surface friction during the process. Azevedo and colleagues [18] found that the viscosity of lubricants plays a significant role in reducing friction. Higher viscosity lubricants result in smoother surfaces, while lower viscosity lubricants result in rougher surfaces, as concluded by the study.

While previous research has helped in reducing the limitations in formability and defects on the sheet itself, it does not completely eliminate wear that may occur on the tool surface or the deformed sheet's surface. Therefore, it is necessary to explore alternative solutions to overcome the limitations and defects that arise in the SPIF process due to the solid tool.

2.2.2 Two points incremental forming (TPIF)

TPIF involves securing the sheet materials in place using a specialised fixture. The external surface of the workpiece is then deformed from top to bottom along the designated tool path. This process is facilitated by a complete or partial die positioned beneath the workpiece,

working in conjunction with a forming tool [19]. In TPIF, the workpiece is formed using two tools in five different configurations: one movable indenter and a small centre support post (**Figure 2-3a**); one movable indenter and a partial die with an upper surface shaped to define the product's profile (**Figure 2-3b**); one movable indenter and a complete positive die defining the entire product shape (**Figure 2-3c**); one movable indenter and a complete negative die defining the entire product shape (**Figure 2-3d**); and two fully movable indenters (**Figure 2-3e**).

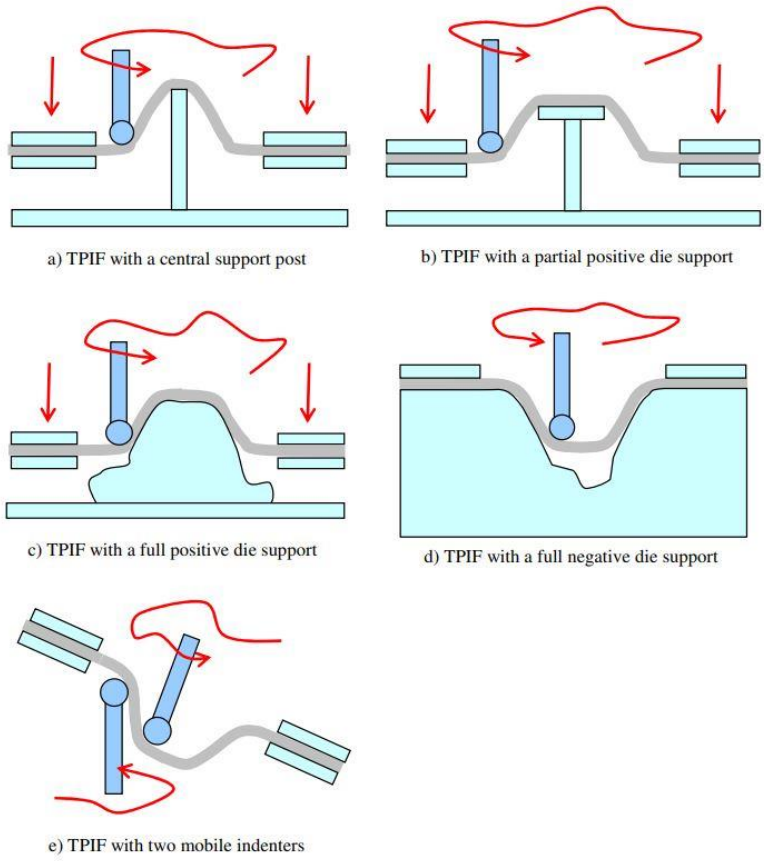

Figure 2-3 Two-point incremental forming (TPIF) configurations [20].

The initial version of TPIF, with a central support post (**Figure 2-3a**), was employed by Matsubara [21] in 1994. In this setup, the depth of the product can be adjusted by either raising the support post or lowering the workpiece frame. Recently, TPIF with a positive die support

(**Figure 2-3b**) has been used to create square-based truncated pyramids, as demonstrated by Hirt and colleagues [22]. Ceretti and colleagues [23] utilised TPIF with a full positive die support (**Figure 2-3c**), to form a vehicle differential housing, which offers greater constraint on the deformation. Giardini and colleagues [24] employed TPIF with a negative die (**Figure 2-3d**) to investigate the effect of working parameters on product quality for a concave shell. Finally, the most flexible ISF setup is TPIF with two mobile indenters , which was invented by Yoshikawa and colleagues [25] in 1999. Meier and colleagues [26] recently implemented this setup using two robot arms, and Maidagan and colleagues [27] achieved synchronization of a robot arm with an X-Y-Z table. While this setup provides the greatest freedom of motion and the ability to shape a variety of products, it is the most challenging in terms of tool path design and machine synchronization.

2.2.3 Summary of the SPIF types

To summarise, the SPIF technique involves gradually deforming a metal sheet by moving a tool along a predetermined path, resulting in the sheet taking the shape of the path. However, SPIF is typically slower compared to other forming methods and may have limitations in terms of material thickness and deformation capabilities.

In contrast, TPIF is another technique used for incrementally deforming metal sheets. It involves following a tool path while utilising a full or partial die underneath the workpiece to aid in the forming process. TPIF requires the simultaneous use of two-point tools.

TPIF offers two significant advantages over SPIF. Firstly, the sheet deformation is more constrained, allowing for greater accuracy. Re-entrant features can also be created depending on the depth to which the indenter(s) penetrate [28]. Tool path optimisation, as indicated by Mostafanezhad and colleagues [29] and Attanasio and colleagues [30], can improve geometric

accuracy, while wall angle and forming force can enhance surface quality.

However, the addition of die supports has limited the flexibility of the TPIF process as the die constrains formability. Heating sources can only be applied to the entire workpiece to avoid affecting the die support. Additionally, TPIF has the disadvantage of requiring specialised tooling for configurations other than those involving two movable indenters. Although TPIF is not a fully flexible process, it has the advantage of requiring only one die, which can be made of inexpensive and soft materials suitable for rapid machining, such as wood or polymer. This is significantly less expensive than using hardened steels, which have traditionally been used in pressing operations.

2.3 Material used in SPIF

The initial and crucial step for the success of the Single Point Incremental Forming (SPIF) process is recognizing the impact of material properties on the deformation process. The significance of this lies in the fact that the majority of calculations associated with sheet deformation heavily rely on the mechanical properties of the material relative to its initial thickness.

2.3.1 Metal

The SPIF technique is a manufacturing approach characterised by its flexibility. The present methodology provides potential practical applications for lightweight metals based on their increased design potentials and work-hardening capabilities. Investigations are being conducted into the possibility of employing this technology for the production of magnesium AZ31 sheet. Ambrogio and colleagues [31] conducted the initial investigation on the SPIF technique as applied to magnesium AZ31 sheets. A space is designed with an insulation and

heating system to achieve efficient thermal control on the sheet, eliminating thermal gradients. The research focused on investigating the formability constraints of AZ31 and the correlations between formability and process parameters through the implementation of a well-designed experiment known as Design of Experiments (DOE). The study conducted experiments within a temperature range of 200-300°C to evaluate the effects of step size, tool diameter, and forming temperature on the results. The experiments have determined that it is possible to enhance formability by utilising magnesium at elevated temperatures. The significance of tool step size and temperature on formability is considerable, whereas the impact of tool diameter is negligible.

Another study conducted by Ji and colleagues [32] investigated the SPIF process for AZ31 sheet across a wide temperature range of 100-250°C. The results indicated that the maximum formability was achieved at a temperature of 250°C. Dabwan and colleagues [33] conducted a study in which they utilised Single Point Incremental Forming (SPIF) on AA1050-H14 aluminium alloy under ambient conditions. The results of their investigation demonstrated outstanding precision in terms of geometric accuracy and surface finish.

Moreover, Torsakul and colleagues [31] conducted a study on the Single Point Incremental Forming (SPIF) process for shaping sheets of Aluminium (AA1100-H14), Brass (JIS H3100 C2801P), and Copper (JIS H3100 C1100P). The study examined the influence of material type, forming angles (30°, 40°, and 50°), and tool revolution speeds (200, 400, and 600 rpm) on the process. According to the study, an 8 mm spherical edge solid tool was used to deform the three different materials to truncated pyramid shape by three different forming angles. As stated in the result, due to the variation in tensile strength coefficient values depending on material type, the forming force results were different. Therefore, the highest force of formability need was to deform the brass sheet, and the lowest force was to deform the Aluminium sheet as seen in

Figure 2-33. Additionally, a notable increase in the forming force was observed when the forming angle was minimised. In contrast, the forming force was reduced with increasing the speed of the tool.

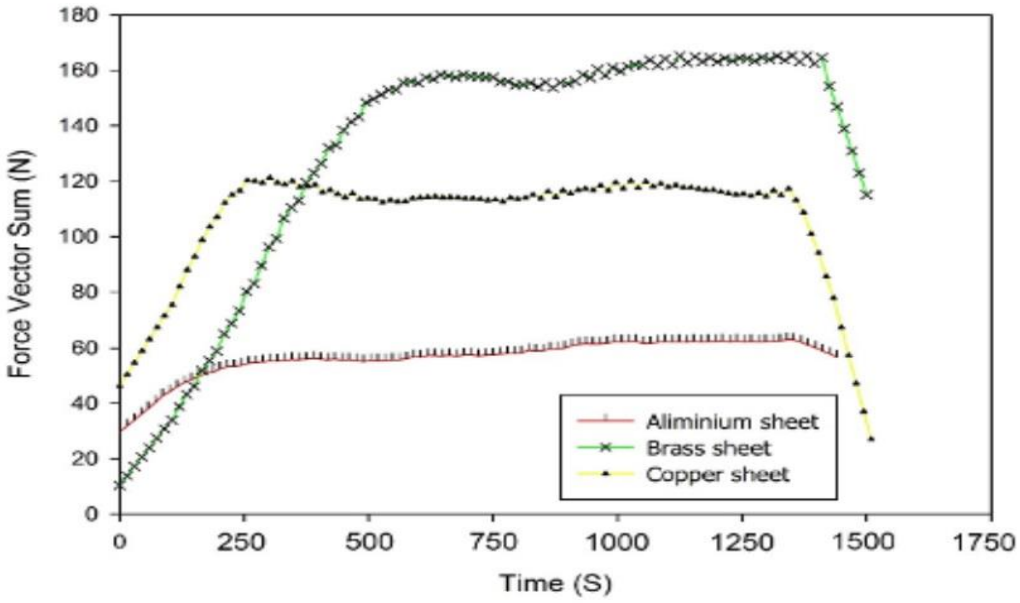

Figure 2-4 The forming force of sheet aluminium, brass and copper at the 30° forming angle and 600 rpm revolution speed [34].

On other hand, the SPIF process can be applied to form high strength material such as titanium. Tanaka and colleagues [35] demonstrated the feasibility of utilising Single Point Incremental Forming (SPIF) technique for processing unalloyed titanium in the production of denture plates. The primary challenge encountered during the manufacturing process was achieving a high-quality surface finish, which required identifying an optimal combination of lubrication and feed rate. According to Hussain and colleagues [36], the proper utilisation of tools and lubrication techniques can enable the application of (SPIF) in commercially pure titanium.

Heat-assisted single point incremental forming (SPIF) systems have been developed in recent years for deforming sheets made of high-strength alloys. Ambrogio and colleagues [9], have

developed a system for SPIF that utilises induction heating to deform sheets of Ti-6Al-4V at temperatures exceeding 600 ℃. Al-Obaidi and colleagues [17] achieved high geometric precision in the deformation of 22MnB5 steel at 750 ℃, using the same heating technique. Li and colleagues [37] designed a high-frequency induction heating SPIF system that provides localised heating to deform Ti-6Al4V sheets with a ball-roller tool, thereby minimising friction at the tool-contact interface. This method has been validated to generate a more ideal surface quality than traditional tools.

2.3.2 Composite

Forming composite materials has become more interesting to the aircraft and naval ship industries due to their superior properties, such as mechanical strength, reduced weight and stiffness, corrosion resistance, non-magnetic properties. The application of the SPIF technique was employed by Jackson and colleagues [38] on a standard sandwich panel consisting of three layers of metal-polymer-metal. The mechanical feasibility of utilising sandwich panels in SPIF was investigated through the examination of four sandwich panels. The study covered an extensive evaluation of the diverse characteristics exhibited by sandwich panels commonly used in industrial settings.

The initial experiments utilised a linear trajectory involving a distance of 100 mm, as well as a small helical tool path with a step increment of 0.1 mm. These methods were employed to assess the reduction in thickness, mechanical damage, and changes in surface quality resulting from deformation. The researchers determined that the utilisation of SPIF processing is feasible for sandwich panels made of Aluminum-polypropylene-Aluminum and Mild steel-polypropylene-Mild steel. This is due to the high ductility of the materials, particularly the faceplates, and the incompressible behaviour of the core.

The thinning phenomenon of sheet metal can be clarified by the principles of the sine law and through-thickness strains. The vertical application of a tool exhibits identical variations with respect to the vertical inclination and the radius of the tool. Abdali and colleagues [39] investigated the formability and failure mode of the bimetal sheet according to the effect of the arrangement of the layers, tool diameter, and step down. The bimetal sheet contained a layer from 1.5 mm Al 1050 and 0.5 mm SUS304 layer, and the tool used was 10 mm and 15 mm hemispherical rigid tool. According to the study, the results show that the maximum formability was achieved when the SUS layer was in contact with the forming tool in the SUS/Al arrangement, as SUS is stiffer material than Al. Additionally, the formability was found to be connected with the size of tool diameter and the step down, and the relationship can be stated as follows: an increase in tool diameter will decrease the formability, and increasing the step down from 0.15-1 mm will decrease the formability. In contrast, fractures always appeared on the SUS layer in both different arrangements due to the reduction in the thickness as shown in **Figure 2-5.**

Similarly, another attempt in forming composite material was made by Al-Obaidi and colleagues [40] who successfully deformed Glass-fiber-reinforced polymers (GFRP) into conical shapes with a variety of wall angles using SPIF assisted by hot air heating.

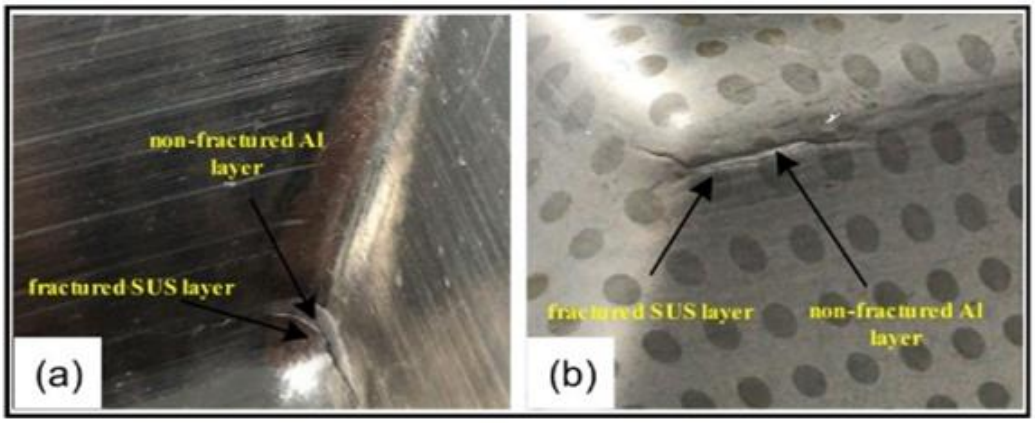

Figure 2-5 Fracture initiation in different layer arrangements

(A) SUS/AI (B) AI/SUS [39].

The GFRP was protected by two teflon layers and two dummy metal sheets. The metallic layers were added to protect the PA6GF47 from tool friction and excessive heating effects. Simultaneously, the teflon layers were added to prevent sliding of the PA6GF47 during the forming process.

2.3.3 Polymers

Polymers play a crucial role in the production of various parts. Over the past few decades, their use has significantly increased in industries such as automotive, aerospace, and biomedical components [41]. Moreover, the modern manufacturing industry has embraced polymers to replace heavy components with lighter alternatives. Franzen and colleagues [12] conducted investigations on polyvinylchloride (PVC) using the ISF method. To assess the formability of PVC, a conical component was used. The study identified three distinct types of mechanical failure that occurred during the forming process. The maximum achievable wall angle during PVC forming ranged between 67 and 72 degrees. The authors aimed to minimise the occurrence of the 'stress whitening' phenomenon, which caused a change in the material's colour during forming. The obtained findings were unexpected.

Martins and colleagues [13] conducted a study on the formability of five different polymer types, including polyoxymethylene (POM), polyethylene (PE), polyamide (PA), polyvinylchloride (PVC), and polycarbonate (PC). The diameter of the rigid tool was 10 and 15 mm, and the thickness of each sheet varied between 2 and 3 mm. The suitability of each material for the SPIF was evaluated based on their individual properties. PE and PA are suitable for components with large wall angles due to their superior ductility. On the other hand, if high precision is required, PVC is the material of choice due to its minimal springback. Additionally, polycarbonate is a suitable option for meeting high surface quality requirements and maintaining its colour during incremental cold forming, as illustrated in **Figure 2-5**. In contrast, POM material showed the poorest overall performance among the investigated polymers due to its limited ductility. Ultimately, alterations in the colour of the polymer were detected after the final step of the procedure.

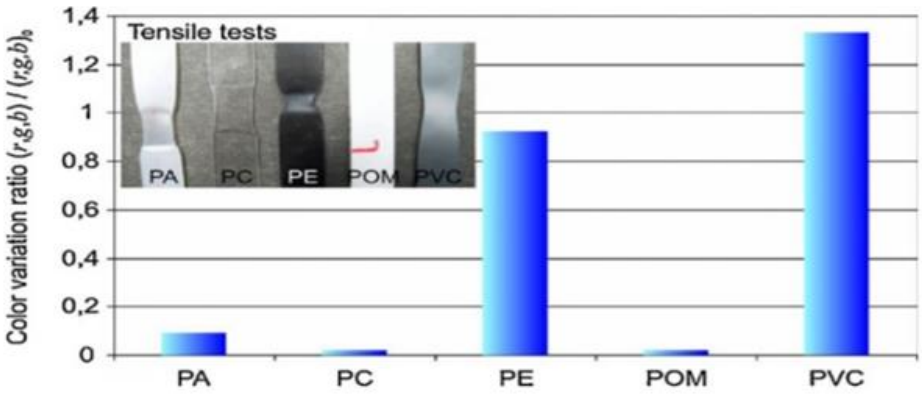

Figure 2-6 Change in colour after forming [13].

In conclusion, the findings of the study indicate a positive correlation between the formability of polymers and the thickness of the material. Moreover, as the tool diameter increases, the maximum forming angle will decrease. Conversely, increasing the thickness of the sheet results in a decrease in springback; however, springback increases as the initial draw angle increases.

2.3.4 Summary of material

In conclusion, the initial focus of research on SPIF was predominantly on the deformation of metal materials due to their superior mechanical properties. Extensive research has been conducted on metals including copper, steel, aluminium, brass, and even superalloys such as titanium.

However, there has been a growing interest in utilising SPIF for forming polymeric and composite materials. This shift is motivated by the advantageous properties exhibited by polymers, such as their higher strength-to-weight ratio and corrosion resistance.

Researchers have made significant efforts to explore the application of SPIF in forming various types of polymer sheets, such as polypropylene, polyoxymethylene (POM), polyethylene (PE), polyamide (PA), polyvinylchloride (PVC), and polycarbonate (PC) [4]. It is important to note, however, that polymers generally exhibit lower formability compared to metals due to their increased brittleness and lower melting points. These characteristics impose limitations on the use of conventional forming techniques for shaping polymers. Therefore, specialised forming techniques specifically tailored for materials with low formability need to be developed.

Polycarbonate is a material with exceptional thermomechanical properties. It possesses a wide range of desirable mechanical characteristics, such as high impact resistance, lightweight nature, ease of manufacturing (with a low glass temperature of 140-160 °C and a rubbery range extending from the glass transition temperature to the optical melting temperature), and flexibility in application. It also exhibits good thermal and electrical insulation properties, high toughness even at low temperatures, weather resistance, high dimensional stability in heat, and overall durability.

Moreover, polycarbonate is highly transparent, cost-effective, and fully recyclable. These additional features make polycarbonate an ideal choice for various applications, including optical and lighting systems, as a substitute for glass, medical packaging, automotive engineering, household goods, electrical components, and safety products [42]. Overall, the exceptional thermomechanical properties and versatility of polycarbonate make it a preferred material in diverse industries, providing solutions for a wide range of applications.

2.4 Single point incremental formation utilising heat assistance

In order to improve the formability, geometric accuracy, and surface quality of conventional SPIF processes for diverse sheet materials, it is essential to minimise the high forming force during the process by using heating sources. Friction stirring, ultrasonic vibration, electric heating, laser heating, and induction heating technologies are the most commonly employed heating sources in SPIF processes. Each heating method has its advantages and limitations in the forming process, as well as significant potential for enhancements.

2.4.1 Incremental Single Point Forming with Friction Stirring

Friction stir-assisted single point incremental forming (FSSPIF) is a heat-assisted SPIF technique in which the workpiece can be heated at the deformation zone between the rapid tool movement and the contact with the workpiece. The first technique was introduced by Buffa and colleagues [43], where the heat was generated from the tool's rotational speed, as illustrated in **Figure 2-7**. This concept was observed during the forming of AA1050-O, AA1050-H24, and AA6082-T6 aluminium alloy sheets using SPIF, which showed an increase in formability and wall angle with increasing tool rotational speed, leading to a rise in the sheet temperature, as seen in **Figure 2-8**. However, while the heating resulting from increased tool rotation improved formability and wall angle, it also resulted in poor surface roughness on the AA7075-O

workpieces, as noted by Liu and colleagues [44].

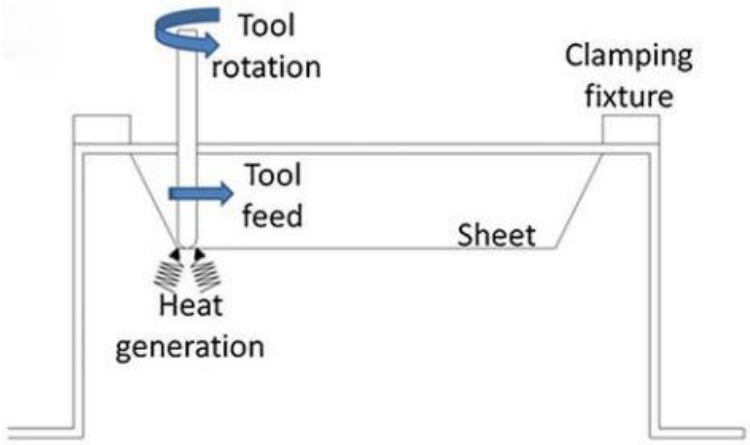

Figure 2-7 Schematic view of friction heat assisted ISF [43].

Nevertheless, the heating-assisted single point incremental forming (SPIF) method exhibits instability and shortcomings when applied to different materials. The findings presented in **Figure 2-9** [45] demonstrate that friction stir SPIF on 3 mm polypropylene sheets resulted in notable wrinkling or tearing. This occurs because local heating can exceed the softening temperature of the thermoplastic polymer due to friction between the surface of the thermoplastic sheet and the tool. Due to the fluctuating temperature increase, FSSPIF cannot be relied upon for manufacturing polymeric materials with high precision and surface quality.

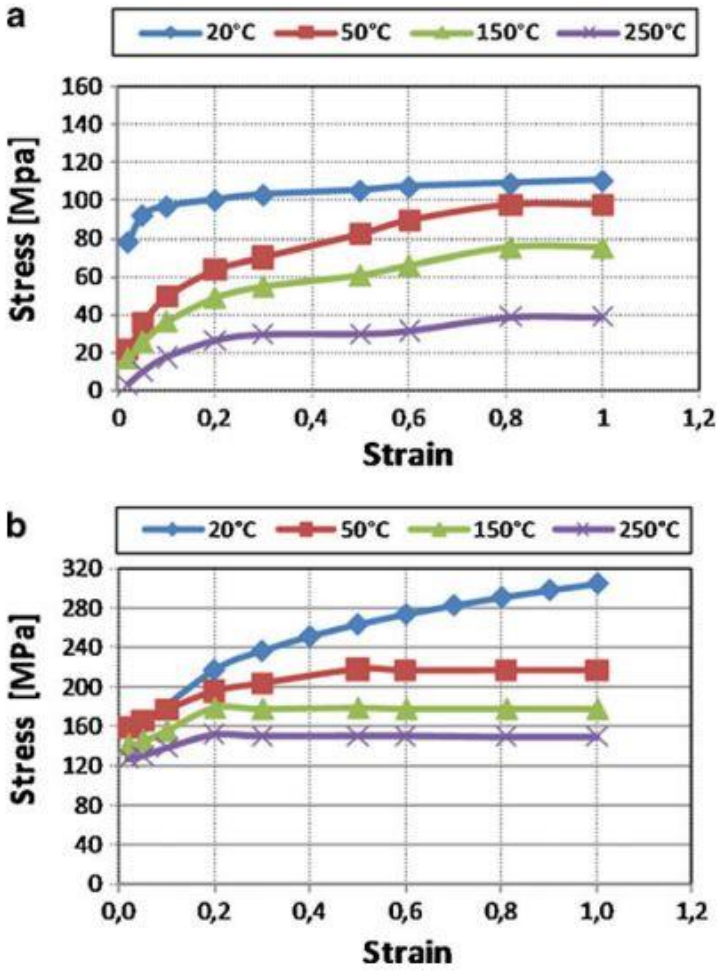

Figure 2-8 Flow stress curves at the varying of temperature a AA1050-H24 and b AA6082-T6 [43].

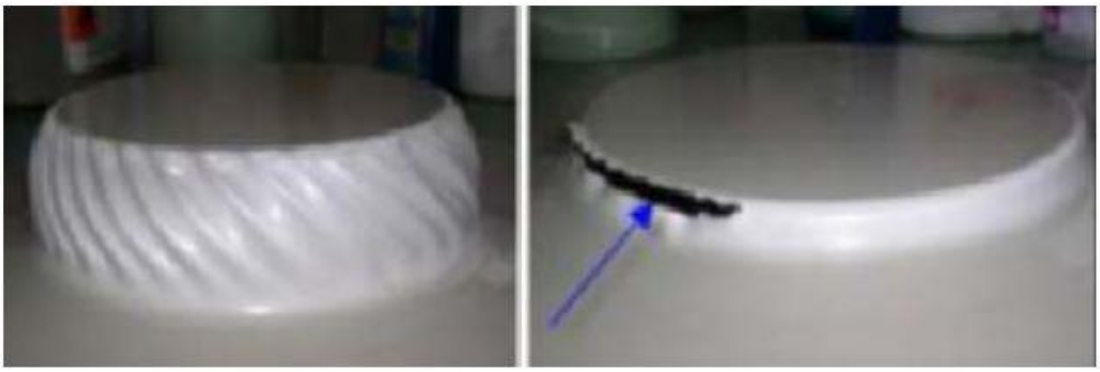

Figure 2-9 Mechanical defects in produced parts [45].

2.4.2 Incremental Single Point Shaping with Ultrasonic Vibration Assistance

UVSPIF (ultrasonic vibration single point incremental forming) has evolved from Ultraviolet (UV) stamping, drawing, drilling, extrusion, and hydroforming processes of metal alloys and polymers [46-51] to overcome forming limitations by applying vibrated-localised deformation to the forming tool. **Figure 2-10(a)** [52] illustrates the standard UVSPIF process, while **Figure 2-10(b)** [52] represents the measured reduction in forming force. It is evident that an average reduction of approximately 500 N in the forming force was observed when Ultrasonic Vibration-Assisted Single Point Incremental Forming (UVSPIF) was applied to form pure titanium bimetal sheets. Baghlani and colleagues [48] implemented a high-frequency vibration feed rate during the drilling process to increase the rotational speed of the tool and facilitate the transfer of temperature to the workpiece through contact. The results showed a significant reduction in the forming force of Inconel 738LC superalloy during the process.

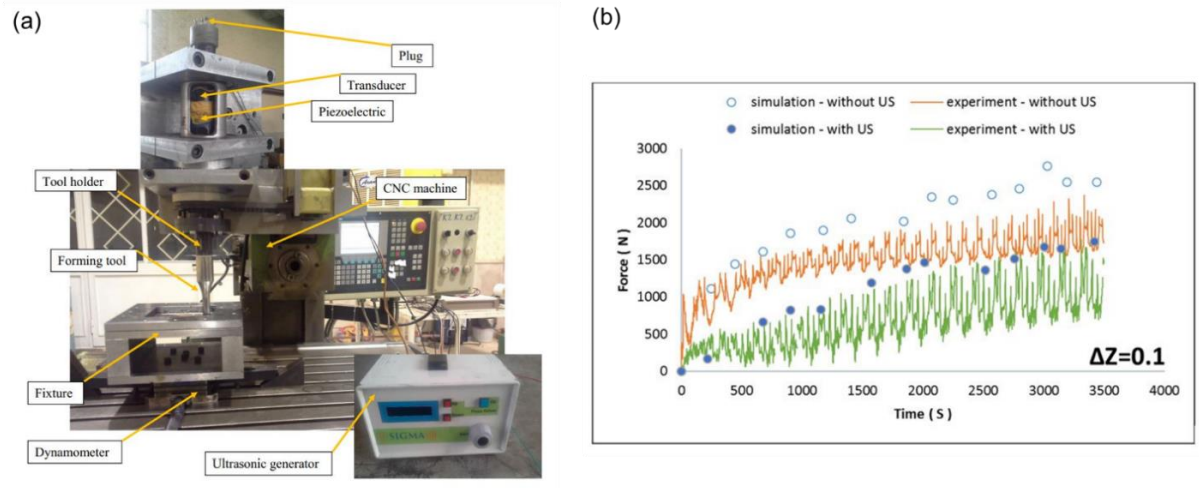

Figure 2-10 UVSPIF technique, (a) UVSPIF illustration, (b) the UVSPIF process's measured forming force [52] .

At an oscillating frequency of 20 kHz, Cheng and colleagues [53] used ultraviolet light to deform sheets of Al 7075 alloy while employing the SPIF and TPIF processes. The study

findings indicated a significant reduction in the applied forming force in both processes, resulting in improved material ductility and formability. The reduction in force magnitude was found to be relatively lower in SPIF compared to TPIF, attributed to energy transfer to membrane vibration. Sun and colleagues [54] observed that employing the UVSPIF technique effectively mitigated springback and waviness, resulting in enhanced geometric precision and surface quality for 2 mm AA-5052 sheets compared to traditional SPIF. Meanwhile, Cheng and colleagues [55] reported a 66.7% reduction in forming force when applying UVSPIF to AA1050-O alloy sheets with a 10 μm vibration amplitude.

Liao and colleagues [56] recently investigated the effects of temperature and ultrasonic vibration on the twist and springback of PEEK sheets. The findings showed that ultrasonic vibration can reduce twist and springback, improve geometric accuracy, and increase molecular chain orientation. However, at 140 °C, the opposite trend was observed due to molecular chain disorientation. Ultrasonic vibration at 60°C and 100°C reduced springback in the blank holder and bottom areas of the part, but it led to side wall bulge when applied at 140°C. Additionally, ultrasonic vibration at 60 °C and 100 °C increased molecular chain orientation and reduced deformation resistance, while at 140 °C, it caused disorientation of molecular chains.

2.4.3 Incremental Single Point Forming with Electric Heating Assistance

The studies [57-59] have established analytical models to investigate the heating and deformation mechanisms of electric heating-assisted SPIF processes. These models aim to increase the temperature for heat-assisted SPIF systems, particularly for high-strength materials.

In the study conducted by Fan and colleagues[60], the "Joule law heating method" was employed to heat the workpieces. This method involves transferring an electric current

generated by a DC generator from the tool to the workpieces, as depicted in **Figure 2-11**. When directing this current through certain alloys like magnesium and titanium, it led to an elevation in the sheet's temperature. Consequently, the ductility of these alloys was enhanced due to electric heating, resulting in increased formability and decreased forming force. Researchers such as Xu and colleagues [61] have compared the heating effects of tool friction and electric heating, and they found that electric heating provides faster and more consistent results compared to heating from friction forces. Moreover, regarding health and safety considerations, they found both approaches present burn risks. However, electric heating introduces the added concern of electric shock. While protective equipment and proper ventilation are essential for both methods, electric heating demands extra measures focused on electrical safety and insulation. Although electric heating may provide more accurate temperature control compared to tool friction heating, continuous monitoring and regulation are imperative for ensuring safety in both cases. On Other hand, when comparing friction heating with electric heating in terms of cost, friction heating is lower in cost as there is no need for a separate heating system as in electric heating [44, 62].

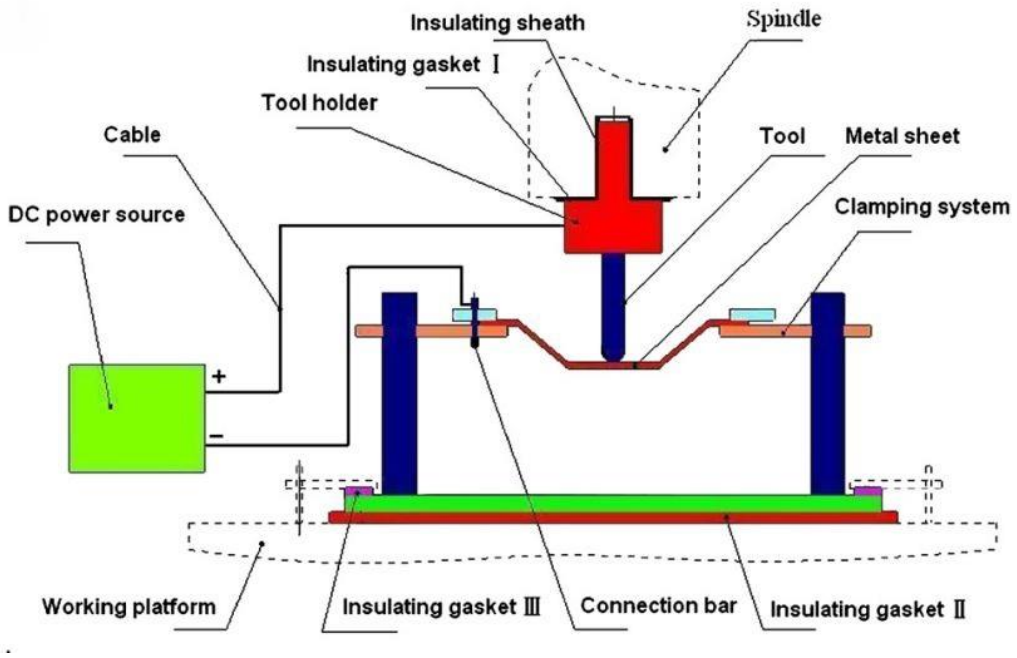

Figure 2-11 Experimental principal of electric hot ISF with local heating [60].

Meier and colleagues [62] , as well as Möllensiep and colleagues [63], developed an approach to apply a temperature of 600 ℃ to steel metal sheets by utilising direct current (DC) to control the robotic arm-operated tools. The research findings indicate a significant decrease in the forming force required to achieve a flexible and precise forming shape for 1mm DC04 steel, with the force measuring approximately 2000 N. According to Joule's law, the transfer of direct current from a tool to a workpiece result in the production of heat, leading to an increase in temperature and flux within the region. To ensure safety, insulation is applied to both the tool and workpiece, providing a limited area for the flow of flux.

In general, heat assisted SPIF demonstrated that increasing the current, and consequently the temperature, increased the sheet's formability. However, there is a limit to the improvement, which is reached when the temperature reaches the point where the sheet begins to burn. Ao and colleagues [64] used a high-power generator to raise the temperature to 820 °C in order to deliver a substantial amount of energy to Ti-6Al-4V sheets.

However, as depicted in **Figure 2-12,** the resulting formed shapes were suboptimal due to the presence of substantial cracks, notable springback, and burn holes. These outcomes can be attributed to the unstable temperature distribution and friction in the process, resulting in electric sparks at the contact area between the tool and workpiece. These sparks caused unpredictable defects along the tool path of the workpiece.

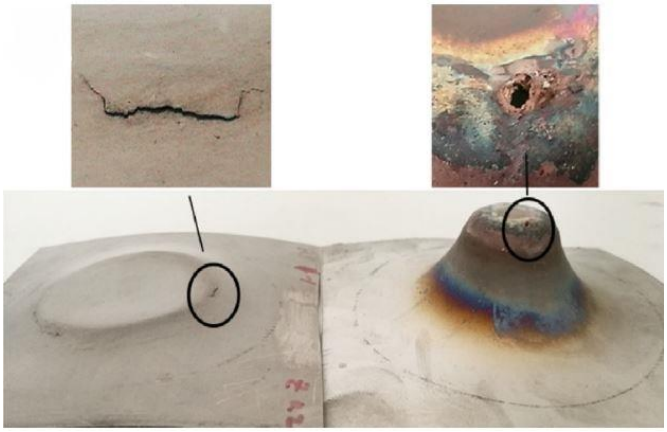

Figure 2-12 Defects on Ti-6Al-4V titanium alloy sheet due to using electric hot incremental forming [64].

As shown in **Figure 2-13**, Ambrogio and colleagues [31] reported that the heat-assisted SPIF process enhanced the formability of AA2024-T3 and titanium grade 5 sheets, with the greatest achievable forming angles of 40° and 45°, respectively, compared to approximately 30° and 20° at room temperature. While AZ31B-O could be formed up to 60°, producing this alloy without heat support proved impossible.

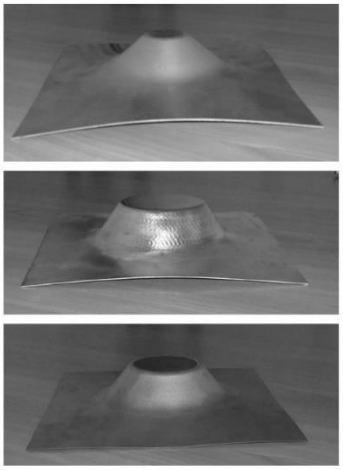

Figure 2-13 Results of experiments on (a) AA2024-T3, (b) AZ31B-O, and (c) Ti6Al4V [31].

Although, Shi and colleagues [65] utilised electric hot incremental forming to form low carbon steel sheets, the experimental results indicate that the current value has little effect on the total height of the parts when the value is lower than 400 A. However, when the value exceeds 400 A, the total height decreases significantly. This phenomenon can be attributed to the abrasion of the tool at high temperatures, which reduces the overall length of the forming tool.

Furthermore, due to the elevated temperatures involved in heat-assisted SPIF, lubrication can also pose a challenge. Additionally, the current flux induces temperature variations across the entire workpiece, and the temperature is not consistently maintained between the contact area under the forming tool and other sections of the workpiece. Moreover, the current flux generates significant Joule heating, leading to visible springback, cracks, wear tracks, and oxidation. Therefore, it is crucial to employ a uniform and elevated temperature heating technique to effectively heat the interface between the forming tool and the workpiece.

2.4.4 Incremental Single Point Shaping with Laser Heating Assistance

The Laser Forming Process operates by utilising the thermal effect induced on a sheet through the application of laser irradiation. The use of a laser device in the SPIF process was introduced by Duflou and colleagues [66], as shown in **Figure 2-14.** Its purpose was to generate localized heat on the surface of the metal sheet opposite to the tool application. The objective of implementing local dynamic heating was to enhance material ductility, improve dimensional precision, and reduce the required process forces. In this study, Laser Single Point Forming Process was employed to deform Al 5182 sheet metals with a thickness of 1.25 mm. By adjusting the beam intensity to 500 W, the temperature could be maintained at 350 °C. Compared to SPIF at ambient temperature, the forming force decreased from 1400 N to 700 N, while the forming angle increased from 32° to 56°. However, despite the lower temperature, heating the surface resulted in decreased surface quality and did not minimise springback during the process.

Lehtinen and colleagues [67] conducted an investigation on the effect of laser heating in Single Point Incremental Forming (SPIF) utilising a 1 kW fibre laser to deform 0.75 mm DC04 steel. While the study focused on investigating laser heating effects on high-strength sheet metal, it was not possible to compare the surface quality achieved with that obtained at room temperature. This is evident from **Figure 2-15(a-b)**, where the heated surface (**Figure 2-15b**) exhibited significant wear and minor cracks, while the product produced at room temperature (**Figure 2-15a**) had a smooth surface with no visible wear or cracks.

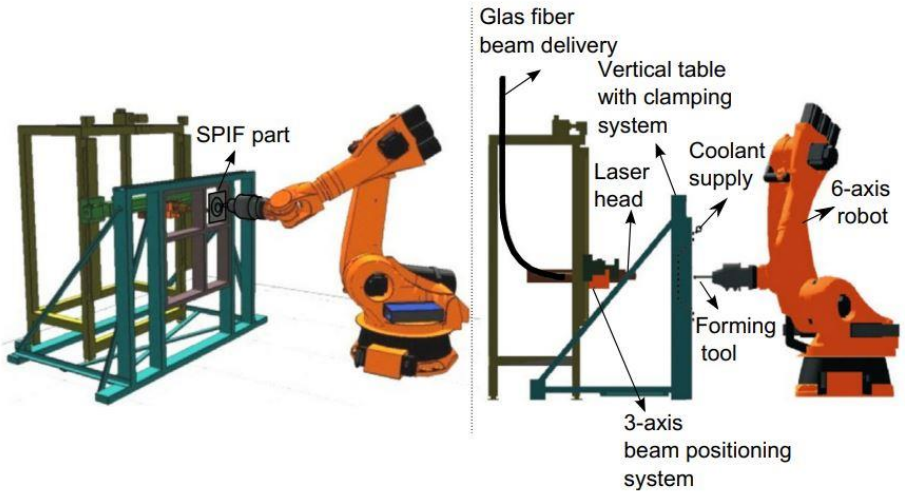

Figure 2-14 Experimental LASPIF configuration [66].

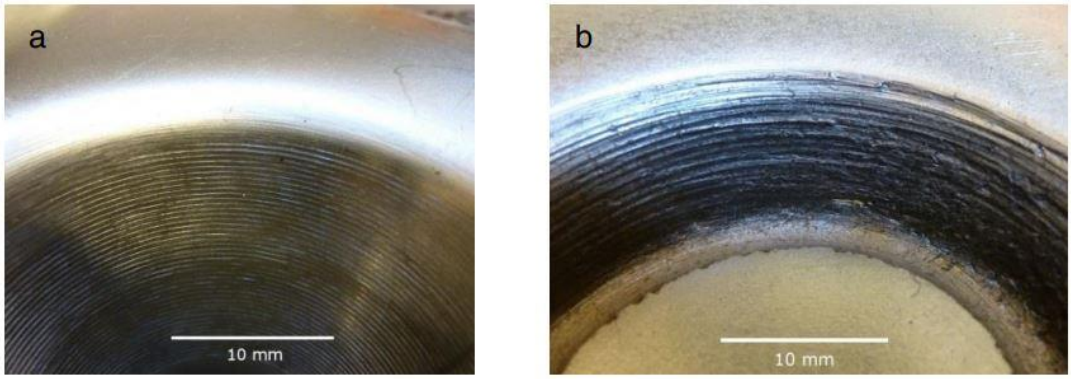

Figure 2-15 Comparing the surface quality of the produced workpiece, (a) without heating, (b) with heating [67].

Figure 2-16 illustrates the high-power (10 kW) fibre laser heating-assisted SPIF system proposed by Göttmann and colleagues [8] and developed in the study conducted by Göttmann and colleagues [68] for 1.5 mm Ti-6Al-4V sheets. The result shows improvement in the formability of the titanium Grade 5 alloy (TiAl6V4) through the use of a combination of laser heating and AISF (Adiabatic Isothermal Shear Forming) [68]. The laser spot system is coupled to the tool to enable synchronized movement. For rapid heating, the laser heating system utilises

beam shaping optics and displacement to direct the laser beam to the targeted area of the tool. Localised heating on the workpiece surface can be achieved by maintaining the temperature at 400 ℃. However, the achieved surface quality does not meet the required standards.

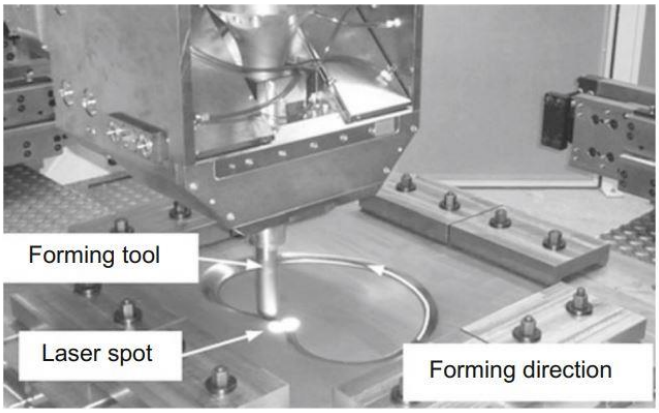

Figure 2-16 Experimental configuration employing laser as a heat source at the tool side [69].

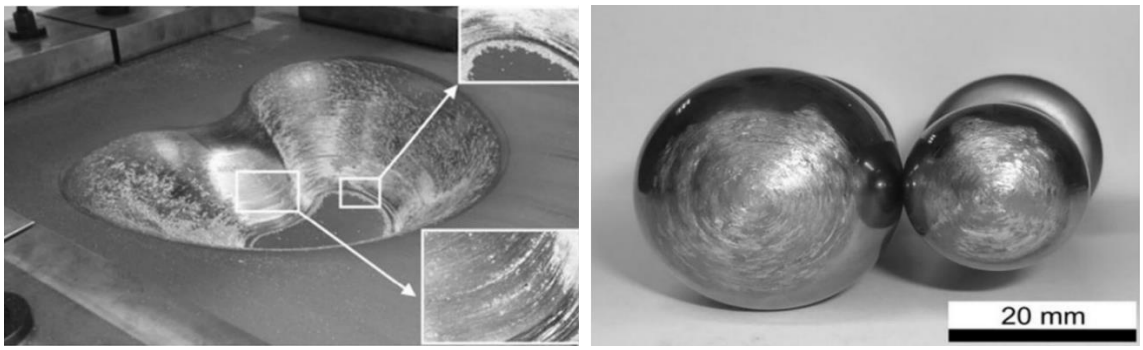

Figure 2-17 Tool erosion and surface finish (a) abrasive debris on a produced workpiece, (b) tool wear on different diameters of tool tips [69].

The use of laser beam heating leads to the rapid dissipation of the lubricant ahead of the tool, resulting in the formation of significant scratches between the tool and surface. **Figure 2-17(a)** demonstrates that material particles have been generated from the surface, leaving a substantial amount of wear debris on the surface. At elevated temperatures, the removal of the tool coating increases the adherence of lubricant and wear debris to the tool. This phenomenon has the

potential to negatively impact both the geometric precision and surface finish of the tool.

2.4.5 Incremental Single Point Shaping with Induction Heating Assistance

In contrast to the heating techniques discussed in earlier sections, the utilization of induction heating assisted SPIF offers the advantages of elevated temperatures, targeted heating, relatively inexpensive equipment, and improved surface quality. **Figure 2-18** illustrates the synchronised induction heating-assisted single-point incremental forming (SPIF) system with a tool-heater developed by Al-Obaidi and colleagues [17] . The induction heating coil is positioned beneath the workpiece and linked to the mounting of the forming tool to ensure synchronized movements.

The research focused on the formation process of dual-phase metal sheets made of 1.6 mm DP 980 steel. Thermal testing was conducted at temperatures of 785 ℃, 790 ℃, and 800 ℃ for wall angles of 45°, 55°, and 60°, respectively, while maintaining an allowable deviation of 30 ℃. The obtained results demonstrate a significant improvement in geometric precision compared to outcomes achieved at ambient temperature, which were insufficient for achieving a fully formed shape. The investigation also revealed enhanced geometric tolerances in the area with uniform induction power, as higher power led to a greater reduction in springback. In this case, higher temperatures result in improved ductility, which enhances geometric precision by reducing forming forces.

Furthermore, Al-Obaidi and colleagues [70] examined induction heating-assisted single-point incremental forming (SPIF) on 1.2 mm HCT 980C steel to obtain a wall angle of 70°. The findings indicate that localised heating of the workpiece at 750 ℃ using 5 kW power can an reduce forming forces by 66.63%.

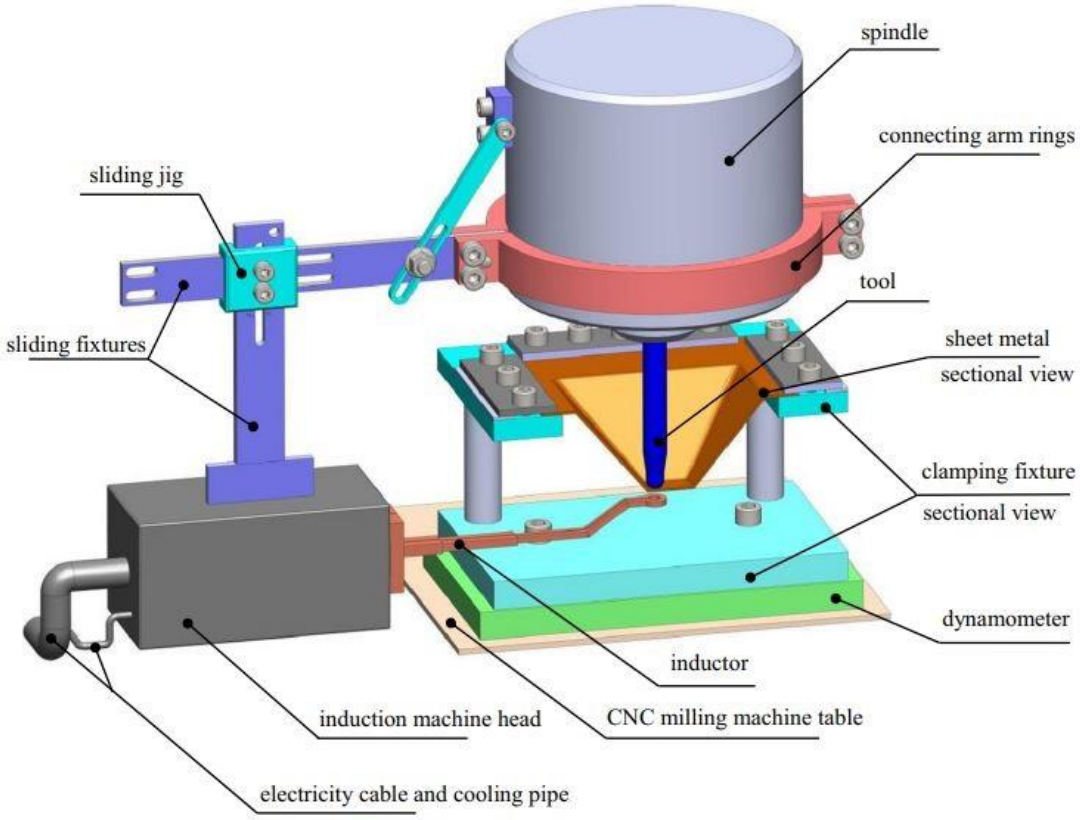

Figure 2-18 Experiential setup for induction heat-assisted SPIF [17].

In comparison to previously mentioned heating-assisted SPIF systems, the induction heater offers advantages of lower cost, easier setup, and higher product quality. The localised and precise heating provided by induction heating improves geometric precision and formability. However, there is still room for further enhancement of surface quality.

Figure 2-19 illustrates the difference in surface quality between electric-heating assisted SPIF and induction-heating SPIF on Ti-6Al-4V sheets using the same MoS2 lubricant and heating temperature. The electric-heating assisted SPIF product [71] shows distinct wear and cracks on the formed surface, whereas the induction-heating SPIF product [37] exhibits better surface quality.

Studies on induction heating have observed that lubricant dissipation is temperature dependent.

At higher temperatures (around 700 ℃), lubricant dissipation increases significantly from the initial stages of the process. To minimise these effects, Li and colleagues [72] implemented a water-cooling channel mechanism to facilitate the flow of liquid lubricant, thereby reducing the temperature at the tool-surface interface. This adaptable methodology ensures consistent heating temperatures throughout the procedure, leading to equiaxed microstructural changes and maintaining a steady DRX (dynamic recrystallization) process.

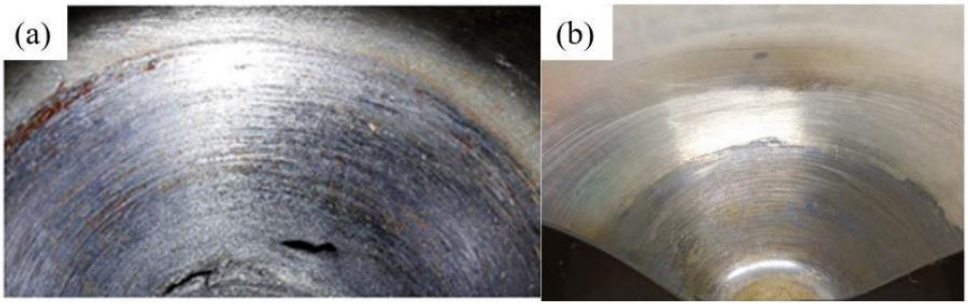

Figure 2-19 Evaluation of surface quality (a) electric-heating assisted SPIF [71], (b) induction-heating assisted SPIF [37].

2.4.6 Summary of the single point incremental sheet technique with heat assistance

In general, the incorporation of various heat sources into the Single Point Incremental Forming (SPIF) process shows potential for improving the ductility of materials, especially those with limited formability at ambient temperatures, and reducing forming forces, resulting in a superior surface finish. However, the utilisation of regional or localised heating methods presents several challenges that need to be addressed.

These challenges include the influence of temperature on formability and geometric accuracy, effects on surface quality due to wear debris and lubricant dissipation, the need for consistent and precise heating of the workpiece, and the design of efficient tools to minimise friction at the contact area. Each of the previous thermal sources has its limitations. For instance,

controlling the heat caused by the rotational speed of the tool is challenging and can lead to severe tool erosion [73]. Ultrasonic vibration may result in uncontrollable temperatures and difficulties in forming high-strength materials, which can exhibit significant springback and unfavourable surface quality.

Electric heating presents challenges in achieving stable and equilibrium heat control, while an increased feed rate for frictional heating can cause wear on the material sheet. Laser beam heating, although effective, can be costly and may lead to surface burns and damage. Induction heating, on the other hand, requires complex lubrication and expensive hardware.

A potential approach to overcome these limitations involves the utilisation of an innovative contactless heating technique such as the contactless single point incremental forming, which can effectively mitigate concerns regarding surface roughness, lubricant, and localised heating without compromising the flexibility of the forming process.

2.5 Forming tool developments

The tool utilised for forming processes plays a crucial role in determining the resultant shapes, geometric precision, and surface characteristics. The majority of studies focus on using a standard hemispherical tool to incrementally shape the sheet into its final form. Various alternative applications have been investigated as potential substitutes for the rigid tool. These include the implementation of diverse typologies of roller ball tips, employment of laser irradiation, and utilisation of water jets. Following are the works found in the literature that use these various shaping techniques.

2.5.1 Conventional tools

According to the experimental designs, the conventional tools used in SPIF typically have a hemispherical shape with diameters ranging from 6 to 25 millimetres [74]. However, in the study depicted in **Figure 2-20,** tools with both hemispherical and flat shapes were designed, with tooltip diameters varying based on the wall angle and step size. Kumar and colleagues [75] conducted a study to examine the forming limits of traditional hemisphere and flat tools, as depicted in **Figure 2-21(a,b)**. The investigation utilised R1 and R2 tools with diameters of 3.76 mm and 7.52 mm for hemispherical-end solid tools, respectively. Additionally, a side diameter of 1.4 mm was used for the corner radius for the flat-end solid tool.

According to the research, the use of hemisphere tools resulted in higher formability compared to flat tools. This can be attributed to the fact that the rounded surface reduces the contact area with the sheet. While the flat tool surface allows for greater geometric precision, the formability is reduced due to the increased tool corner. The size of the tool plays a crucial role in determining geometric precision and formability. Smaller tool sizes are beneficial in achieving smaller step sizes, which are essential for producing highly precise geometries and complex shapes. Nevertheless, the reduction in contact area leads to an increase in forming force, thereby raising the probability of crack formation when shaping deep geometries.

Figure 2-20 SPIF Tool shapes [74].

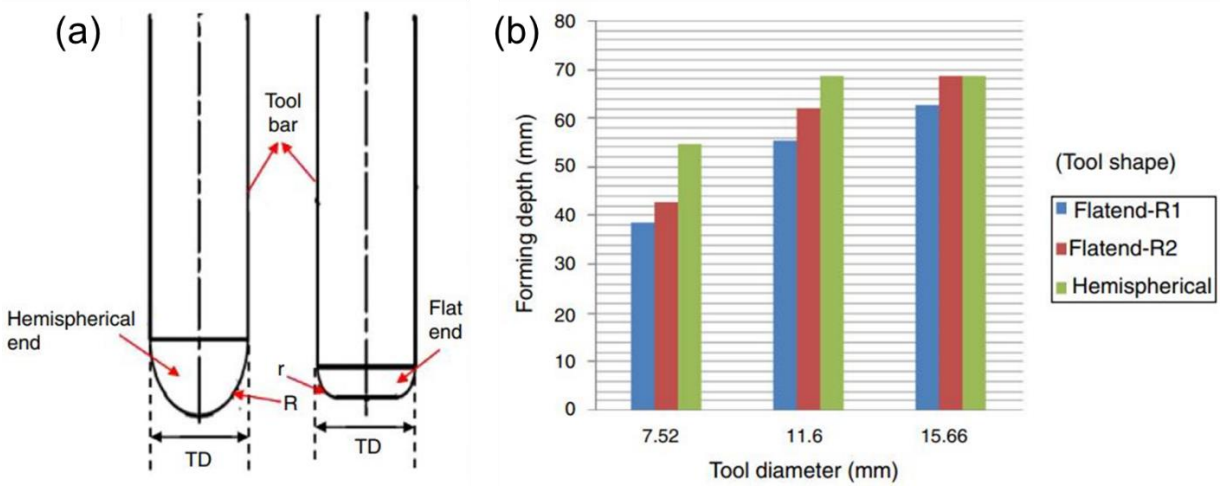

Figure 2-21 Standard tools and the associated impacts (a) Tools geometry, (b) The impact of tool diameter on forming depth [75].

2.5.2 Free rotational ball tools

Shim and colleagues [76] created a shaping tool with a freely revolving ball on the tool tip, as shown in **Figure 2-22**. The primary benefits of this approach include reduced forming stress, decreased friction, and an enhancement of surface finish. As illustrated in **Figure 2-23**, the researchers utilised a free-ball tip tool to assess the formability of AA1050 sheet metal during the fabrication of diverse geometries, including triangles, squares, pentagons, hexagons, octagons, circles, and squares with rounded corners. The study of these shapes was carried out until a crack appeared. The strains of the deformed grids, both major and minor, were measured around the area of cracks. To understand the deformation of SPIF, Finite Element analysis was conducted and compared to the experimental data. The research findings have validated that the deformation is restricted to the closest region of the tool's contact area. In general, the results revealed that near equi-biaxial stretching occurred at the corner, while near plane-strain stretching occurred along the straight side for all shapes except the circle. The circular structure presented a significantly greater magnitude of minor strain compared to all other shapes. Since the corners suffer more deformation than the straight sides, cracking has occurred there

frequently.

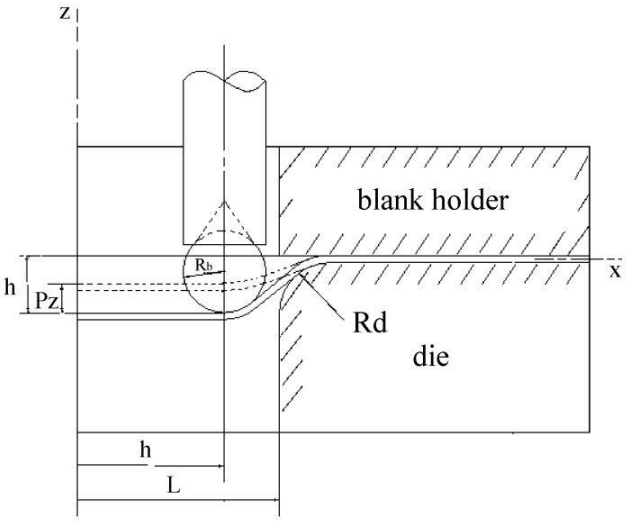

Figure 2-22 Schematic diagram of a ball-roller tool [76].

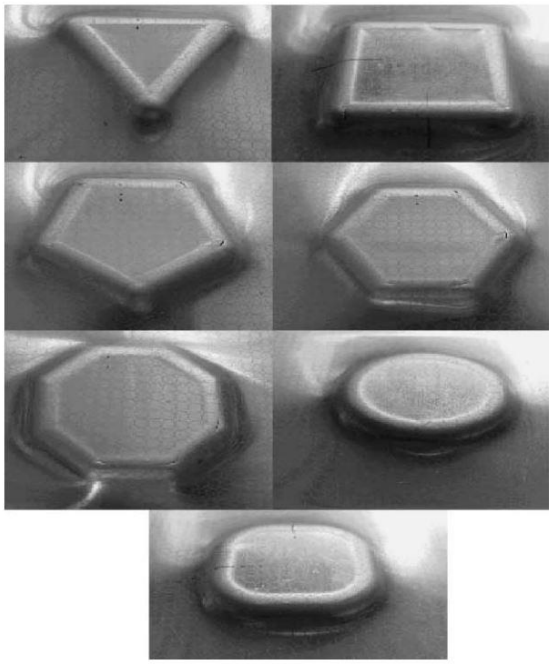

Figure 2-23 Different AA1050 shapes generated by a ball rolling tool [76].

2.5.3 Oblique roller ball and vertical roller ball

The authors Lu and colleagues [16] conducted an investigation on a recently developed tool known as the Oblique Roller Ball (ORB) , as displayed in **Figure 2-24**. A 3-axis CNC machine was used to control the ball roller, which was mounted to the tool body and always faced the workpiece. The primary objective of the ORB tool is to minimise the impact of the tool on the finished surface quality. A series of experiments were conducted to determine the final surface quality, formability, and deformation behaviour to evaluate the effectiveness of the developed ORB tool. The study conducted a comparative analysis of various forming tool topologies, including the conventional rigid tool (a), the Vertical Roller Ball (VRB) tool (b), and the ORB tool (c), through experimental works. The tools subjected to experimental testing are displayed in **Figure 2-25**.

Regarding the material of the sheet, various aluminium alloys were utilised. The experiments were conducted with a lubricated rigid tool and non-lubricated VRB and ORB tools. The research results indicated that the utilisation of roller-ball tools resulted in greater surface quality and reduced friction compared to the use of rigid tools. The ORB tool resulted in surfaces with low roughness values, whereas the rigid tool produced surfaces with the highest roughness values. When comparing the VRB and ORB tools, equal roughness values were discovered with no significant difference. Therefore, the rigid and ORB tools were used to assess the frictional influence on SPIF formability. The deformation behaviour suggests that the main source of the Through-Thickness-Shear (TTS) was friction between the tool and the sheet. Overall, the ORB tool demonstrated significant benefits, including lowered friction, reduced forming load, increased formability, and enhanced final surface quality. Nevertheless, the surface roughness of the resultant part displayed an increase compared to the original surface. The utilisation of the ORB tool in a 3-axis CNC milling machine has demonstrated its

benefits by optimising the process of creating wall angles.

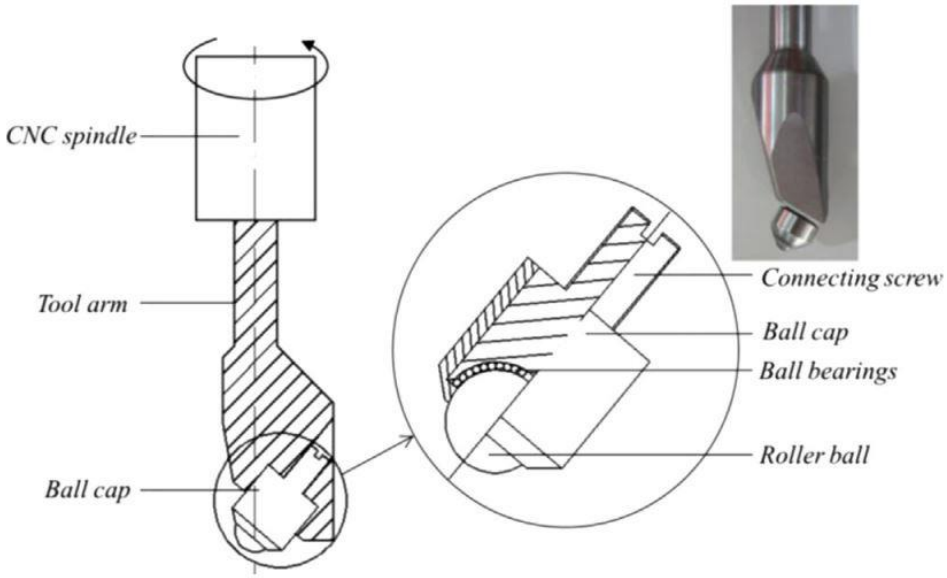

Figure 2-24 The ORB tool's schematic and physical structure [16].

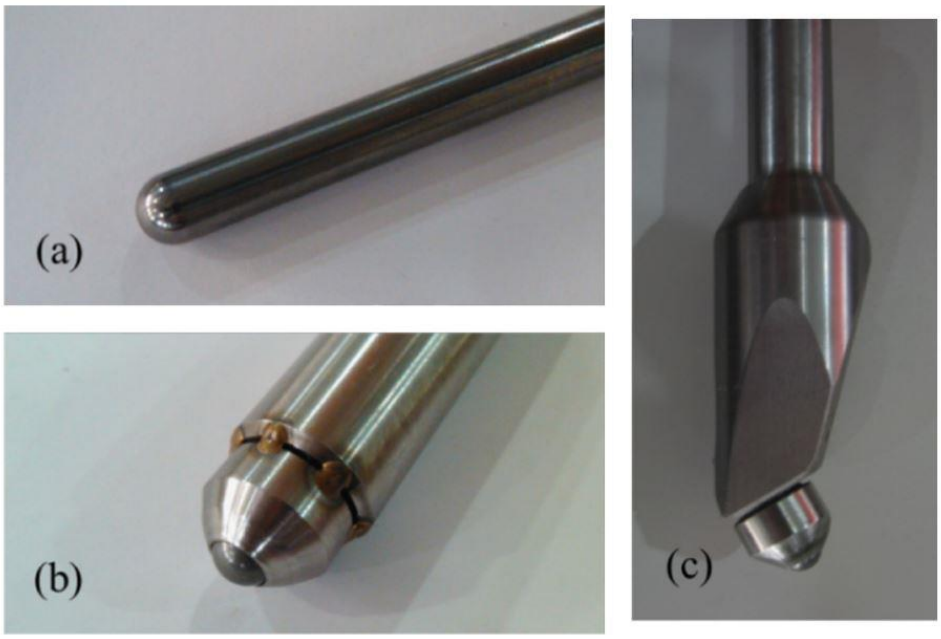

Figure 2-25 Various types of tools. (a) Rigid tool, (b) VRB tool, and (c) ORB tool [16].

2.5.4 Water jet forming tool

The possibility of utilising alternative tools has been suggested, such as the implementation of an unconventional tool like the waterjet tool. Water Jet forming (WJ) employs a water jet in substitution for a rigid forming tool. The benefits behind this approach include increased flexibility, improved surface integrity, reduced tooling needs, decreased equipment expenses, minimised environmental impact, and optimised contact conditions. However, WJ is less accurate, consumes more energy, and requires more time than other established forming tools [77].

The utilisation of high-speed WJ as a dieless Incremental Sheet Forming (ISF) technique has been proposed by Jurisevic and colleagues [77]. To enhance the characterisation process, the concept of relative jet diameter (k) was introduced. This parameter is determined by dividing the diameter of the water jet (dWJ) by the thickness of the sheet (t). The study identified essential process parameters and utilised empirical predictions to determine technological windows. The findings suggest that WJ has the potential as an alternative to SPIF. The study established two separate operational regions, determined by the water pressure (pW) and relative jet diameter (k), and a final process parameter defined by the WJ distance (h_{SO}), as seen in **Figure 2-26**.

Through experiments, numerical evaluations were conducted for each situation. The initial technological window (1) was constrained at its upper boundary by the amount of surface pressure required to initiate erosion. The lower limit was determined by the required magnitude of the water jet (WJ) force necessary to initiate plastic deformation in a blank with a specified thickness (t). Due to the material dependence of both limiting lines, technological windows must be identified independently for each workpiece material. A second technical window (2) is represented by the water pressure (pW) and the distance (hSO) between the forming WJ and

the workpiece. The technological window was defined based on the variables of water pressure and relative jet diameter. The observation indicates that the phenomenon was constrained by erosion, which occurs under conditions of elevated water pressures and reduced distances. However, an absence of plastic deformation will occur if the water pressure is too low, and the distance is too great. The process operation area is determined by the sheet material.

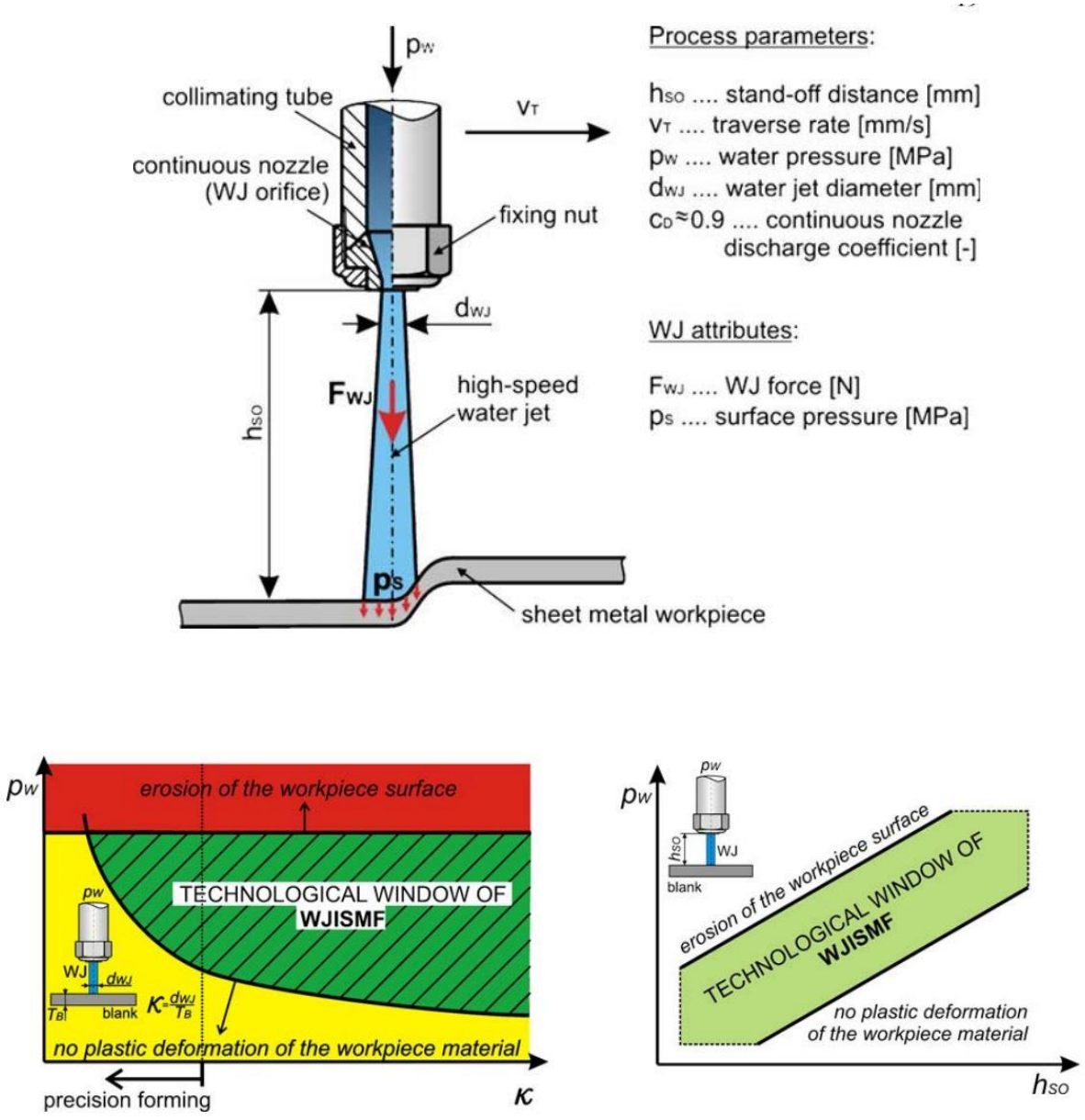

Figure 2-26 The technological components of the WJ process [77].

Petek and colleagues [78] conducted an analysis of the WJ process. The objective of their research was to investigate the key parameters that have a significant impact on both the WJ and conventional SPIF processes. The experimental study involved the fabrication of a basic pyramid structure using aluminium sheet material with a thickness of 0.23 mm. The study revealed that the optimal range of horizontal step and wall angle resulted in identical effects between the two processes. Based on the results of the conducted experimental research, it can be concluded that the utilisation of a rigid tool is more suitable for scenarios involving larger wall angles ranging from 44º to 60º and smaller horizontal steps ranging from 0.2 mm to 0.8 mm. With a rigid tool and a horizontal step size of 0.2 mm, the greatest wall angle obtained was 60º. In contrast, the application of WJ demonstrated higher efficiency in larger horizontal steps ranging from 0.8 mm to 1.6 mm and smaller wall angles between 22º to 26º. The primary distinguishing factor between the two forming tools is the controlling concept. When employing a rigid tool, the most important process parameter was the definition of the loads that were acting on the surface of the worksheet. While the water pressure (pW) and the distance (hSO), which define the forces acting on the worksheet surface, are the primary parameters for WJ. The results of this investigation indicate that utilisation of the rigid tool results in enhanced process accuracy, lower energy consumption, and reduced machining time compared to the utilisation of the WJ method.

2.5.5 Summary of the tool design

In summary, the formability, geometric accuracy, and surface quality of formed shapes are influenced by the type, shape, and tool diameter. This section provides an analysis of the advantages and disadvantages associated with the use of traditional tools, freely rotational tools, ball-roller tools, and water jet tools in the context of single point incremental forming (SPIF), based on the findings of conducted studies.

Regarding the solid tool, the sheet's formability is limited, noticeable wear tracks are present, there is a high possibility of cracking, and the use of lubrication is necessary. The ball roller tool involves complicated design and manufacturing processes that come with significant expenses. As for the water jet tool, it incurs significant costs in terms of both components and operation. Additionally, it employs a wet process, exhibits reduced precision, unsustainable due to water loss, and requires additional safety precautions. Therefore, it is crucial to consider a novel concept that can effectively address the limitations of traditional equipment while also offering a reduced level of cutting or high-impact risks compared to water jet technology, a lower cost, greater precision, and sustainability.

2.6 Coatings and lubricants

SPIF systems commonly use graphite lubrication, machine oil, and MoS2 paste/spray as lubricants. In the context of the heat-assisted single point incremental forming (SPIF) process, conventional lubricants are considered insufficient for achieving optimal levels of surface finish and geometric precision. This section aims to conduct a comparative analysis of various lubricant types, including paste, spray, and liquid, in terms of their impact on surface quality and geometric accuracy.

2.6.1 Lubricants and coatings used in ISF

The impact of lubrication and coating on surface quality in ISF processes is significant. The choice of lubricant or coating depends on the materials involved, process parameters, and temperature. The efficacy of lubrication and coating in SPIF processes conducted at room temperature is influenced by the sheet materials used due to significant variations in surface roughness and yield strength, which affect the exertion of forming forces. High forming forces can influence tool motion and reduce the performance of the lubricant or coating, leading to

geometric inaccuracy and cracks.

For example, Azevedo and colleagues [18] concluded that the selection of the right lubricant viscosity depends on the hardness of the material to achieve the best result. In their study, they examined the surface finish of steel (DP780) and aluminium (AA1050-T4) after applying different types of lubricants (Repsol SAE 30, Total Finarol B5746, Moly Slip AS 40, Weicon AL-M (all-round), and Moly Slip HSB (high-speed bearing)). The study found that SAE 30 provides a smoother surface finish when applied to AA1050-T4, while Finarol B5746 oil gives a rougher surface finish, as shown in **Figure 2-27**. Conversely, for the steel material, Finarol B5746 oil provides a smoother surface finish, while SAE 30 gives a rougher surface finish, as shown in **Figure 2-28**. Therefore, high-hardness materials require lower-viscosity lubricants, and vice versa.

Figure 2-27 The surface quality of 1050 aluminium cones for lubricants (a) SAE 30, and (b) Finarol B5746 [18].

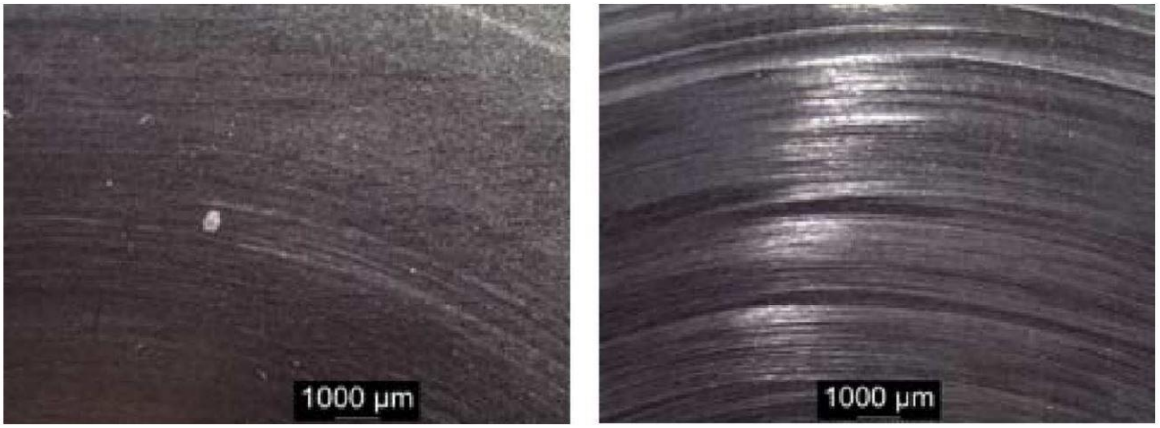

Figure 2-28 The surface quality of DP 780 steel cones for lubricants (a) Finarol B5746, and (b) SAE 30 [18].

Another study conducted by Sornsuwit and colleagues [79] examined the efficacy of MoS2 on stainless steels SUS 304 and SUS 316L, as well as Grade 2 titanium (Ti Gr2). MoS2 is a self-mixed paste consisting of MoS2 particles and petroleum jelly in a ratio of 4:1. In all experiments, the tool diameter is 10 mm, the workpiece thickness is 1 mm, and the feed rate is 3140 mm/min. **Figure 2-29** displays the surface quality of each material, showing a decline in lubricant performance correlated with the yield strength of the materials. Specifically, Ti Gr2 exhibited the poorest surface quality on the deforming surface. The formability and surface roughness are depicted in **Figure 2-30**. The results indicate that Ti Gr2 displayed the highest surface roughness distribution when compared with the surface roughness of SUS304 and SUS316L when using same lubricants. Nevertheless, MoS2 remains the optimal lubricant for Ti Gr2 sheets compared to alternative lubricants.

On the other hand , Hussain and colleagues [80] observed the poor surface finish in titanium parts due to regular lubrication escaping the tool-sheet contact area. Consequently, they found that the combining a micro-arc oxidation coating on the sheet and MoS2 paste as lubricant improved the surface finish of the titanium due to the lack of adherence of sheet material to the

tool tip.

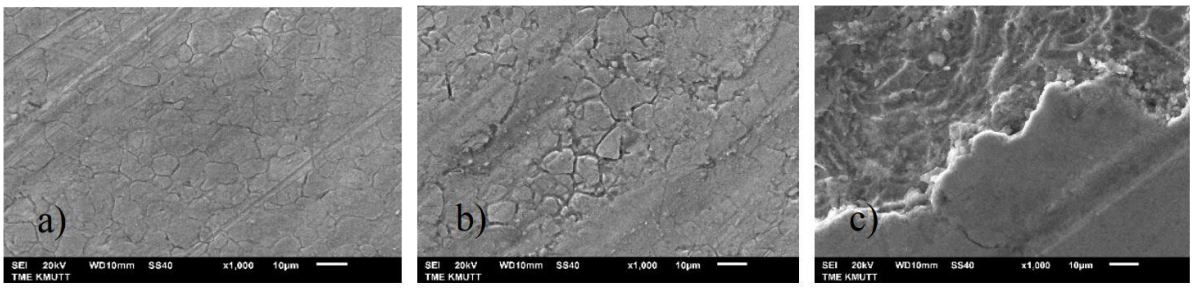

Figure 2-29 The surface of a shaped materials when MoS2 is used as a lubricant to at x1000 magnification; a) SUS 304, b) SUS 316L, c) Ti Gr2 [79].

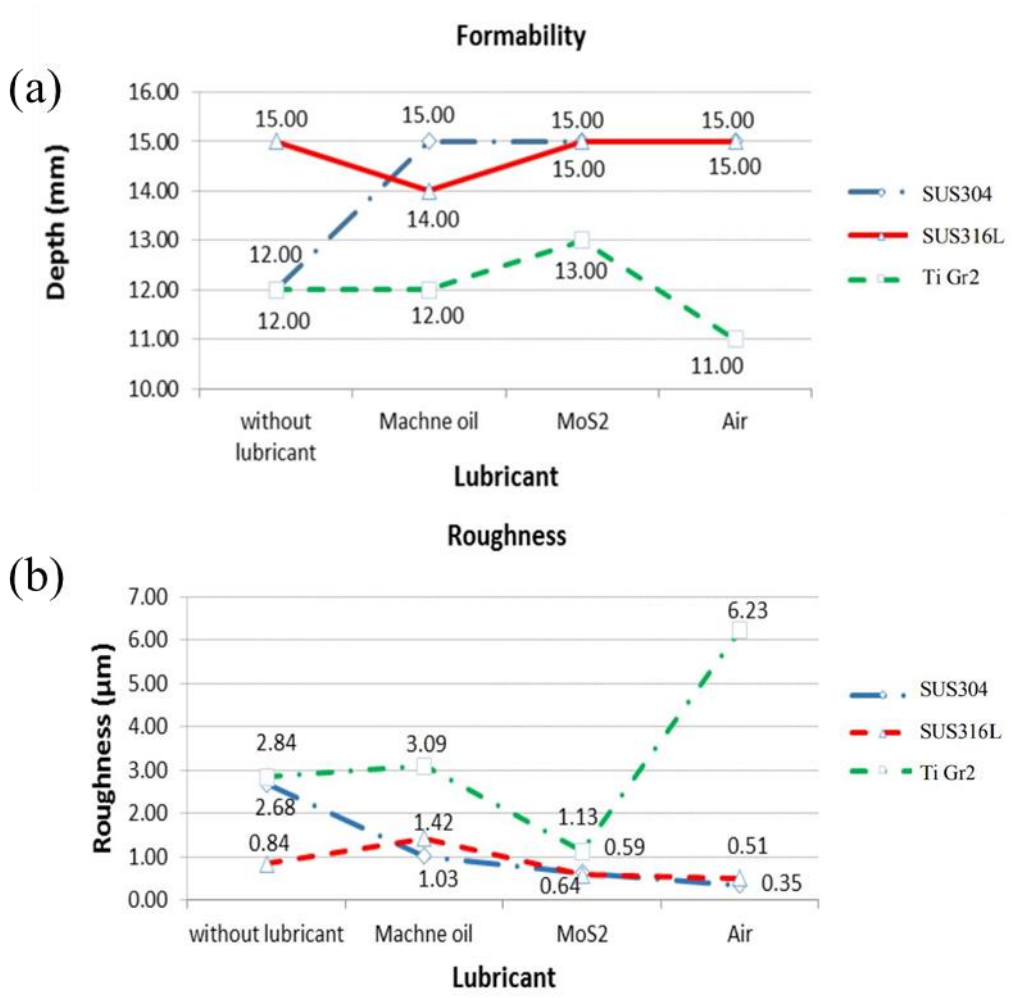

Figure 2-30 Surface roughness and formability, (a) formability, (b) roughness [79].

On the other hand, when it comes to the heat-assisted SPIF process for high-strength materials, conventional coatings may not be effective at elevated temperatures. The commonly used spray, paste, or liquid lubricants tend to dissipate during this process [81, 82]. To address this issue, Li and colleagues [82] developed a lubricant mixture consisting of WS2 powder and high-temperature lubricating oil. This mixture has been found to reduce the adherence of the lubricant during electric heating-assisted SPIF of Ti-6Al-4V sheets at 500°C. Similarly, Liu and colleagues [83] implemented a water-cooling mechanism for the tool to lower the temperature of the ball-roller tool tip. In a subsequent study, Li and colleagues [72] further improved the design of the forming tool by introducing a liquid MoS2 flow, which served the dual purpose of lubricating the forming surface and cooling down the ball-roller tool tip. This approach provides sufficient lubrication to prevent frictional dissipation and minimise thermal expansion of the tool and contact surface consistently.

Additionally, Fan and colleagues [84] found that a solid lubricant coating containing a nickel matrix with MoS2 material enhances the surface quality and prevents high-temperature oxidation of the Ti-6Al-4V titanium sheet formed by the electric hot incremental forming method. In their study, three types of solid lubricants (graphite, MoS2, and boron nitride) were investigated. However, graphite lubricant proved to be ineffective for deforming Ti-6Al-4V titanium sheets as it caused the appearance of numerous micro-pits on both the tool and sheet metal surfaces due to electric sparks generated during the electric hot incremental forming process. When examining the surface roughness of the Ti-6Al-4V sheet treated with MoS2 and boron nitride lubricants, it was noted that the boron nitride-treated sheet exhibited double the surface roughness compared to the MoS2-treated one. The MoS2-treated sheet had an average surface roughness of 21.5 µm, while the boron nitride-treated sheet had a surface roughness of 41.4 µm.

Lastly, polymeric materials exhibit relatively high frictional resistance between the sheet surface and the tool. Thermoplastic polymers may experience a temperature rise above their softening point due to localized heating. While this can increase the formability of the SPIF process, it also leads to unstable sheet deformation. To address this issue, Hussain and colleagues [85] used machine oil as a lubricant when deforming polymer materials using SPIF.

2.6.2 Summary of lubricants and coating

In conclusion, lubrication plays an essential role in enhancing the formability of SPIF, improving surface quality, and reducing tool wear. However, the use of lubricants increases the cost of the SPIF method due to the additional expense of the lubricant itself and the cleaning process. Furthermore, it is important to note that the effectiveness of lubrication may vary depending on the material being formed and the specific SPIF process used.

On the other hand, applying lubricant is time-consuming as it requires an additional cleaning step. Moreover, it may have a negative impact on the environment and the surface quality of the workpiece. Additionally, it is important to consider the potential health and safety risks associated with using lubricants, such as skin irritation or inhalation of fumes. Proper safety measures should be taken to minimise these risks and ensure a safe working environment for all personnel involved in the SPIF process.

The limitations associated with the use of lubricants in SPIF present opportunities for further investigation and advancement of alternative techniques that can offer comparable advantages while reducing the related expenses and hazards. To overcome the use of lubricants, it is suggested to explore methods that eliminate direct contact between the tool and sheet.

2.7 Numerical simulation analysis

This section examines the accuracy of several forms of numerical analysis (implicit and explicit) in estimating geometric precision, thickness distribution, forming force, and temperature. Additionally, it explores the utilisation of a computational fluid dynamics (CFD) model in SPIF to predict heat transfer values, as well as calculate the force and temperature of the fluid when used as a non-conventional forming tool. Moreover, the investigations conducted involved microstructural finite element (FE) analysis, such as crystal plasticity finite element method (CPFEM), representative volume element (RVE), cellular automata (CA), are discussed in terms of their ability to accurately predict the microstructural behavior of SPIF or other relevant metal forming processes.

2.7.1 FE modelling (implicit and explicit)

In order to anticipate the mechanical response during the Single Point Incremental Forming process, a numerical modeling approach has been developed utilising constitutive laws from existing literature, which are defined by the user for Finite Element (FE) simulation. Currently, user-defined processing and post-processing tasks can be performed using commercial software such as ABAQUS, LS-DYNA, and ANSYS.

In the context of finite element modeling for single point incremental forming processes, it is common to consider the tool parts as rigid bodies while defining the sheet materials as deformable objects. The tool's motion in the FE model corresponds to the experimental SPIF process, which can be assigned to path displacements and temperature conditions. Due to the complex forming shape and step size, the simulation may require a high number of discrete increments. Silva and colleagues [86] stated that the quantity of increment points was determined by the tolerance setting within the CAM program. Utilising a 0.01 mm tolerance,

for example, generated an estimated 400 increment points per meter for the hyperbolic cone, while the pyramid in the finite element simulation exhibited 8 points per meter due to its straight sides. The vertical step down was set at a value of 0.5mm, and the coefficient of friction was modeled using Amonton-Coulomb's law with a value of zero ($\mu = 0$).

Prior to running a simulation to solve a FE problem, it is necessary to consider specific computational features and the amount of time required for computation. For example, ABAQUS standard simulation provides two solver types: explicit and implicit. The explicit solver computes the data output based on the present state, resulting in a simple calculation process that requires less computational time for a single explicit increment. However, it cannot be used for large time increments due to the exponential growth of errors, which would make the calculation process unstable.

On the other hand, the implicit solver utilises the previous state to calculate the data output, involving a coupled system that requires non-linear algorithms such as the Newton-Raphson method. It is important to note that the implicit solver demands more computational time and memory compared to the explicit solver, as a larger number of equations need to be solved during an incremental process.

The explicit solver is commonly used in SPIF simulation to account for material quasi-static behavior and minimise computational time. In contrast, the implicit solver requires more computation time and presents a higher probability of generating non-convergence results due to the complex details of tool-workpiece contact. In a study conducted by Durgun and colleagues [87], a comparison was made between explicit and implicit solvers in an ABAQUS simulation of Single Point Incremental Forming (SPIF) processes. The workpiece consisted of 7300 S4R shell elements and seven thickness elements. The comparison of geometric and strain

measurements among explicit, implicit, and optical methods is presented in **Figure 2-31**. Based on the results, it can be concluded that both types of solvers are in agreement with the optical measurement and explicit solver, suggesting a comparatively stronger correlation than the implicit solver. Additionally, the research revealed that the implicit solver exhibits a greater computational duration compared to the explicit solver.

Yamashita and colleagues [88] utilised the dynamic explicit finite element software LS-DYNA to analyse of a quadrangular pyramid with varying heights. Various toolpaths were experimented with to investigate their impact on the deformation characteristics. The distribution of strain in thickness and the magnitude of the force generated during the tool's movement were examined. The results indicate that the inertial effect on deformation is related to the density of the sheet material and the travelling speed of the tool. After careful examination and optimisation, the optimal computing conditions for running simulations in LS-DYNA was determined. The findings suggested that numerical simulations with an explicit strategy can be used to optimise the SPIF toolpath.

Kulkarni and colleagues [89] employed a coupled thermomechanical model to simulate the convective heat-assisted single-point incremental forming (CHASPIF) setup. Accurate modeling of the SPIF setup primarily involves integrating the circular forming area of the blank and the tool's tip. The coupled thermo-mechanical simulation model was developed in ANSYS 17.0 CAE software. The Finite Element Analysis (FEA) model includes a movable heat load that depends on the toolpath and its corresponding temperature. In the ANSYS software, the localised convective heating is approximated as a series of sector shapes, which are modeled as equivalent nodal convective heat transfer coefficient (HTC) loads.

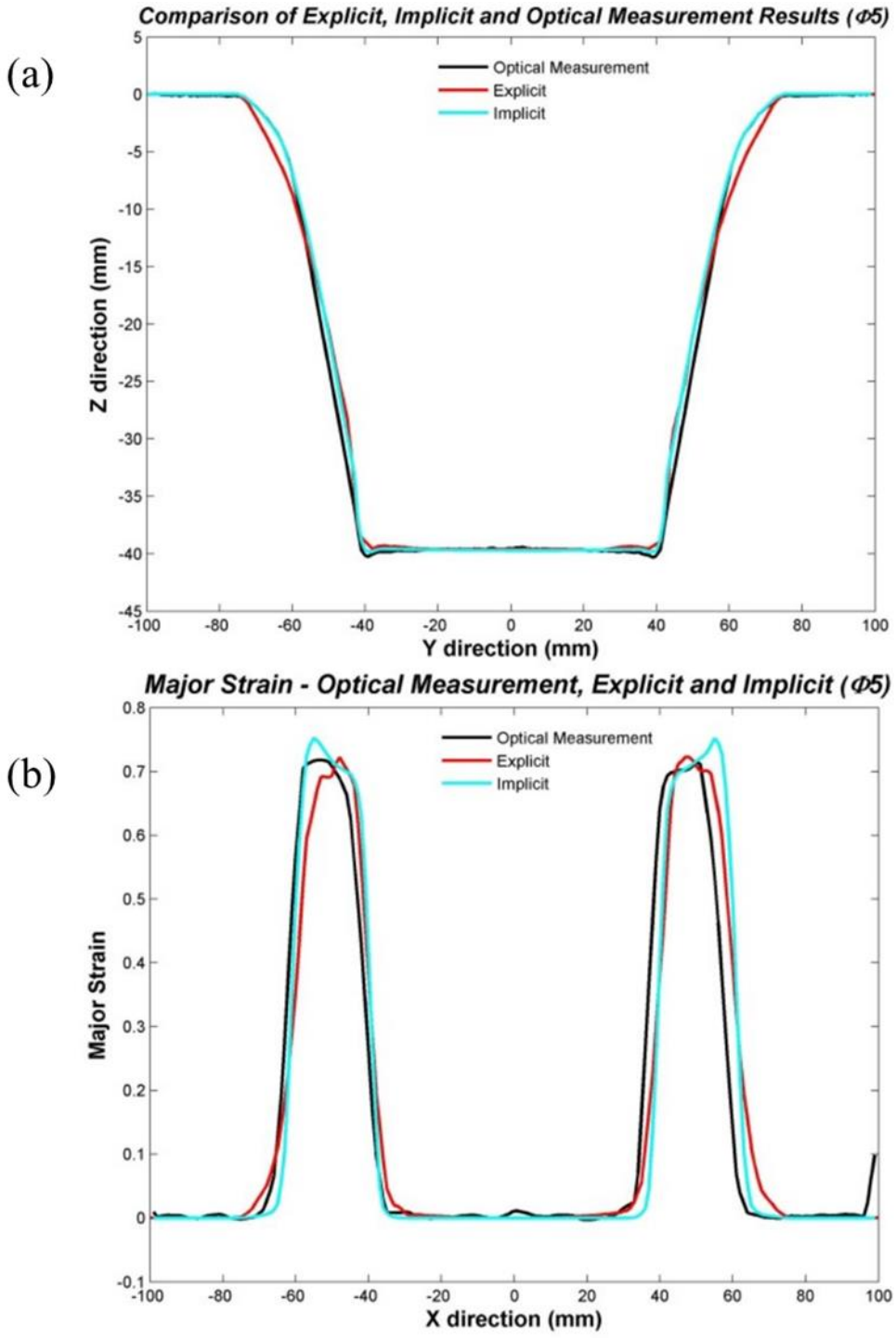

Figure 2-31 Comparison of explicit and implicit analysis in terms of geometry and strain (a) profile comparison, (b) strain comparison [87].

This process is illustrated in **Figure 2-32** [90]. Nodes within each heated spot region are identified and HTC values are assigned based on the tool's position at each time step. APDL

scripts repeat this process for each time step. Furthermore, simulating SPIF at ambient temperature can be achieved by omitting the placement of a localised thermal load. The structural and thermal finite element analysis matrices can be obtained simultaneously by utilising the Mechanical ANSYS Parametric Design Language (MAPDL) solver.

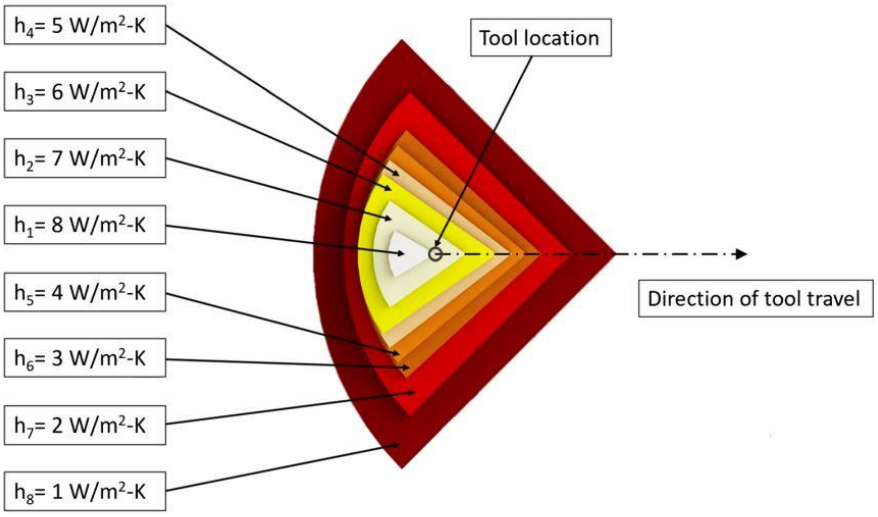

Figure 2-32 Simulation of HTC value distribution using a series of sectors [90].

2.7.2 Computational fluid dynamics (CFD) model

Since the use of heat assistance in SPIF has proven its effectiveness in enhancing the process experimentally, studying the implementation of this technique in numerical analysis becomes even more significant to validate those results. The phenomenon of SPIF with localised heating has been the subject of experimental investigation, while the availability of simulation models for such processes is limited. Computational Fluid Dynamics (CFD) modeling has emerged as a powerful and efficient tool for understanding the hydrodynamics of heat transfer in SPIF heat assistance and water jet SPIF, owing to the progress made in computer software.

Lu and colleagues [91] utilised computational fluid dynamics (CFD) simulations through the

ANSYS/Fluent software to assess the velocity and pressure distributions of water jets for four distinct nozzle design concepts. In the analysis, the viscous turbulence model k was used, and the simulations implemented the SIMPLEC algorithm. The time step increments for all design concepts were established to be 1e−6. The selected water flow rate was 8.6 liters per minute, accompanied by an inflow velocity of 2.852 meters per second. The density of water was measured to be 998.2 kg/m3, while the density of air was found to be 1.025 kg/m3.

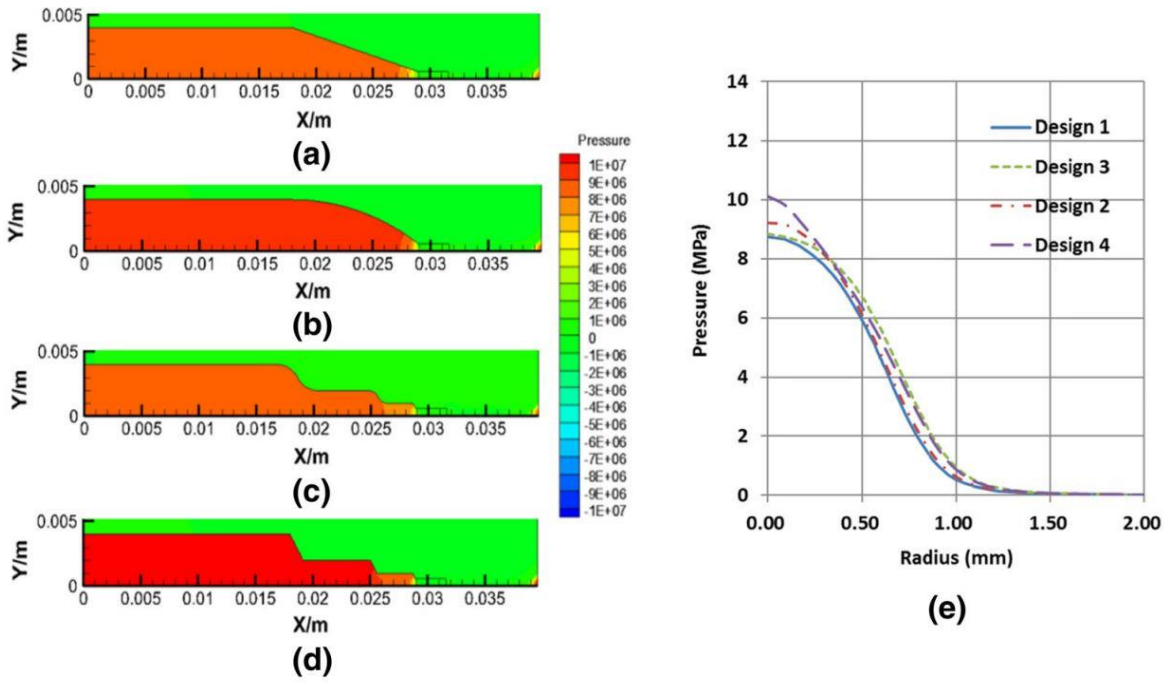

Figure 2-33 Water jet pressure inside the nozzle is compared (a) Design 1, (b) Design 2, (c) Design 3, (d) Design 4 ,and (e) Pressure distributions around the radius of the sheet [91].

The water jet pressure fluctuations during its passage through the nozzle channel were modeled and illustrated in **Figure 2-33(a-d)** using computational fluid dynamics (CFD) simulations. **Figure 2-33e** depicts the pressure distributions along the radial direction of the forming sheet. After that, to study the deformation of the sheet, the forming pressure distribution was computed through computational fluid dynamics (CFD) simulations and applied to the

deformable sheet using the ABAQUS user subroutine function, VDLoad, for the ISF-WJ process.

2.7.3 Crystal Plasticity Finite Element Method (CPFEM), Representative Volume Element (RVE), and Cellular Automaton (CA)

The utilisation of crystal plasticity finite element method (CPFEM) and representative volume element (RVE) can provide analysis at the mesoscopic and microscopic scales for SPIF operations. This approach allows for simulating plasticity behavior at the experimental or partial scale and the strain-stress behavior at the grain level for specific parts during the process, rather than conducting a macroscopic scale analysis.

Esmaeilpour and colleagues [92, 93] conducted research that employed a combination of CPFEM and RVE methodologies to simulate the single point incremental forming (SPIF) process on a sheet of 7075-O aluminum. The plasticity properties obtained from CPFEM were imported and used as inputs in the RVE model. The researchers utilised electron backscatter diffraction (EBSD) to determine grain orientations in crucial regions of the workpiece. In a similar vein, Groeber and colleagues [94] employed DREAM.3D software to construct a RVE model that accurately represented the plasticity behavior.

Chuan and colleagues [95] conducted a study where they combined crystal plasticity finite element method (CPFEM) with cellular automata (CA) to investigate the phenomenon of dynamic recrystallization (DRX) during isothermal hot compression. Their findings provided theoretical evidence for the effectiveness of using crystal plasticity and DRX behavior in simulating the hot deformation process of steel alloys.

In another investigation by Li and colleagues [96], a combination of CPFEM, RVE, and cellular automaton (CA) methods was used to examine the effects of induction heating on grain

orientation, crystal texture, and dynamic recrystallization (DRX) during single-point incremental forming (SPIF) of Ti-6Al-4V. **Figure 2-33** illustrates a novel approach for investigating the macroscopic scale strain-stress behavior using CPFEM. This method involves transferring the collected properties to the Representative Volume Element (RVE) model that corresponds to the crucial forming regions throughout the process. Additionally, a CA modeling technique is employed to predict grain growth using the crystal plasticity outcomes obtained from CPFEM and RVE as input.

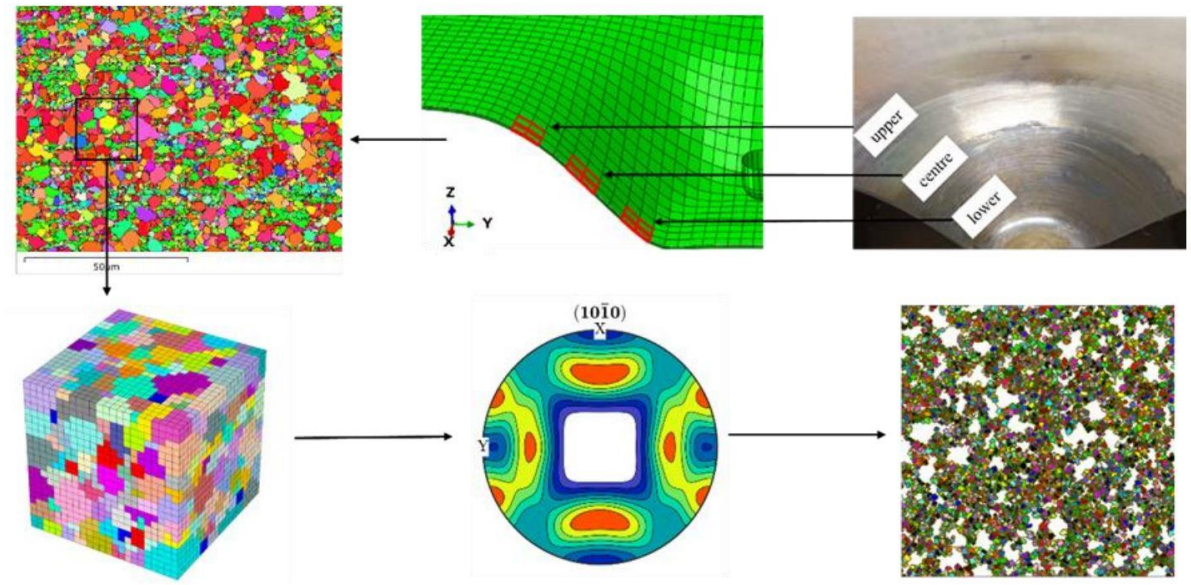

Figure 2-34 Diagram for heat assisted SPIF microstructural evolution [96].

The methodology of this study involved collecting grain orientation data from EBSD, which was subsequently used at an experimental scale. The resulting grain-level stress-strain data was integrated into a RVE to generate crystal texture, utilising the MATLAB toolbox MTEX [97] . This approach was employed to investigate the DRX behavior. The study utilised single crystal constitutive models that consider elastic lattice distortion and plastic deformation while disregarding the effects on lattice geometry. The research outcomes facilitated the generation

of stress and strain data at the grain level, which were utilised to form DRX evolution and misorientation angles for crystal texture.

2.7.4 Summary of Analysis of numerical simulations

Numerical analysis has the capability to evaluate the mechanical and thermal characteristics of experimental-scale SPIF processes. Previous studies have primarily focused on tool-sheet interactions. Various Finite Element Method (FEM) approaches have been developed to incorporate heat assistance into conventional SPIF, such as heating the tool itself or utilising fluid-solid interaction. Most of the studies used the explicit model rather than the implicit model due to less computational time, efficiency for small incremental points, and approximately constant increment size. However, the explicit type is limited when it comes to large incremental times, and the mass scaling affects accuracy and computational time.

On the other hand, the implicit type shows great promise in linear to mildly non-linear models and is efficient for large time increments. CFD modeling was utilised to simulate the water jet forcing in water jet SPIF, which was later combined with FEM as fluid-solid interaction. In this case, the CFD was used to simulate the water jet pressure distribution on the sheet without applying any heating. In terms of analysing the microstructure, CPFEM played a significant role in studying the material's microstructure. The topic of CPFEM holds potential for further research in the future, and subsequent investigations will be conducted for polymers after completing this thesis.

2.8 Forming limits

The formability limits of Single Point Incremental Forming (SPIF) and Two-Point Incremental Forming (TPIF) are determined by the influence of various factors. These factors include

lubrication, movement between the tool and sheet, sheet thickness, tool radius, vertical pitch, tool speed, tool path design, and the properties of the sheet material.

2.8.1 Wall thickness and sine law

The investigation on wall thickness in Single Point Incremental Forming (SPIF) was conducted by Jeswiet and colleagues [98]. The researchers generated multiple cones

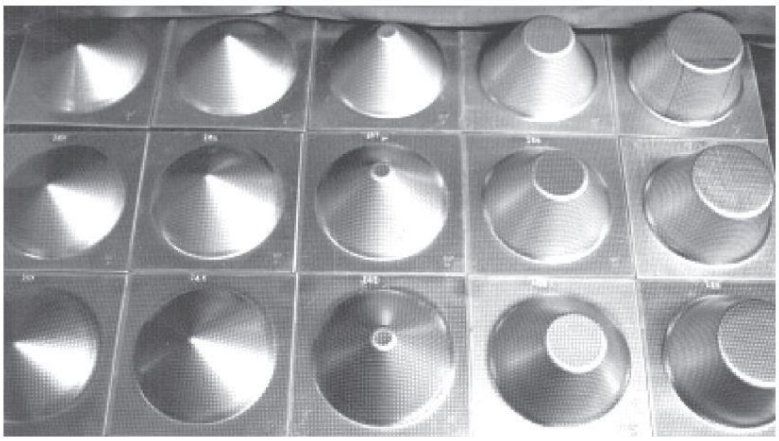

Figure 2-35 Multiple cones with different wall angles [98].

with varying wall angles (represented by θ in **Figure 2-33**) and observed that the sine law is applicable when the wall angle is small. As depicted in **Figure 2-33**, a thinning band occurs as the wall angle increases. The thickness of the wall exceeds the estimation by the sine law within this range. Furthermore, the study found that the measurable thickness of minor wall angles, such as 30°, is slightly lower than the prediction by the sine law. Moreover, the variation between the measured thickness and the anticipated thickness according to the sine law decreases as the wall angle increases in thinning strips.

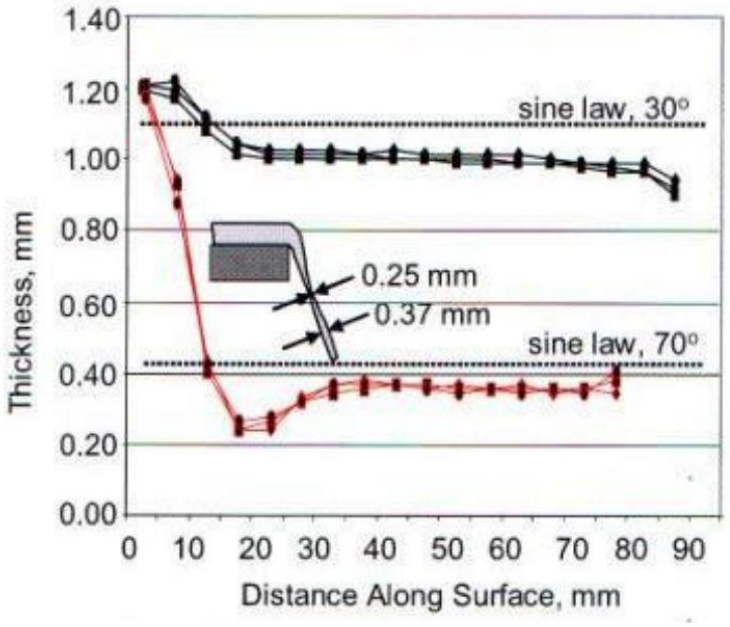

Figure 2-36 Measurements of wall thickness for 30° and 70° cones [99].

Moreover, Wei and colleagues [99] conducted experiments to investigate the thickness distribution in single point incremental forming (SPIF). The researchers observed the formation of irregular and complex shapes and determined that the thickness of the walls can be described by the following equation:

$$t = t0 \cos \alpha \quad \text{.....2.1}$$

Where:

t represents the workpiece's ultimate thickness, t0 represents the workpiece's initial thickness, and α is the wall angle.

Based on the information presented in **Figure 2-33**, it can be suggested that **Equation 2.1** represents an alternative form of the sine law. However, due to the substitution of the wall angle instead of the half apex angle, the resulting equation can be described as a cosine function. The

present investigation will employ the cosine law for the prediction of wall thickness in all relevant areas.

2.8.2 Assessment of formability

In several sheet metal forming procedures, the measure of formability is commonly conveyed through a forming limit diagram (FLD), which indicates the highest strains that can be obtained prior to the start of necking. According to previous research [98], in the SPIF process, the reduction in wall thickness is directly proportional to the increase in wall angle. Consequently, the sheet will fracture once the thinning limit is exceeded. As a result, there is a maximum wall angle that a sheet can withstand without cracking. The maximum wall angle in the SPIF method is commonly referred to as the formability threshold, which has been agreed upon by scholars to be calculated using the maximum angle of the wall, as evidenced by various studies [36, 100, 101].

The frustum of a cone is typically employed as the geometric form used to indicate the maximum angle of a wall. To determine the maximum angle of a frustum wall, the angle is gradually increased in small increments until the maximum value is reached without causing any fractures. Several researchers have identified the creation of a forming limit curve (FLC) within the minor-major strain space to demonstrate the formability in single point incremental forming (SPIF), as shown in **Figure 2-33**. According to the research conducted by Iseki and colleagues research [102], it has been suggested that the tension-tension quarter of the forming limit curve could demonstrate a simple trend with a downward slope in the FLC context. Subsequently, Park and colleagues [32] arrived at a similar conclusion.

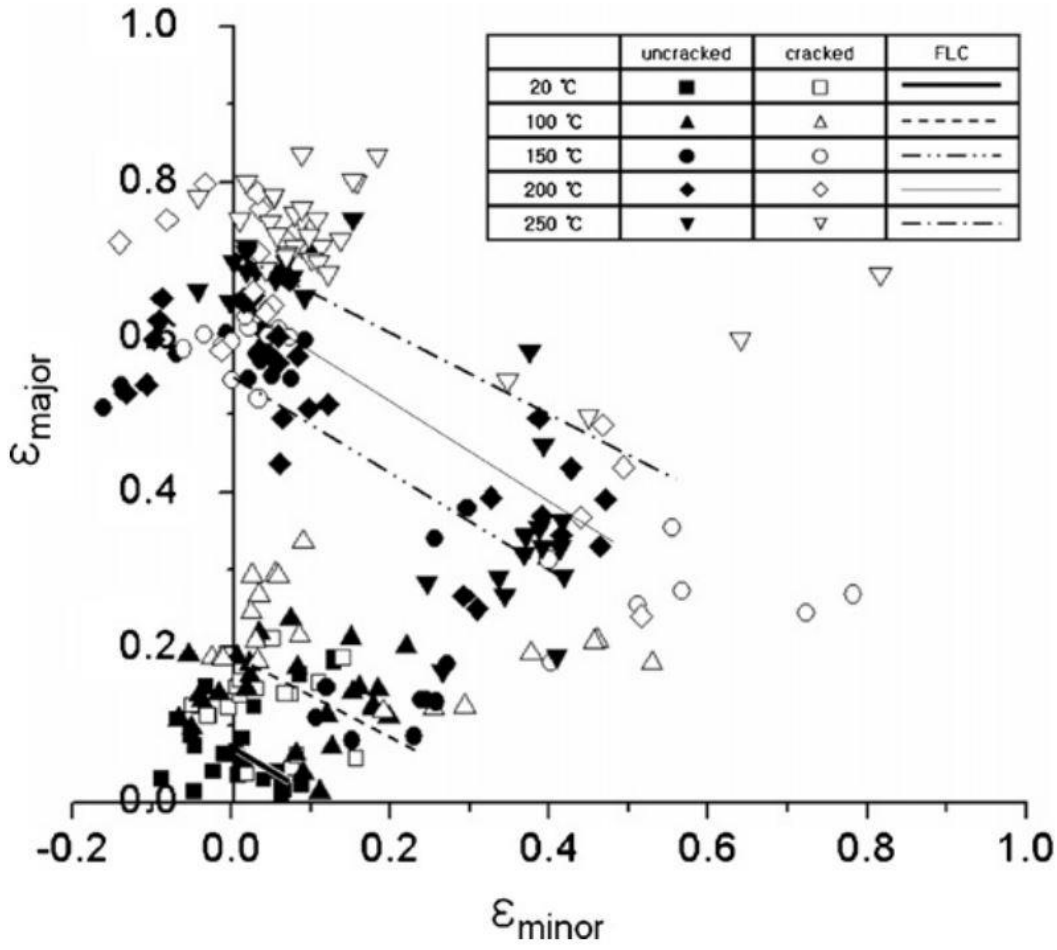

Figure 2-37 FLC of magnesium alloy AZ31sheet at various temperatures [32].

Jeswiet and colleagues [2] proposed a forming limit diagram as a means of predicting the formability of various complex designs. The study conducted by Malwad and colleagues [103] aimed to investigate the impact of wall angle, step size, and tool diameter on formability through experimental methods. Formability analysis was conducted on AA8011 utilising conical shapes featuring varying wall angles of 55º, 65º, and 75º. Subsequently, a multistage examination was conducted to evaluate the maximum achievable forming wall angle as a function of depth, utilising a continuous variation of wall angle ranging from 35º to 90º. The experimental findings indicate that a reduction in thickness was achievable when the wall angle was large. However, a consistent distribution of thickness along the wall was observed for

angles less than 65º. When the wall angle was increased, stretching became a more significant factor than shearing. For lesser wall angles, shearing was the primary cause of deformation. Finally, cone formation reached the desired depth without fracture using constant wall angle forms. However, the utilisation of multistage tests with variable wall angles resulted in an earlier occurrence of fracture compared to the utilisation of constant wall angle shapes.

2.8.3 Formability and experimental parameters

Various parameters can impact the formability of Single Point Incremental Forming (SPIF). Jeswiet and colleagues [98] conducted a study to examine the impact of sheet thickness on the formability of aluminum sheet while keeping other parameters constant. The results indicated a linear increase in formability with increasing sheet thickness. Hirt and colleagues [101] also found this to be true for DCO4 steel sheets.

Park and colleagues [104] conducted a study on the formability of a material, examining the impact of four distinct parameters: tool size, step size, tool type, friction at the sheet/tool interface, and plane anisotropy of the sheet component. The reported results are as follows: Utilisation of a ball-shaped tool instead of a spherical tool is advantageous for modifying formability. Large values of step size and tool size are not recommended for achieving favorable formability. A minimal amount of friction is conducive to reducing the stress state and positively impacting the formability. Conversely, excessive friction can lead to sheet and tool wear and a consequent reduction in formability. Additionally, Micari and colleagues [105] conducted a study on the impact of tool size and step size and found that an increase in these two factors leads to a decrease in formability. Hirt and colleagues [106] performed a finite element analysis (FEA) to investigate the impact of step size on formability, and confirmed this finding. The study demonstrated that enhanced formability can be attributed to a decrease in step size, resulting in a reduction in the mean stress level within the component's wall.

According to Jeswiet and colleagues [2] , formability is negatively affected by an increase in forming speed in a linear scenario. It has been discovered that an increase in spindle speed has a beneficial impact on formability due to the corresponding rise in heat at the point of contact between the sheet and tool.

2.8.4 Effect of bending and springback

The occurrence of material springback is common in all sheet metal forming procedures, which results in inaccurate geometry of the final shape. In Incremental Sheet Forming (ISF), three different types of springback have been identified. The first type is continuous local springback, which happens along with the tool's displacement. The second type is global springback that occurs after the loads are removed and disconnected from clamps. The third type occurs after any trimming has been performed [2].

The magnitude of springback in the SPIF process is influenced by various factors such as sheet thickness, feed rate, spindle speed, tool size, step size, and residual stresses. Mehdi and colleagues [107] examined springback and its effect on the geometrical and dimensional accuracy of ISF technology. They established an analytical model to determine the optimum process parameters for minimised springback. The study revealed that an increase in tool diameter, feed rate, spindle speed, and sheet thickness, coupled with a decrease in vertical step size, individually contribute to the reduction of springback.

2.8.5 Summary of forming limits

To summarise, the formability capacity in traditional single incremental point forming is limited by factors such as tool diameter, wall angle, step size, and feed rate. All of which are associated with the solid and roller-ball tools. The thinning ratio is influenced by the forming angle, which in turn is influenced by the step size. Furthermore, springback is affected by

factors such as tool diameter, feed rate, spindle speed, sheet thickness, and vertical step. The findings suggest that reducing springback can be achieved by increasing the tool diameter, feed rate, spindle speed, and sheet thickness while simultaneously reducing the vertical step size.

However, the absence of conventional mechanical forming tools has the potential to overcome these limitations and enhance material formability. Contact-less forming tools can facilitate the formation of complex shapes and reduce the occurrence of springback while achieving high levels of deformation due to the heat present during the forming process.

2.9 Characterisation techniques in ISF

Empirical insights into the process of ISF can be obtained through experimental analysis methods, which offer advantages over numerical simulations in terms of accuracy. Empirical measurements have been conducted to analyse various process characteristics, including geometry, strains, tool force, thickness after forming, and surface finish. The results of these measurements are then documented as follows.

2.9.1 Dimensions and geometries measurement methodologies

The geometric measurements and accuracy of sheets produced by incremental sheet forming (ISF) have been evaluated at various stages of the forming process (during and after), including in-machine measurements of mounted sheets. In the field of ISF, three primary techniques have been employed for measuring geometry and geometric precision: coordinate measuring machines (CMMs), laser scanners, and 3D stereovision systems.

Coordinate measuring machines (CMMs) are commonly used to obtain measurements of the geometry of sheets produced by incremental sheet forming after they have been removed from the machine. These machines are widely accessible in various engineering workshops. Meier

and colleagues [108] utilised a CMM to measure diverse frustums of pyramids, while Hirt and colleagues [109] used the same equipment to measure cross-sectional areas for comparison with a Finite Element (FEM) model. However, this method is laborious, time-consuming, cannot be used for in-machine sheet measurements (before springback due to clamp removal). Additionally, manual positioning of the stylus can lead to inaccuracies.

Laser scanners and stereovision systems are more suitable for fast measurement of complete three-dimensional surfaces and can be used while the sheet remains in the machine. Laser scanners can determine the geometry of a sheet by scanning across its surface. Duflou and colleagues [110] and Ambrogio and colleagues [111] employed laser scanning techniques to measure the accuracy of formed sheets. Duflou and colleagues [110] reported an accuracy of ±15µm, while Ambrogio and colleagues [111] used a Minolta Vivid 300 laser scanner to achieve precise measurements of formed sheets after their removal from the machine. To prevent high reflectance, a non-reflective surface, such as varnish, is applied to sheets that have been measured by a laser scanner.

In comparison to a laser scanner, stereovision systems capture the complete surface area in a single imaging process without the need for scanning. Strain determination involves comparing a surface pattern's current position with a pattern from a previous time, measured using calibrated CCD cameras. Hirt and colleagues [109] utilised the ARAMIS stereovision system, while Watzeels and colleagues [112] employed the LIMESS system. Stereovision systems provide quick and precise 3D measurements of sheet surface deformation. However, a potential issue arises when the sheet surface is partially obstructed during machine mounting, resulting in incomplete surface measurement. Additionally, the painted patterns necessary for optical systems may be eliminated during the forming process, and the analysis of three-dimensional images may require several seconds. In general, 3D stereovision systems provide an easy way

to measure sheet surface deformation. However, their utilisation is mainly restricted by cost and accessibility limitations.

Measuring the thickness of a sheet in ISF presents challenges due to the need for accurate measurements on opposing surfaces. Typically, scanners or CMM can only access one side, making it difficult to achieve rapid and automated measurements. The micrometre can be utilised to manually measure the thickness at specific points on a cut cross-section of the sheet with an accuracy up to 0.001mm, as demonstrated by Bambach and colleagues [113]. Ambrogio and colleagues [114] employed a CMM to determine the positions of points located on opposing sides of the sheet, which allowed the calculation of sheet thickness.

2.9.2 Strains measurement methodologies

In the field of Incremental Sheet Forming (ISF), three distinct techniques have been utilised for the purpose of measuring surface strains on the sheet. These methods include the use of strain gauges, surface grid measurement, and the implementation of stereovision systems.

The utilisation of strain gauges has been observed by Kitazawa and colleagues [115] to measure the change in strains at specific locations on the sheet surface during the forming procedure. Nevertheless, these methods are constrained by challenges such as complicated attachment procedures, restricted capacity to gauge strain across a limited surface area at different spots, and exposure to failure when subjected to high strains.

A common and alternative approach for measuring strains throughout the entire surface of a sheet after forming involves comparing the dimensions of a circular grid attached to the surface prior to forming with those after forming. In order to prevent grid damage, it is necessary to apply the grid pattern to the surface that is not in contact with the tool for all of the techniques

mentioned above. According to Jeswiet and colleagues research [116] , the implementation of etching as a method for applying the grid may lead to a reduction in forming limits due to the creation of stress concentrations. As a result, printing techniques may be a more ideal choice.

The determination of major and minor surface strains was carried out through the measurement of the major and minor diameters of deformed ellipses of the grid after its forming. This was achieved using either a transparent measuring string (Lamminen and colleagues [117]) or a toolmaker's microscope (Kitazawa and colleagues [115]). The maximum and minimum strains were then calculated based on the obtained measurements. Regardless, one of the drawbacks of the grid-based technique with circles is that the strain route cannot be determined.

On the other hand, an optical system, as explained earlier, can be utilised for the purpose of measuring displacement, allowing for quick calculation of strains across the sheet's surface during the entire process. Sainz and colleagues [118] assessed the strain on polycarbonate specimens deformed by SPIF using the offline automated 3D deformation digital measurement system ARGUS®, which relies on a circle grid. This approach utilizes photogrammetry, or remote sensing, to calculate three-dimensional geometry from a series of two-dimensional images.

Grid-based methods are presently the most frequently employed approach for measuring surface strains in ISF due to their simplicity, affordability, and suitability for the entire surface. Nonetheless, when it comes to strain analysis, optical systems provide the fastest results but are a costly alternative.

2.9.3 Tool force measurement methodologies

In the context of Incremental Sheet Forming (ISF), three distinct methodologies have been employed for the measurement of tool force. These include the utilisation of a force dynamometer for the measurement of reaction forces on the workpiece support, the use of strain gauges for the measurement of forces on the tool post, and the measurement of reaction forces on the workpiece support with load cells.

Duflou and colleagues [119, 120] measured reactions on the workpiece support using a Kistler 9265B six component table force dynamometer, which demonstrated high repeatability, as shown in **Figure 2-33**. Additionally, Bologa and colleagues [121] employed a force dynamometric table to quantify forces along two axes. However, one drawback of the force dynamometer is that it has not been utilised to measure tool force simultaneously with tool position. Consequently, it remains difficult to identify the tool force components with respect to the tool's immediate direction, and only the tool forces within a fixed coordinate system are determined.

As a substitute, Jeswiet and colleagues [122] conducted measurements of tool force using strain gauges located on the tool post. Since then, this method has not gained widespread adoption due to its associated drawback of poor accuracy. The reason for this is that horizontal force components are calculated using bending moments with a small bending arm, which leads to imprecise results.

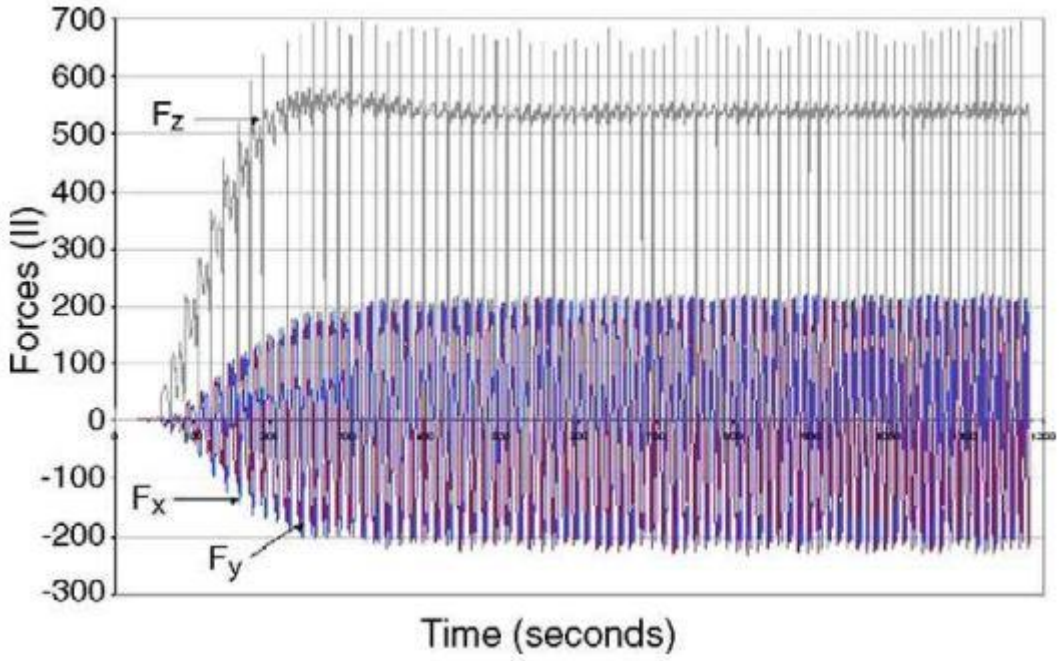

Figure 2-38 Using a dynamometer, three force components (Fx, Fy, and Fz) were measured [120].

To overcome these constraints, the ISF apparatus located at Cambridge University is the only specialized mechanism that includes an integrated system enabling the simultaneous assessment of tool force and tool position. Allwood and colleagues [123] placed the workpiece frame on six load cells to measure forces in three dimensions in real-time.

2.9.4 Surface roughness measurement methodologies

Various methodologies are utilised to measure surface roughness in Incremental Sheet Forming (ISF). These methods are crucial for assessing the quality and precision of formed parts. Two main techniques are used to evaluate the surface roughness in ISF.

One technique is Contact Profilometry, which involves using instruments like stylus profilometers or atomic force microscopes (AFM) to physically scan the surface with a mechanical probe or sharp tip. It measures parameters such as average roughness (Ra),

maximum height of the profile (Rz), and root mean square roughness (Rq). Abd Ali and colleagues [124] utilised a Mitutoyo SJ-410 (Kawasaki, Japan) roughness tester with accuracy resolution of 0.001µm at a measurement range of 80µm to assess the surface quality of bimetal parts by measuring the average surface roughness (Ra), as shown in **Figure 2-33**. Another study by Murugesan and colleagues [125] employed Mitutoyo Surface test SJ-400 surface roughness tester to investigate the surface finish of AA3003-H18 Al sheets using different parameters of tool radius, step-size, and feed rate. Moreover, Kilani and colleagues [126] used DIAVITE DH-7 tester for measuring the surface roughness of aluminium sheet with accuracy of measuring range up to 19.99 µm. As seen in **Figure 2-33**, in accordance with the ISO4287 standard, three categories of roughness measurements were conducted. The first is the arithmetic mean roughness value Ra, the second is the total roughness profile height Rt, and the third is the average roughness depth Rz. However, this method has drawbacks such as being very sensitive to vibrations and the stylus can potentially leaving marks on the surface of the part.

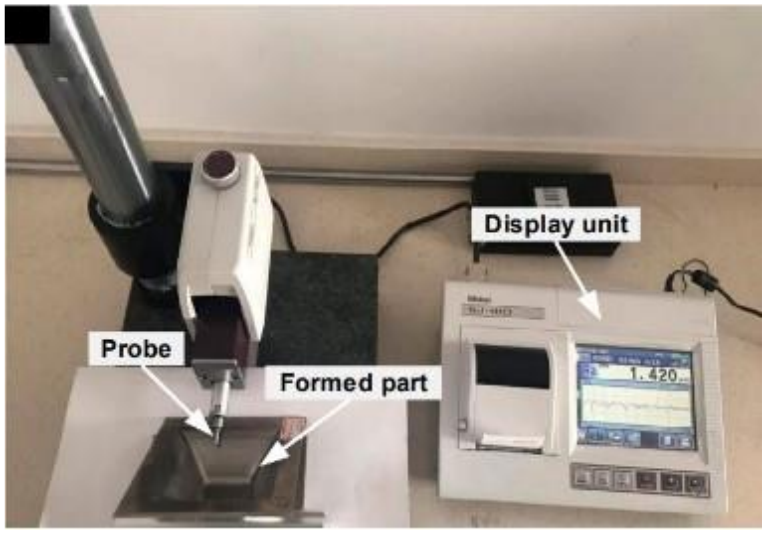

Figure 2-39 Surface roughness measurement by Mitutoyo SJ-410 [124].

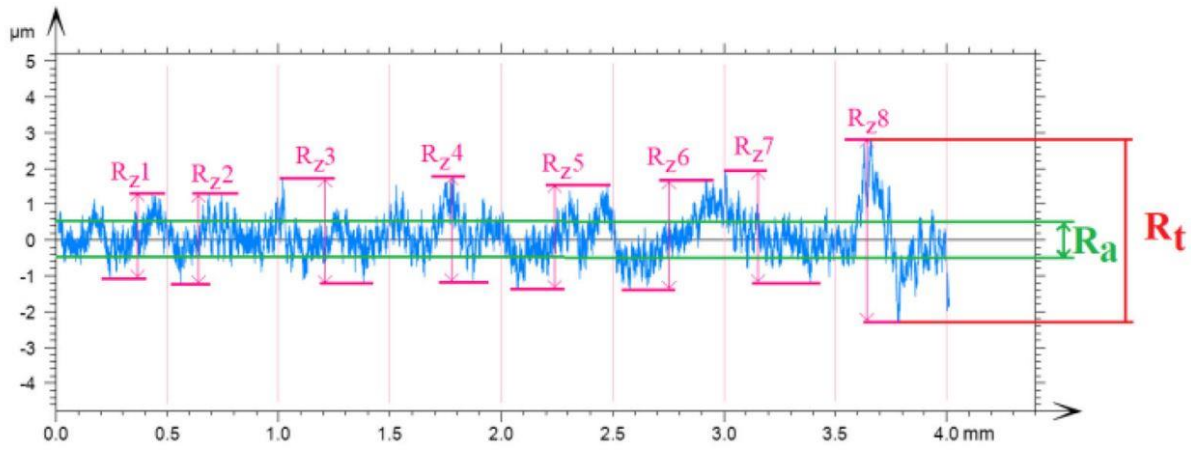

Figure 2-40 Profilometer indication of surface roughness [126].

Conversely, non-contact profilometry is an alternative methodology utilised for gauging surface roughness. This technique utilises interference patterns to evaluate surface height fluctuations and includes methods such as white light interferometry and coherence scanning interferometry. Hagan and colleagues [127] have accurately measured surface roughness using white light interferometry across various process conditions with accuracy from 3 µm to 40 nm. Li and colleagues [82] employed the Alicona Infinite Focus, a precise optical 3D surface measurement system, to assess the surface roughness of Ti-6Al-4V alloy sheets in their original and deformed states and subsequently conducted a comparative analysis.

As a result, it is crucial to select an appropriate methodology based on the specific requirements of the ISF process and the desired accuracy of surface roughness measurement.

2.9.5 Summary of characterisation techniques in ISF

To summarise, when it comes to measuring geometries, commonly used methods include coordinate measuring machines (CMMs), laser scanners, and 3D stereovision systems. Among these methods, CMMs are the most widely used due to their ease of use and availability. They are commonly employed for measuring geometrical accuracy and can also be helpful in

measuring the thickness of the sheet from the opposite direction.

In terms of strain measurement, grid-based methods are the most commonly used in SPIF processes. These methods are affordable and suitable for transparent materials.

For measuring tool force, dynamometers, strain gauge sensors, and load cells are used. However, strain gauge sensors are the most commonly utilised method. These sensors are attached to the tool and provide real-time feedback on the applied force.

Regarding measuring surface roughness, there are two main techniques: contact profilometry using the Mitutoyo SJ-410 and non-contact profilometry using the Alicona. The most commonly used method is contact profilometry, as it is less costly and easier to access.

Overall, there are various methods and tools available to measure different aspects of geometrics, strain, tool force, and surface roughness in manufacturing processes. The choice of method depends on the specific requirements of the application and the available resources.

2.10 Summary

Based on the above literature review, several aspects of ISF processes have been covered, including the types of ISF processes, materials used, heating strategies, tool design, lubrication and coating techniques, numerical modeling, formability, and commonly used characterisation procedures. However, key gaps in the literature that still exist are the following:

1. The use of TPIF is limited to configurations involving two movable indenters. It requires specialised tooling and partial die or support techniques, making it less flexible.

2. Conventional SPIF has limitations in terms of material thickness and deformation

capabilities due to the solid tool used. The tool's shape, size, and type restrict formability and effect the probability of defects occurring.

3. Conventional SPIF negatively effects surface quality due to friction from the solid tool (dents, scratches, or distortions).

4. Lubricants and coatings can reduce friction but not eliminate it completely. Their effectiveness varies depending on the material and SPIF process used. Additionally, they can lead to material contamination and incur extra costs for procurement and cleaning. Some lubricants and coatings may also contain harmful chemicals that can have adverse effects on the environment, making it necessary to prioritise environmentally friendly options.

5. The water jet tool is expensive to acquire and operate. It is a wet process with reduced precision, lacks environmental sustainability, and requires additional safety precautions. Moreover, it can be challenging to deform low-strength materials and thin sheets due to the high-force impact of the water jet, which may result in damage or surface imperfections such as dents, scratches, or distortions.

6. Compared to metals, polymers generally have lower formability due to their increased brittleness and lower melting points. These characteristics limit the use of conventional forming techniques for shaping polymers.

7. Therefore, it is crucial to consider a novel concept that can effectively address the limitations of traditional equipment. This concept should offer reduced risks compared to water jet technology, lower costs, environment-friendly, enhanced precision, elimination of defects on the sheet material, improved formability, eliminating extra

steps (lubrication or cleaning), and enhanced surface finish.

2.11 References

1. Behera, A.K., B. Lu, and H. Ou, Characterization of shape and dimensional accuracy of incrementally formed titanium sheet parts with intermediate curvatures between two feature types. The International Journal of Advanced Manufacturing Technology, 2016. 83: p. 1099-1111.

2. Jeswiet, J., et al., Asymmetric single point incremental forming of sheet metal. CIRP annals, 2005. 54(2): p. 88-114.

3. Behera, A.K., B. Lu, and H. Ou, Characterization of shape and dimensional accuracy of incrementally formed titanium sheet parts. 2015.

4. Ham, M. and J. Jeswiet, Single point incremental forming and the forming criteria for AA3003. CIRP annals, 2006. 55(1): p. 241-244.

5. Strano, M., Technological representation of forming limits for negative incremental forming of thin aluminum sheets. Journal of manufacturing processes, 2005. 7(2): p. 122-129.

6. Leonhardt, A., et al., Experimental study on incremental sheet forming of magnesium alloy AZ31 with hot air heating. Procedia Manufacturing, 2018. 15: p. 1192-1199.

7. Honarpisheh, M., M. Abdolhoseini, and S. Amini, Experimental and numerical investigation of the hot incremental forming of Ti-6Al-4V sheet using electrical current. The International Journal of Advanced Manufacturing Technology, 2016. 83: p. 2027-2037.

8. Göttmann, A., et al., A novel approach for temperature control in ISF supported by laser and resistance heating. The International Journal of Advanced Manufacturing Technology, 2013. 67(9-12): p. 2195-2205.

9. Ambrogio, G., et al., Induction heating and cryogenic cooling in single point incremental forming of Ti-6Al-4V: process setup and evolution of microstructure and mechanical properties. The International Journal of Advanced Manufacturing Technology, 2017. 91: p. 803-812.

10. Davarpanah, M.A., et al., Effects of incremental depth and tool rotation on failure modes and microstructural properties in Single Point Incremental Forming of polymers. Journal of materials processing technology, 2015. 222: p. 287-300.

11. Silva, M., L. Alves, and P. Martins, Single point incremental forming of PVC: Experimental findings and theoretical interpretation. European journal of mechanics-A/Solids, 2010. 29(4): p. 557-566.

12. Franzen, V., et al., Single point incremental forming of PVC. Journal of Materials Processing Technology, 2009. 209(1): p. 462-469.

13. Martins, P.A.F., et al., Single point incremental forming of polymers. CIRP Annals, 2009. 58(1): p. 229-232.

14. Panjwani, D., et al., A novel approach based on flexible supports for forming non-axisymmetric parts in SPISF. The International Journal of Advanced Manufacturing Technology, 2017. 92: p. 2463-2477.

15. Sousa, R., Incremental sheet forming technologies. Reference module in materials

science and materials engineering. 2016, Elsevier, Amsterdam. https://doi. org/10.1016/B978-0-12-803581-8.04055-8.

16. Lu, B., et al., Mechanism investigation of friction-related effects in single point incremental forming using a developed oblique roller-ball tool. International Journal of Machine Tools and Manufacture, 2014. 85: p. 14-29.

17. Al-Obaidi, A., V. Kräusel, and D. Landgrebe, Hot single-point incremental forming assisted by induction heating. The International Journal of Advanced Manufacturing Technology, 2016. 82(5-8): p. 1163-1171.

18. Azevedo, N.G., et al., Lubrication aspects during single point incremental forming for steel and aluminum materials. International Journal of precision engineering and manufacturing, 2015. 16(3): p. 589-595.

19. Silva, M. and P. Martins, Two-point incremental forming with partial die: theory and experimentation. Journal of Materials Engineering and Performance, 2013. 22: p. 1018-1027.

20. Jackson, K. and J. Allwood, The mechanics of incremental sheet forming. Journal of materials processing technology, 2009. 209(3): p. 1158-1174.

21. Matsubara, S., Computer numerical control incremental forming. Journal Japan Society Technology of Plasticity, 1994: p. 35(406): pp. 1258-1263. .

22. Hirt, G., J. Ames, and M. Bambach, Validation of FEA for asymmetric incremental sheet forming by on-line measurements of deformation and tool forces. Prod. Engng, 2006. 13(1): p. 39-44.

23. Ceretti, E., C. Giardini, and A. Attanasio, Experimental and simulative results in sheet incremental forming on CNC machines. Journal of Materials Processing Technology, 2004. 152(2): p. 176-184.

24. Giardini, C., et al. Analysis of the influence of working parameters on final part quality in sheet incremental forming. in PROCEEDING OF THE 3RD INTERNATIONAL CONFERENCE AND EXHIBITION ON DESIGN AND PRODUCTION OF DIES AND MOLDS 2004. 2004. M. Akkok, B. Kaftanoglu, J. Tamaki, T Kuriyagawa, MAS Arikan, T. Balkan.

25. Yoshikawa, T. A study on incremental sheet metal bulging using pair of upper and lower tools. in Spring conference on technology of Plasticity. 1999.

26. Meier, H., et al. Two point incremental forming with two moving forming tools. in Key Engineering Materials. 2007. Trans Tech Publ.

27. Maidagan, E., et al. A new incremental sheet forming process based on a flexible supporting die system. in Key Engineering Materials. 2007. Trans Tech Publ.

28. Bagudanch, I., M. Sabater, and M.L. Garcia-Romeu, Single point versus two point incremental forming of thermoplastic materials. Advances in materials and processing technologies, 2017. 3(1): p. 135-144.

29. Mostafanezhad, H., et al., Optimization of two-point incremental forming process of AA1050 through response surface methodology. Measurement, 2018. 127: p. 21-28.

30. Attanasio, A., et al., Asymmetric two points incremental forming: improving surface quality and geometric accuracy by tool path optimization. Journal of materials

processing technology, 2008. 197(1-3): p. 59-67.

31. Ambrogio, G., L. Filice, and F. Gagliardi, Formability of lightweight alloys by hot incremental sheet forming. Materials & Design, 2012. 34: p. 501-508.

32. Ji, Y. and J. Park, Formability of magnesium AZ31 sheet in the incremental forming at warm temperature. Journal of materials processing technology, 2008. 201(1-3): p. 354-358.

33. Dabwan, A., et al., Study of the effect of process parameters on surface profile accuracy in single-point incremental sheet forming of AA1050-H14 aluminum alloy. Advances in Materials Science and Engineering, 2020. 2020.

34. Torsakul, S. and N. Kuptasthien, Effects of three parameters on forming force of the single point incremental forming process. Journal of Mechanical Science and Technology, 2019. 33(6): p. 1-7.

35. Tanaka, S., Incremental sheet metal forming process for pure titanium denture plate. Proc. 8th ICTP, 2005, 2005.

36. Hussain, G., L. Gao, and N. Hayat, Empirical modelling of the influence of operating parameters on the spifability of a titanium sheet using response surface methodology. Proceedings of the Institution of Mechanical Engineers, Part B: Journal of Engineering Manufacture, 2009. 223(1): p. 73-81.

37. Li, W., M.M. Attallah, and K. Essa, Experimental and numerical investigations on the process quality and microstructure during induction heating assisted incremental forming of Ti-6Al-4V sheet. Journal of Materials Processing Technology, 2022. 299:

p. 117323.

38. Jackson, K., J. Allwood, and M. Landert, Incremental forming of sandwich panels. Journal of Materials Processing Technology, 2008. 204(1-3): p. 290-303.

39. Abd Ali, R., et al., Formability and failure analyses of Al/SUS bilayer sheet in single point incremental forming. The International Journal of Advanced Manufacturing Technology, 2019. 105(7): p. 2785-2798.

40. Al-Obaidi, A., A. Kunke, and V. Kräusel, Hot single-point incremental forming of glass-fiber-reinforced polymer (PA6GF47) supported by hot air. Journal of Manufacturing Processes, 2019. 43: p. 17-25.

41. Gordon, J., M.J. Gordon Jr, and M.J. Gordon, Industrial design of plastics products. 2003: Wiley-Interscience.

42. Kyriacos, D. Chapter 17 – Polycarbonates. 2017.

43. Buffa, G., D. Campanella, and L. Fratini, On the improvement of material formability in SPIF operation through tool stirring action. The International Journal of Advanced Manufacturing Technology, 2013. 66(9-12): p. 1343-1351.

44. Liu, Z., Friction stir incremental forming of AA7075-O sheets: investigation on process feasibility. Procedia Engineering, 2017. 207: p. 783-788.

45. Le, V., A. Ghiotti, and G. Lucchetta, Preliminary studies on single point incremental forming for thermoplastic materials. International Journal of Material Forming, 2008. 1(1): p. 1179-1182.

46. Jimma, T., et al., An application of ultrasonic vibration to the deep drawing process. Journal of Materials Processing Technology, 1998. 80: p. 406-412.

47. Murakawa, M. and M. Jin, The utility of radially and ultrasonically vibrated dies in the wire drawing process. Journal of Materials Processing Technology, 2001. 113(1-3): p. 81-86.

48. Baghlani, V., et al., Ultrasonic assisted deep drilling of Inconel 738LC superalloy. Procedia Cirp, 2013. 6: p. 571-576.

49. Shen, X.-H., et al., A study of surface roughness variation in ultrasonic vibration-assisted milling. The International Journal of Advanced Manufacturing Technology, 2012. 58: p. 553-561.

50. Mousavi, S.A., H. Feizi, and R. Madoliat, Investigations on the effects of ultrasonic vibrations in the extrusion process. Journal of materials processing technology, 2007. 187: p. 657-661.

51. Bagudanch, I., et al., Forming force and temperature effects on single point incremental forming of polyvinylchloride. Journal of materials processing technology, 2015. 219: p. 221-229.

52. Sakhtemanian, M., M. Honarpisheh, and S. Amini, A novel material modeling technique in the single-point incremental forming assisted by the ultrasonic vibration of low carbon steel/commercially pure titanium bimetal sheet. The International Journal of Advanced Manufacturing Technology, 2019. 102: p. 473-486.

53. Cheng, R., et al., Applying ultrasonic vibration during single-point and two-point

incremental sheet forming. Procedia Manufacturing, 2019. 34: p. 186-192.

54. Sun, Y., et al., Study on the springback effect and surface property for ultrasonic-assisted incremental sheet forming of aluminum alloy. Symmetry, 2021. 13(7): p. 1217.

55. Cheng, Z., et al., Ultrasonic assisted incremental sheet forming: Constitutive modeling and deformation analysis. Journal of Materials Processing Technology, 2022. 299: p. 117365.

56. Liao, J., S. Zhou, and X. Xue, Twist springback and microstructure analysis of PEEK sheets in ultrasonic-assisted thermal incremental forming. The International Journal of Advanced Manufacturing Technology, 2022. 121(7-8): p. 5269-5282.

57. Li, Z., et al., Electric assistance hot incremental sheet forming: an integral heating design. The International Journal of Advanced Manufacturing Technology, 2018. 96: p. 3209-3215.

58. Magnus, C.S., Joule heating of the forming zone in incremental sheet metal forming: part 1: state of the art and thermal process modelling. The International Journal of Advanced Manufacturing Technology, 2017. 91: p. 1309-1319.

59. Min, J., et al., Thermal modeling in electricity assisted incremental sheet forming. International Journal of Material Forming, 2017. 10: p. 729-739.

60. Fan, G., et al., Electric hot incremental forming: A novel technique. International Journal of Machine Tools and Manufacture, 2008. 48(15): p. 1688-1692.

61. Xu, D., et al., A comparative study on process potentials for frictional stir-and electric

hot-assisted incremental sheet forming. Procedia Engineering, 2014. 81: p. 2324-2329.

62. Meier, H. and C. Magnus. Incremental sheet metal forming with direct resistance heating using two moving tools. in Key Engineering Materials. 2013. Trans Tech Publ.

63. Möllensiep, D., et al., Regression-based compensation of part inaccuracies in incremental sheet forming at elevated temperatures. The International Journal of Advanced Manufacturing Technology, 2020. 109: p. 1917-1928.

64. Ao, D., et al., Formability and deformation mechanism of Ti-6Al-4V sheet under electropulsing assisted incremental forming. International Journal of Solids and Structures, 2020. 202: p. 357-367.

65. Shi, X., et al., Electric hot incremental forming of low carbon steel sheet: accuracy improvement. The International Journal of Advanced Manufacturing Technology, 2013. 68: p. 241-247.

66. Duflou, J., et al., Laser assisted incremental forming: formability and accuracy improvement. CIRP annals, 2007. 56(1): p. 273-276.

67. Lehtinen, P., T. Väisänen, and M. Salmi, The effect of local heating by laser irradiation for aluminum, deep drawing steel and copper sheets in incremental sheet forming. Physics Procedia, 2015. 78: p. 312-319.

68. Göttmann, A., et al., Laser-assisted asymmetric incremental sheet forming of titanium sheet metal parts. Production Engineering, 2011. 5: p. 263-271.

69. Göttmann, A., et al., Laser-assisted asymmetric incremental sheet forming of titanium

sheet metal parts. Production Engineering, 2011. 5(3): p. 263-271.

70. Al-Obaidi, A., V. Kräusel, and D. Landgrebe, Induction heating validation of dieless single-point incremental forming of AHSS. Journal of Manufacturing and Materials Processing, 2017. 1(1): p. 5.

71. Vahdani, M., et al., Electric hot incremental sheet forming of Ti-6Al-4V titanium, AA6061 aluminum, and DC01 steel sheets. The International Journal of Advanced Manufacturing Technology, 2019. 103: p. 1199-1209.

72. Li, W., K. Essa, and S. Li, A novel tool to enhance the lubricant efficiency on induction heat-assisted incremental sheet forming of Ti-6Al-4 V sheets. The International Journal of Advanced Manufacturing Technology, 2022. 120(11-12): p. 8239-8257.

73. Grün, P., et al., Formability of titanium alloy sheets by friction stir incremental forming. The International Journal of Advanced Manufacturing Technology, 2018. 99: p. 1993-2003.

74. McAnulty, T. and P. Gupta, J. Jeswiet, D. Adams, M. Doolan. Adv. Manuf, 2015. 3: p. 253-262.

75. Kumar, A., et al., Parametric effects on formability of AA2024-O aluminum alloy sheets in single point incremental forming. Journal of Materials Research and Technology, 2019. 8(1): p. 1461-1469.

76. Shim, M.-S. and J.-J. Park, The formability of aluminum sheet in incremental forming. Journal of Materials Processing Technology, 2001. 113(1-3): p. 654-658.

77. Jurisevic, B., K. Kuzman, and M. Junkar, Water jetting technology: an alternative in incremental sheet metal forming. The International Journal of Advanced Manufacturing Technology, 2006. 31(1-2): p. 18-23.

78. Petek, A., et al., Comparison of alternative approaches of single point incremental forming processes. Journal of materials processing technology, 2009. 209(4): p. 1810-1815.

79. Sornsuwit, N. and S. Sittisakuljaroen. The effect of lubricants and material properties in surface roughness and formability for single point incremental forming process. in Advanced Materials Research. 2014. Trans Tech Publ.

80. Hussain, G., et al., Tool and lubrication for negative incremental forming of a commercially pure titanium sheet. Journal of materials processing technology, 2008. 203(1-3): p. 193-201.

81. Li, W., M. Attallah, and K. Essa, Experimental and numerical investigations on the process quality and microstructure during induction heating assisted increment forming of Ti-6Al-4V sheet. Journal of Materials Processing Technology, 2021. 299: p. 117323.

82. Li, Z., et al., A novel current-carrying lubrication in electric hot incremental forming of Ti–6Al–4V titanium sheet. Journal of the Brazilian Society of Mechanical Sciences and Engineering, 2022. 44(5): p. 216.

83. Liu, R., et al., Development of novel tools for electricity-assisted incremental sheet forming of titanium alloy. The International Journal of Advanced Manufacturing Technology, 2016. 85: p. 1137-1144.

84. Fan, G., et al., Electric hot incremental forming of Ti-6Al-4V titanium sheet. The International Journal of Advanced Manufacturing Technology, 2010. 49(9): p. 941-947.

85. Hussain, G., A. Mahna, and A. Iqbal, Response surface analysis of cold formability of polymers in incremental sheet forming: effect of parameters and associated thermal softening. International Journal of Precision Engineering and Manufacturing, 2016. 17: p. 613-621.

86. Silva, M.B. and P.A.F. Martins, 3.02 - Incremental Sheet Forming, in Comprehensive Materials Processing, S. Hashmi, et al., Editors. 2014, Elsevier: Oxford. p. 7-26.

87. Durgun, I., et al., Simulation for Incremental Sheet Forming Process: a Comparison of Implicit and Explicit Finite Element Analysis with Experimental Data. 2013.

88. Yamashita, M., M. Gotoh, and S.-Y. Atsumi, Numerical simulation of incremental forming of sheet metal. Journal of materials processing technology, 2008. 199(1-3): p. 163-172.

89. Kulkarni, S.S. and G.M. Mocko, A finite element simulation model of convective heat-assisted single-point incremental forming of thermoplastics. The International Journal of Advanced Manufacturing Technology, 2020. 111(11): p. 3305-3317.

90. Kulkarni, S.S. and G.M. Mocko, Experimental investigation and finite element modeling of localized heating in convective heat-assisted single-point incremental forming. The International Journal of Advanced Manufacturing Technology, 2020. 107: p. 945-957.

91. Lu, B., et al., A study of incremental sheet forming by using water jet. The International

Journal of Advanced Manufacturing Technology, 2017. 91(5): p. 2291-2301.

92. Esmaeilpour, R., et al., Calibration of Barlat Yld2004-18P yield function using CPFEM and 3D RVE for the simulation of single point incremental forming (SPIF) of 7075-O aluminum sheet. International Journal of Mechanical Sciences, 2018. 145: p. 24-41.

93. Esmaeilpour, R., et al., Experimental validation of the simulation of single-point incremental forming of AA7075 sheet with Yld2004-18P yield function calibrated with crystal plasticity model. The International Journal of Advanced Manufacturing Technology, 2021. 113: p. 2031-2047.

94. Groeber, M.A. and M.A. Jackson, DREAM.3D: A Digital Representation Environment for the Analysis of Microstructure in 3D. Integrating Materials and Manufacturing Innovation, 2014. 3(1): p. 56-72.

95. Chuan, W., Y. He, and L.H. Wei, Modeling of discontinuous dynamic recrystallization of a near-α titanium alloy IMI834 during isothermal hot compression by combining a cellular automaton model with a crystal plasticity finite element method. Computational materials science, 2013. 79: p. 944-959.

96. Li, W., et al., Crystal plasticity model of induction heating-assisted incremental sheet forming with recrystallisation simulation in cellular automata. The International Journal of Advanced Manufacturing Technology, 2022. 123(3-4): p. 903-925.

97. Niessen, F., et al., Parent grain reconstruction from partially or fully transformed microstructures in MTEX. Journal of Applied Crystallography, 2022. 55(1): p. 180-194.

98. Young, D. and J. Jeswiet, Wall thickness variations in single-point incremental forming. Proceedings of the Institution of Mechanical Engineers, Part B: Journal of Engineering Manufacture, 2004. 218(11): p. 1453-1459.

99. Wei, H., L. Gao, and S. Li. Investigation on thickness distribution along bulge type incrementally formed sheet metal part with irregular shapes. in Proceeding of the International Manufacturing Conference, Jinan, China. 2004.

100. Hussain, G., L. Gao, and N. Hayat, Forming parameters and forming defects in incremental forming of an aluminum sheet: correlation, empirical modeling, and optimization: part A. Materials and Manufacturing Processes, 2011. 26(12): p. 1546-1553.

101. Junk, S., G. Hirt, and I. Chouvalova. Forming strategies and tools in incremental sheet forming. in Proceedings of the 10th International Conference on Sheet Metal, Belfast. 2003.

102. Iseki, H., Forming limit of incremental sheet metal stretch forming using spherical rollers. J. Jpn. Soc. Technol. Plasticity, 1994. 35(406): p. 1336.

103. Malwad, D. and V. Nandedkar, Deformation mechanism analysis of single point incremental sheet metal forming. Procedia Materials Science, 2014. 6: p. 1505-1510.

104. Kim, Y. and J. Park, Effect of process parameters on formability in incremental forming of sheet metal. Journal of materials processing technology, 2002. 130: p. 42-46.

105. Filice, L., L. Fratini, and F. Micari, Analysis of material formability in incremental forming. CIRP Annals, 2002. 51(1): p. 199-202.

106. Hirt, G., et al., Forming strategies and process modelling for CNC incremental sheet forming. CIRP Annals, 2004. 53(1): p. 203-206.

107. Vahdati, M., M. Sedighi, and H. Khoshkish. An analytical model to reduce spring-back in incremental sheet metal forming (ISMF) process. in Advanced materials research. 2010. Trans Tech Publ.

108. Meier, H., O. Dewald, and J. Zhang. A new robot-based sheet metal forming process. in Advanced Materials Research. 2005. Trans Tech Publ.

109. Hirt, G., M. Bambach, and S. Junk. Modelling of the incremental CNC sheet metal forming process. in Proceedings of the 10th International Conference on Sheet Metal. 2003.

110. Duflou, J., et al. Achievable accuracy in single point incremental forming: case studies. in Proceedings of the 8th European Scientific Association for material Forming Conference on Material Forming. 2005.

111. Ambrogio, G., et al., Influence of some relevant process parameters on the dimensional accuracy in incremental forming: a numerical and experimental investigation. Journal of materials processing technology, 2004. 153: p. 501-507.

112. Watzeels, K., et al. Experimental validation of the finite element simulation of the first stroke in single point incremental forming. in 8th ESAFORM Conference on Material Forming. 2005. The publishing House of the Romanian Academy.

113. Bambach, M., et al. Initial experimental and numerical investigations into a class of new strategies for single point incremental sheet forming (SPIF). in Proc. Esaform.

2005.

114. Ambrogio, G., et al. Sheet thinning prediction in single point incremental forming. in Advanced materials research. 2005. Trans Tech Publ.

115. Kitazawa, K. Incremental sheet metal stretch-expanding with CNC machine tools. in Proc. 4th ICTP. 1993.

116. Jeswiet, J., D.J. Young, and M. Ham. Non-traditional forming limit diagrams for incremental forming. in Advanced Materials Research. 2005. Trans Tech Publ.

117. Lamminen, L. Incremental sheet forming with an industrial robot–forming limits and their effect on component design. in Advanced Materials Research. 2005. Trans Tech Publ.

118. Rosa-Sainz, A., et al., Experimental investigation of polycarbonate sheets deformed by SPIF: formability, micro-mechanisms of failure and temperature analysis. Journal of Materials Research and Technology, 2023. 25: p. 7546-7565.

119. Duflou, J.R., A. Szekeres, and P. Vanherck. Force measurements for single point incremental forming: an experimental study. in Advanced Materials Research. 2005. Trans Tech Publ.

120. Duflou, J., et al., Experimental study on force measurements for single point incremental forming. Journal of Materials Processing Technology, 2007. 189(1-3): p. 65-72.

121. Bologa, O., V. Oleksik, and G. Racz. Experimental research for determining the forces

on incremental sheet forming process. in 8th ESAFORM Conference. Cluj-Napoca, Romania. 2005.

122. Jeswiet, J., J.R. Duflou, and A. Szekeres. Forces in single point and two point incremental forming. in Advanced Materials Research. 2005. Trans Tech Publ.

123. Allwood, J., N. Houghton, and K. Jackson. The design of an incremental sheet forming machine. in Advanced Materials Research. 2005. Trans Tech Publ.

124. Abd Ali, R., et al., Experimental investigation and optimal prediction of maximum forming angle and surface roughness of an Al/SUS bimetal sheet in an incremental forming process using machine learning. Materials, 2019. 12(24): p. 4150.

125. Murugesan, M., et al., Investigation of Surface Roughness in Single Point Incremental Sheet Forming Considering Process Parameters. Int. J. Mech. Eng. Robot. Res, 2021. 10: p. 443-451.

126. Kilani, L., et al., Effects of rolling ball tool parameters on roughness, sheet thinning, and forming force generated during SPIF process. The International Journal of Advanced Manufacturing Technology, 2020. 106.

127. Hagan, E. and J. Jeswiet, Analysis of surface roughness for parts formed by computer numerical controlled incremental forming. Proceedings of the Institution of Mechanical Engineers, Part B: Journal of Engineering Manufacture, 2004. 218(10): p. 1307-1312.

3 Chapter Three: Hot-Air Contactless Single-Point Incremental Forming

Mohammad Almadani [a,b], Ahmet Guner [a], Hany Hassanin[c] , Khamis Essa [a]

[a] *Mechanical Engineering, University of Birmingham, Edgbaston, Birmingham, B15 2TT, UK*

[b] *Department of Mechanical Engineering Technology, Yanbu Industrial College, Yanbu Al-Sinaiyah City, 41912, Kingdom of Saudi Arabia.*

[c] *School of Engineering, Technology, and Design, Canterbury Christ Church University, B15 2TT, UK*

This research was published as a full-length research article in Journal of Manufacturing and Materials Processing:

Mohammad Almadani, Ahmet Guner, Hany Hassanin, and Khamis Essa, *Hot-Air Contactless Single-Point Incremental Forming*. Journal of Manufacturing and Materials Processing. 2023, 7, 179. http://doi.org/10.3390/jmmp7050179.

Credit authorship contribution statement

Mohammad Almadani: Conceptualisation, Investigation, Methodology, Validation, Formal analysis, Writing - original draft.

Ahmet Guner: Writing - review & editing, Resources of lab equipment, Supervision.

Hany Hassanin: Writing - review & editing, Resources of lab equipment, Supervision.

Khamis Essa: Writing - review & editing, Resources of lab equipment, Supervision, Project Administration**.**

Research contributions:

This chapter aims to complete the objective 1 and 2 which cover the following insights:

- A novel sheet forming process named Hot Air Contactless Single-Point Incremental Forming (HASPIF) is developed using a commercial 3D printer equipped with a hot air nozzle as a deforming tool.

- The HASPIF eliminates physical contact between the forming tool and the polymer sheet, reducing manufacturing costs and eliminating the need for a rigid tool.

- A case study was conducted using a polycarbonate (PC) sheet and a setup consisting of a nozzle, heating tube, heater, temperature controller, air compressor, and a computer numerical control system with a clamped frame.

- The HASPIF achieved high accuracy in deforming the PC sheet and outperformed the

traditional SPIF process and addresses both the quality of the workpieces and the challenges faced by solid tools due to wear from the forming process.

- The study's findings are significant in providing a solution to challenges in the traditional SPIF process and open a new direction in incremental sheet forming for polymers, composites, and metals.

3.1 Abstract

Single-point incremental forming (SPIF) has emerged as a time-efficient approach to manufacturing that offers increased material formability compared to conventional sheet-metal forming techniques. However, the physical interaction between the forming tool and the sheet poses challenges, such as tool wear and formability limits. This study introduces a novel sheet-forming technique called contactless single-point incremental forming (CSPIF), which uses hot compressed air as a deformation tool, eliminating the requirement for physical interaction between the sheet and a rigid forming tool. In this study, a polycarbonate sheet was chosen as the case-study material and subjected to the developed CSPIF. The experiments were carried out at an air temperature of 160 °C, air pressure of 1 bar, a nozzle speed of 750 mm/min, and a step-down of 0.75 mm. A Schlieren setup and a thermal camera were used to visualize the motion of the compressed hot air as it travelled from the nozzle to the sheet. The results showed that the CSPIF technique allowed for the precise shaping of the polycarbonate sheet with minimal springback. However, minor deviations from the designed profile were observed, primarily at the starting point of the nozzle, which can be attributed to the bending effects of the sample. In addition, the occurrence of sheet thinning and material buildup on the deformed workpiece was also observed. The average surface roughness (Ra) of the deformed workpiece was measured to be 0.2871 microns.

Keywords: contactless; polycarbonate; deformation behavior; formability

3.2 Introduction

In the past decade, the manufacturing industry has seen significant changes driven by the growing need for product customization and the integration of Industry 4.0 technologies. 3D printing, a key Industry 4.0 technology, has revolutionized work processes and increased the demand for advanced manufacturing techniques, especially for small-batch custom products. One crucial process for small to medium-sized customized sheet-material production is single-point incremental forming (SPIF) [1]. This cost-effective technology allows for the creation of highly customized shapes and components in a single step from metal sheets, without the need for dedicated dies. SPIF, utilizing computer numerically controlled (CNC) technology, offers high precision and accuracy, enabling the production of complex shapes with reduced lead time and low forming forces, resulting in high formability. These advantages align perfectly with the adaptable and flexible manufacturing processes required by Industry 4.0 [2].

Since its introduction in Matsubara labs in Japan by Leszak et al. [3], single point incremental forming (SPIF) has seen significant advancements and widespread adoption in various industries. Notably, it plays a crucial role in aerospace, where it achieves precision shaping of Ti–6Al–4V alloy [4, 5], in automotive manufacturing for customized parts from steel and aluminum alloys [6], and in the medical field for biomedical implant production [7]. SPIF, however, presents challenges, including elastic springback, which can compromise geometric precision and final component shape. Material thinning during sheet forming can also reduce product precision, but optimizing parameters like feed rate, tool path, and spindle speed can minimise defects, and improve geometry accuracy [8]. The use of edge stiffeners [9] and multistage incremental forming [10, 11] can further enhance precision. Another issue is poor surface finish, impacting aesthetics and mechanical properties due to the incremental nature of the process. Surface quality depends on factors such as spindle speed, forming tool radius,

vertical increment, and feeding rate. Taguchi methods can help optimise settings and identify key factors affecting surface roughness [12]. High tool wear is a significant limitation, caused by repeated tool-material contact, leading to increased costs due to frequent replacements. This is dependent on material properties such as hardness, sheet thicknesses, and the intricacy and dimensions of the parts. Extended use of tools may be required for larger parts, resulting in more frequent tool changes or maintenance. Reducing tool wear in SPIF involves adjusting sheet metal properties, optimizing process parameters, and using coolants and lubricants [13-15].

In SPIF research, the initial focus has been on metallic materials, but there is now growing interest in exploring other materials like polymers, thermoplastics, and composites. Shifting from metals to polymers shows promise for future SPIF technology development [16]. These materials, although challenging to shape, have diverse applications, discovered a wide range of uses, and SPIF provides a solution to traditional polymer processing problems. These applications include commercial automobiles, lightweight racing cars, aircraft, UAVs, and aerospace vehicles. Polymers have found several uses in the biomedical industry, which is another significant sector. Furthermore, SPIF's mold-free process allows the cost-effective production of small batches and unique parts [17]. Additionally, localized deformations by SPIF enable the creation of objects from a variety of thermoplastics, from polyethylene [18] to polycarbonate, all at ambient temperatures [19].

During SPIF of polymers, heat is often used to reduce the strength, which can enhance the formability of brittle polymers using various heating methods. These methods raise the forming temperature of the metal and thermoplastic sheets [20, 21]. For example, Ambrigio et al. [22] employed a similar heating system for forming PMMA sheets using ISF. On the other hand, Conte et al. [23] used a 2 kW heater within an insulated chamber within a refractory-coated

metallic structure. Okada et al. [24] employed a halogen lamp to heat and deform a thermoplastic CFRP sheet, while in another study a heating coil is used to heat a PC sheet of an SPIF process [25].

In SPIF of polymers, the main failure modes can occur. First, there can be an in-plane fracture caused by ductile tearing where the inclined wall meets the corner of the formed part in the circumferential direction because of the stress buildup. Second, wrinkles can form adjacent to the inclined wall of the formed part near the corner due to twisting of the workpiece due to the solid forming tool [19]. It was found that the SPIF of polymers has a more pronounced springback than metals [26]. Durante et al. [19] showed that the tool design affects the amount of springback in the forming process, while the toolpath strategy does not have a significant effect. Bagudanch et al. [27] found that applying heat to the workpiece after forming reduces springback. Decreasing the initial drawing angle, increasing the original sheet thickness, and reducing the step size can also decrease springback.

Achieving a satisfactory surface finish in polymer-forming processes, similar to SPIF in metal forming, faces challenges due to springback in polymer sheets and the incremental SPIF process. Lubricants like grease and liquid types reduce tool friction, enhancing surface quality. Forming settings, such as spindle speed and tool parameters, influence material roughness [28]. A roller ball tool can also improve surface finish [29], especially at lower temperatures. Tool material, geometry, and paths also impact surface quality [30].

Despite polymer SPIF advancements, issues like geometric precision, wrinkling, tool wear, and rough surfaces persist due to tool-polymer interaction. To combat tool wear, Water Jet Incremental Sheet Forming (WJISF) emerges, originating from water jet cutting. This is promising for automotive, micro-electronics, medical, and aerospace industries, requiring a

multi-axial machine and pressure pump. Since no lubricants are involved, WJISF warrants more research in terms of complex shapes and different alloys [31].

This research aimed to develop another contactless single incremental forming, which uses hot compressed air as a deforming tool without any physical contact. The goal of this process is to eliminate the physical interaction between the tool and the polymeric material, therefore reducing defects and lowering the cost of rigid tool production and lubricants. The experimental findings, deformation behavior, and workability of this new process are evaluated using polycarbonate as a demonstration material, and its design is described.

3.3 Materials and Methods

3.3.1 Design of the Contactless Incremental Point Forming

The hot-air contactless single-point incremental forming process is based on traditional single-point incremental forming, but with a difference - it uses pressured hot air rather than a rigid tool. In the traditional SPIF process, a clamping mechanism is used to hold the polymer or metal sheet securely in place. The material is then deformed using a rigid forming tool, which is driven by a control system to move along a predetermined path and shape the sheet into the desired form. **Figure** 3-1**b** shows a schematic of the contactless single point incremental forming process. Similar to traditional SPIF, a clamping frame is used to clamp the workpiece. A nozzle supplied with a controlled-temperature hot air nozzle is used to deform the workpiece according to the programmed CNC code.

The design of the HASPIF setup involves several key components, including five-bar air compressors, an in-line air and gas heater pipe, a PID temperature controller, a single-phase SSR, a 5 mm hose, an electric vacuum, and a 3D coordinate controller, which is implemented

using a 3D printer setup, see **Figure** 3-1**(b,c)**. All these elements are essential in ensuring the smooth and efficient operation of the system. For example, the 3D coordinate controller setup is used to control the movement and speed of the nozzle, while a specially built steel fixture is used to clamp the sheet in place and prevent material flow into the forming area. Additionally, the air compressor is linked to the in-line gas heater pipe through an 8.5 mm hose and provides compressed air to the heater, which in turn heats the air and maintains a consistent temperature using a thermocouple and SSR relay connected to the PID temperature controller. The inlet of the heater is connected to the hose through a 3/4" female × 3/8" push fit, and the thermocouple is attached at the exit of the heater for hot air temperature measurement. The electric connection of the heater and the thermocouple is managed by the SSR relay, which is connected to the temperature controller to maintain the required temperature. Finally, a stainless-steel nozzle, with a 33 mm inlet diameter and 5 mm outlet diameter, has been designed and implemented at the outlet of the heater to further regulate the flow of air and gas.

3.3.2 Nozzle Design and Manufacturing

The aim of the nozzle design is to develop a nozzle that can apply pressure to a polymer material without having physical contact with it. This is crucial because direct contact can negatively affect the polymer's quality. To attain this objective, the nozzle must generate a precisely controlled flow of pressurised air, producing a force on the polymer material while avoiding direct contact. Additionally, the nozzle must be able to manage the elevated temperatures and pressures that come with delivering pressurised air from a compressor and air heater. To meet this requirement, the nozzle needs to be made of moderate-temperature materials like alloy steel.

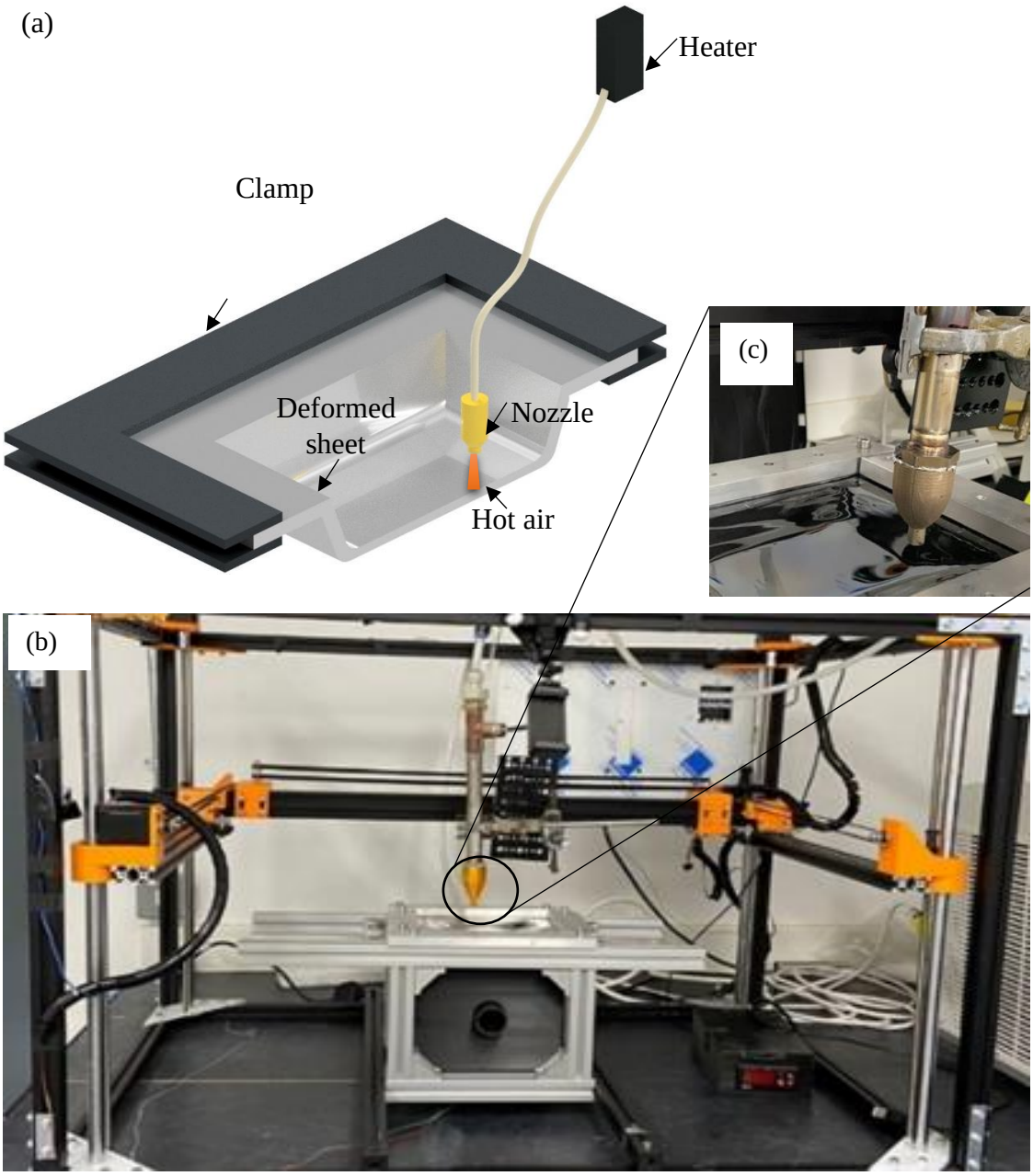

Figure 3-1 (a) A schematic diagram of CSIPF, (b) The experimental setup, (c) The air nozzle in operation. Video: https://www.dropbox.com/s/w0n4n3narl0dgvi/Contact-less%20SPIF.mp4?dl=0 (acceded on:1 September 2023)

SolidWorks was used to create the CAD model of the nozzle, which included the reducer, the inlet, and the outlet, see **Figure** 3-1**a**. The nozzle has been specifically designed to accommodate a thermocouple, which enables the measurement of the high-temperature

compressed air flowing through the nozzle. To facilitate the attachment of the thermocouple, a small aperture has been created on the upper side of the nozzle, beneath the thread that runs from the outer chamber to the inner chamber. The hole was then sealed to create a pathway for the thermocouple to reach the inlet of the nozzle. This design allowed for the accurate measurement and management of the temperature of the hot compressed air at the inlet of the nozzle. The ability to measure the temperature provided valuable information about the inlet temperature of the hot air that is used to deform the polymer sheet.

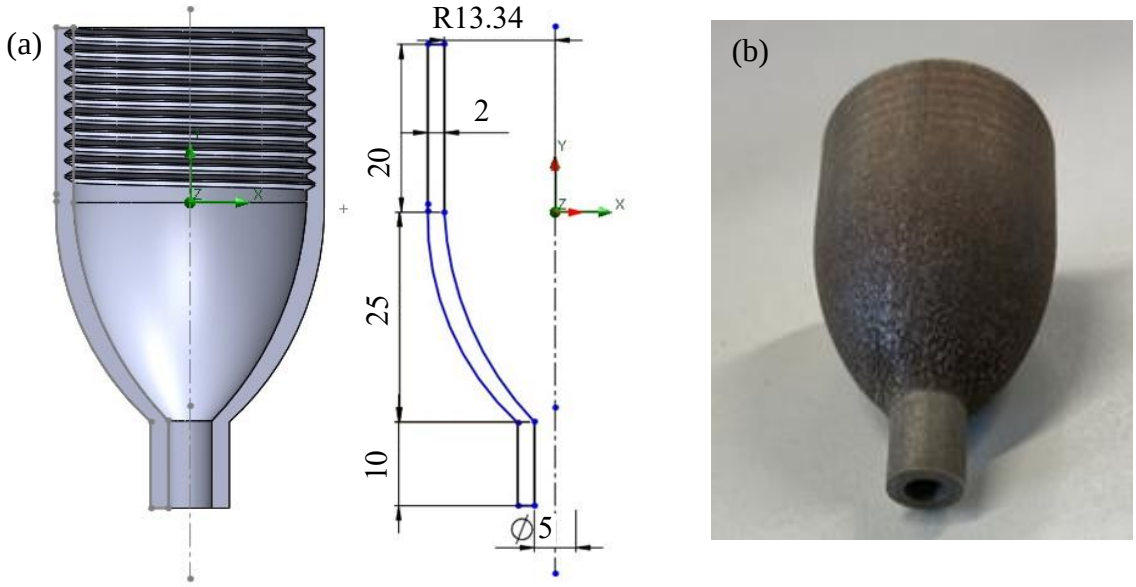

Figure 3-2 (a) CAD design of the nozzle, (b) 3D-printed steel nozzle.

The alloy steel nozzle was produced using a metal laser powder bed fusion printer (Concept Laser-M2 cusing). The 3D metal printer has a continuous wave ytterbium fiber laser with a nominal laser power of 200 W. The built chamber is maintained in a controlled argon atmosphere, ensuring a safe and controlled environment during the 3D printing. The material used in the fabrication process was the gas-atomized steel powders from Concept Laser. The fabricated nozzle is shown in **Figure** 3-1**b**.

3.3.3 Sheet Material

The polymeric material for this project was Lexan® 9030 polycarbonate (PC) with dimensions of 205 mm length, 170 mm width and 0.75 mm thickness. As depicted in **Table** 3-1, the properties of this PC sheet boast high impact resistance, transparency, and temperature stability. To fully comprehend the behavior of the PC sheet under varying temperatures, stress and strain curves were analysed from room temperature to 160 °C. These curves, which demonstrate the correlation between temperature and mechanical properties of the PC sheet, were sourced from previous research studies [32, 33]. The literature shows that, at temperatures that exceed the glass transition temperature threshold, strain hardening disappears. As a result, a forming temperature of 160 °C was utilised for the CSPIF process.

Table 3-1. Properties of Lexan® 9030 polycarbonate (PC) [32, 33].

Thickness	0.75 (mm)
Density	1.2 (g/cm)
Young's modulus	2.3 (Gpa)
Yield stress	60 (Mpa)
Poisson's ratio	0.38
Maximum elongation	110%

Thermal conductivity	0.2 (W/m.°C)

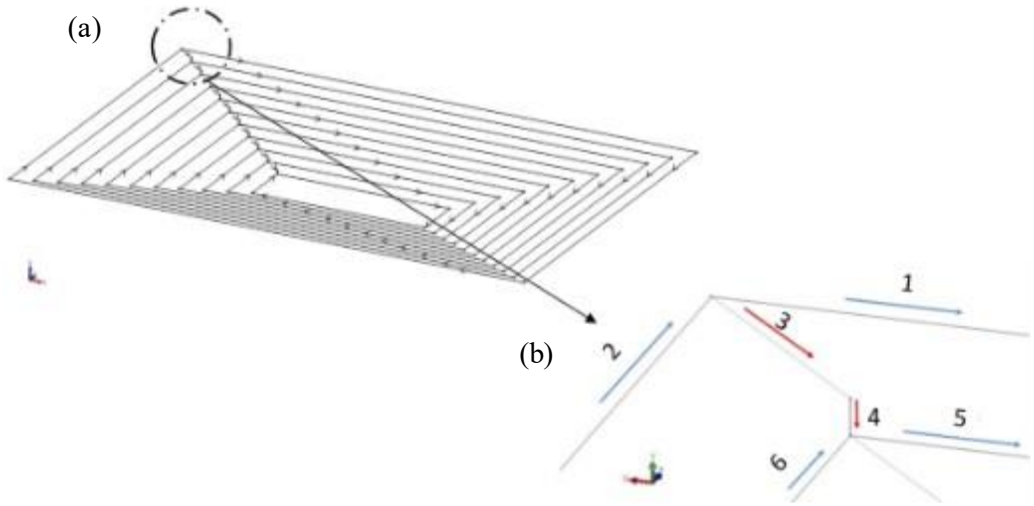

Figure 3-3 Truncated pyramid path trajectory (a) Full path, (b) Path movement.

The path, shaped like a truncated pyramid, was created using consecutive parallel loops. It commenced with a 152 mm × 120 mm rectangle in the initial loop. Each loop rectangle decreases by 5 mm from each side and concludes with a 62 mm × 30 mm rectangle in the last loop, with each loop step-down of 0.75 mm. As illustrated in **Figure** 3-3**b**, the initial trajectory follows a straight path in both clockwise directions, denoted as "1" and "2", until it returns to its starting point. Subsequently, it shifts along the x and z-axis, as indicated by direction "3", before proceeding in "4" direction along the y-axis to initiate the subsequent descent. This movement pattern continues until the last path.

3.3.4 Process Parameters

The contactless process of deformation relied on five parameters, including air pressure, air

temperature, nozzle speed, the gap between the nozzle and the polymer sheet, and step-down thickness, which are outlined in **Table** 3-2. These parameter choices were influenced by the most efficient parameters used in the conventional SPIF process, particularly the feed rate and step-down, in conjunction with those relevant to the new tool. Additionally, new parameters, including air pressure, air temperature, and initial gap, were introduced through experimental determination to optimise the performance of the newly implemented hot compressed air tool.

The process began with the activation of the air heater and the adjustment of its temperature to 160 °C, as specified by the controller. The air compressor was then turned on to deliver compressed air with a pressure of 1 bar to an 8.5 mm plastic hose. One end of the hose was attached to the air compressor and the other end was attached to the air heater. As the compressed air flowed through the heating element inside the heater, it was heated to the required temperature. The hot compressed air was then directed to the nozzle located at the outlet of the heater. When the nozzle was used, it increased the velocity of the air, which resulted in an increased forming force and the concentration of pressure in a specific area of the polycarbonate sheet. This prevented the occurrence of friction force that could have resulted from the use of a conventional tool tip during the deformation process. Using compressed air as the forming force instead of a solid tool, significantly reduced the risk of surface fractures or wear tracks on the polycarbonate.

Table 3-2. Process parameters.

Air pressure	1 (bar)
Air temperature	160 (°C)
Nozzle speed	750 (mm/min)
Initial gap	6 (mm)
Step-down	0.75 (mm)

3.3.5 Visualization of the Air Flow

An RS T-10 smart thermal camera was used to capture the thermal images and compare the result of the temperature that heated the nozzle itself with the value of the temperature on the PC sheet during the deformation. Conversely, a Z-type Schlieren setup was employed to visualize the air flow from the nozzle to the polymer sheet [34]. It comprised two concave mirrors, a spotlight serving as the light source, and a razor edge, see **Figure** 3-4. In addition, the setup included a digital single-lens reflex (DSLR) camera. The red lines in the setup indicate the light emitted from the LED pinhole, the blue lines indicate the parallel lights between the mirrors, and the green light represents the light that reaches the focal point.

The Schlieren setup was utilised to observe the motion of the hot compressed air as it traveled from the nozzle to the polymer sheet. The configuration of the system was such that the hot

compressed reducer was positioned in the centre, the nozzle was directed downwards, and the camera was equipped with a 100 mm micro lens. To attain optimal images quality, the Schlieren system underwent calibration using a high-density gradient-producing candle. To enhance the image, the light and razor edge were positioned at one focal length from the mirror direction. The camera was positioned beneath the razor edge. A gap of 6mm was maintained as the hot compressed air was expelled from the nozzle towards the polymer sheet. The temperature and pressure of the hot air inside the nozzle were found at 160 °C and 1 bar, respectively. The camera was positioned in such a way that it captured the movement of the hot air as it emerged from the nozzle and made contact with the sheet below it.

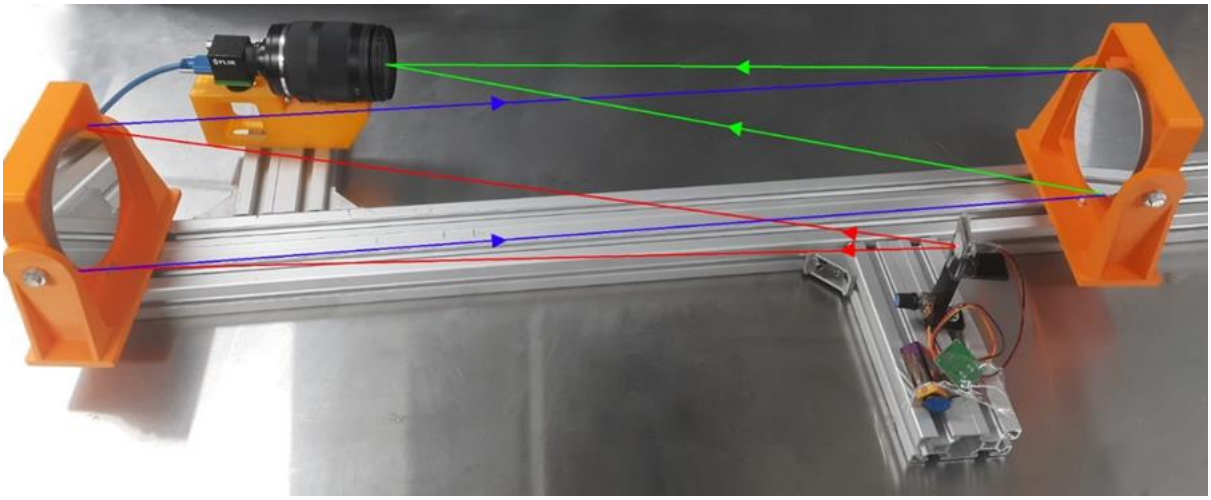

Figure 3-4 The Schlieren setup.

3.4 Results and Discussion

3.4.1 Forming Force and Air Thermal flow

The air flow from the compressed air nozzle has a significant impact on the proposed forming process. The high-pressure air coming out of the nozzle creates a thrust that is used to deform the PC (polycarbonate) sheet. The axial (z-axis) force during the incremental forming process

was measured by calculating the value of the air pressure and the affected area on the PC sheet. The pressure input of the nozzle was adjusted at 1 bar, and the affected area was determined using the results of the thermal and Schlieren images. Based on the affected area, the forming force was calculated to be 2.17 N, which is a rather small amount, taking into account the inlet pressure. However, this small forming force is sufficient to deform a polycarbonate sheet when combined with an elevated temperature. The results of the thermal image shown in **Figure** 3-5**a** show that the temperature-affected area diameter was equal to 18.67 mm (an area equal to 273.77 mm2) while the pressure zone diameter from the Schlieren image was equal to 5.26 mm (an area equal to 21.73 mm2) **Figure** 3-5**b** in an open-air system, the pressure drops significantly right after the air leaves the nozzle tip. However, the temperature does not decrease at the same rate, which results in variations in the affected areas measured by the thermal camera and those by the Schlieren. **Figure** 3-5**b** shows the hot compressed air flow coming out of the nozzle. Moreover, the affected area on the sheet from the air is obvious. As a result, the diameter of the affected area on the sheet is equal to 6 mm when comparing that area with the outlet diameter of the nozzle (5 mm).

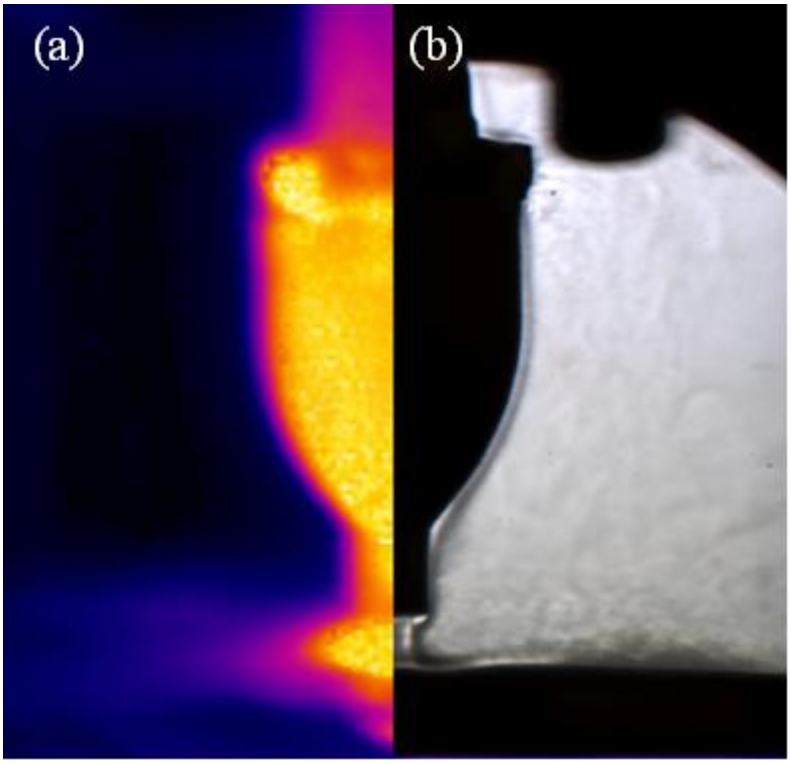

Figure 3-5 Air flow using (a) thermal camera, (b) the Schlieren method.

3.4.2 Geometric Profile of the PC workpiece

The precision and accuracy of the deformed workpiece fabricated using the proposed contactless incremental forming technique were determined using a Mitutoyo coordinate measuring machine, the Euro-CA776 (CMM), with an accuracy of (1.7 + 0.3L/100) µm. The measuring strategy employed involved sensing discrete points using a trigger probe positioned along the cross-section of the workpiece, from one edge to the other. The coordinates for each point were determined from both the top and bottom sides. The top-side measurements provided the profile data, while measurements of the bottom side were used to calculate the sheet thickness on the surface. The CMM was used to calculate the profile and thickness of the deformed part and compare it to the target geometry.

Figure 3-6 illustrates the comparison between the CAD drawing and the measured profile after

being fabricated using CSPIF. The CAD drawing profile data were obtained using SolidWorks by generating a G-code of the path from the edge to the middle. To ensure the validity of the results, the profiles obtained through experimentation were measured by scanning the workpiece using a CMM, eliminating any unclamping and cooling errors and ensuring an accurate assessment of the precision of the proposed method.

As shown in **Figure** 3-6, observations made before unclamping revealed minimal springback at the base of the pyramid and a pillow effect in the centre. The results suggest that the CSPIF system can deform polycarbonate sheets accurately. The obtained profile formed at 160 °C closely resembles the CAD design drawing profile, which demonstrates the effectiveness of the proposed technology.

Additionally, the bending effect at the nozzle starting point produces a deviation from the ideal profile as the PC sheet is being deformed. This deviation between the digital model and the deformed workpiece or the error in manufacturing has a significant impact on the final product's quality and accuracy, especially when working with precision parts [35, 36]. To mitigate these effects, it is crucial to consider the fixture design, nozzle placement, and the starting position of the thermal nozzle when performing the deformation process. Moreover, the use of the RS T-10 smart camera enabled the monitoring of the temperature distribution during the deformation process, which was crucial to understanding the reasons behind the deviation from the ideal profile. The temperature reached a maximum of 205 °C at the overlapped areas, where the heat tails intersected, highlighting the significance of temperature control in the deformation process, see **Figure** 3-7. Proper consideration of fixture design, nozzle placement, and starting position of the nozzle is essential to prevent overlapping and minimise deviation from the desired profile.

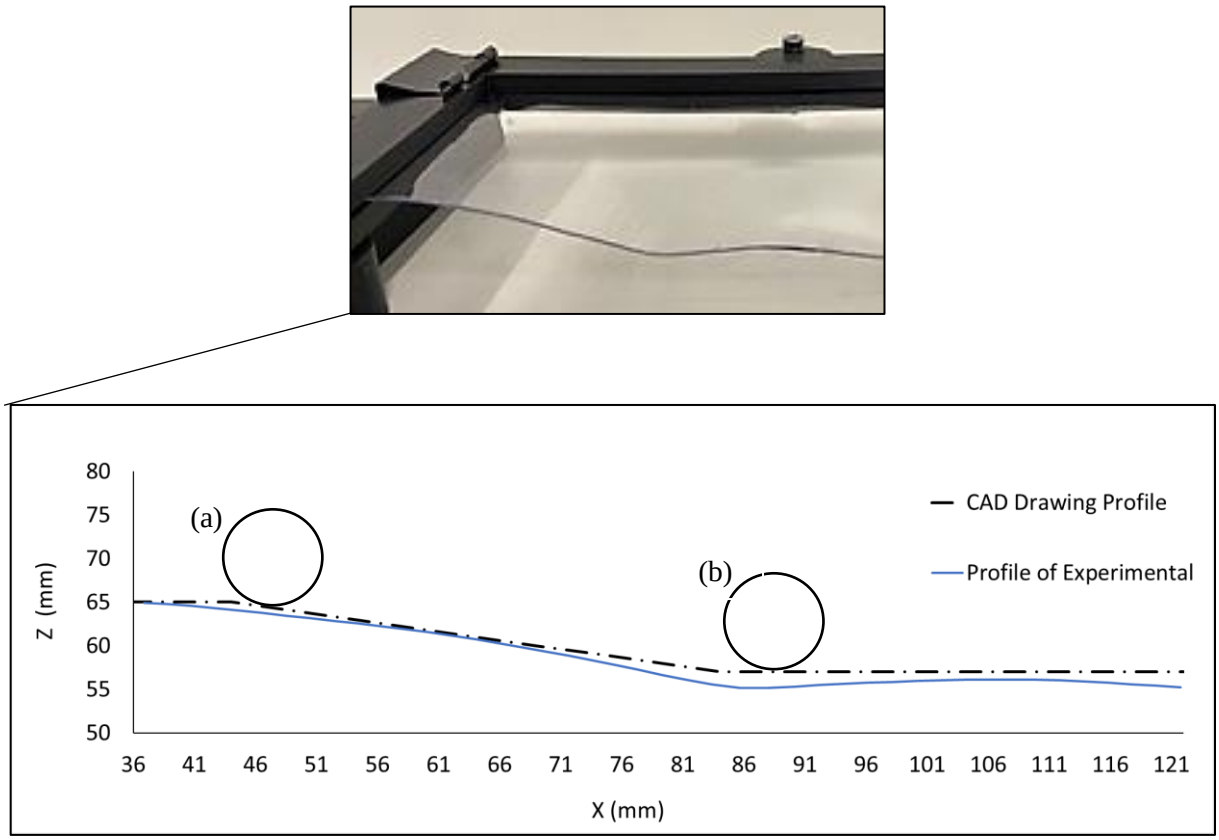

Figure 3-6 Comparison between CAD drawing and deformed PC workpiece using CIPF technique. (a) Deflection at the base of the shape (b) Deflection near the centre of the shape.

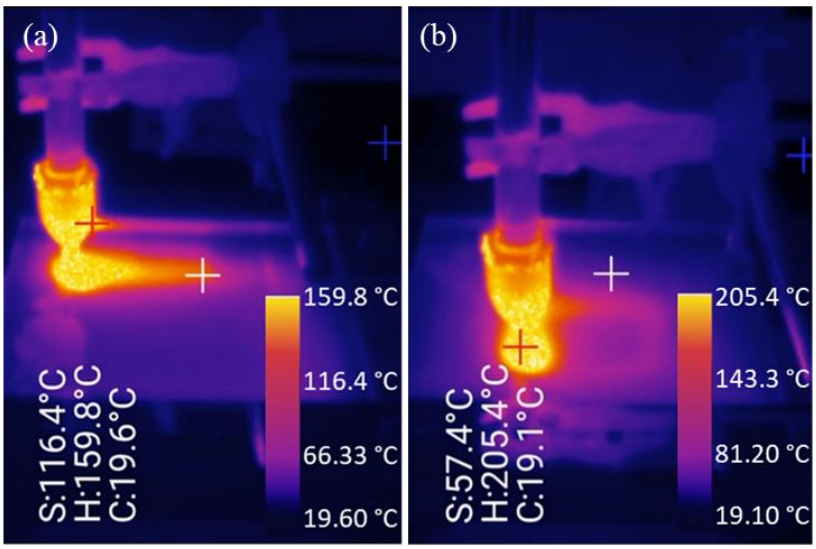

Figure 3-7 Temperature tail at the (a) First path and (b) Last path with tail overlapping. S, H, and C represent surrounding, hot, and cold spots, respectively.

3.4.3 Thickness Distribution

The thickness distributions of both the CAD design and experimental results are depicted in **Figure** 3-8, with the data collected from the edge to the centre of the workpiece. The thickness was calculated using **Equation 3.1**. The values of *X, Y,* and *Z* displacements were determined using a coordinate measuring machine (CMM) on both the workpiece bottom and top surfaces. The theoretical thickness distribution was derived through the application of the sine law, as expressed in **Equation 3.2**, which was found to be useful in determining the workpiece thickness, according to the study by Cao et al. [37] on the ISF (incremental single forming) process. The measurements were taken at 18 different locations, as shown in **Figure** 3-8**a**.

$$\mathbf{t}=\sqrt{(\boldsymbol{x1}-\boldsymbol{x2})^2+(\boldsymbol{y1}-\boldsymbol{y2})^2+(\boldsymbol{z1}-\boldsymbol{z2})^2} \quad \textbf{(3.1)}$$

Where t is the polymeric sheet thickness, *x1*, *y1*, and *z1* are the top surface route node coordinates, and *x2*, *y2*, and *z2* are the bottom surface path node coordinates. The sine law equation, which gives an estimate of the actual thickness of the sheet based on the original thickness, is used to get the theoretical thickness distribution, as shown in the following equation:

$$t_f = t_0 \times \mathrm{Sin}((\pi/2) - (\alpha)) \quad \textbf{(3.2)}$$

The thickness of the workpiece, represented by t_f, can be determined **Equation 3.2**, where t_0 represents the workpiece's initial thickness and α is the wall angle, as illustrated in **Figure** 3-8**b**. The percentage thinning was proportional to the formability of the polymer sheets [38].

$$\text{Percentage Thinning} = (\text{Initial Thickness} - \text{Thickness})/\text{Initial Thickness} \quad \textbf{(3.3)}$$

The equation was introduced by Hussain and Gao [39] in their previous paper, which focused

on determining the thickness distribution in SPIF. A similar method was adopted by Lu et al. [40] to calculate the theoretical thickness in double-sided ISF. Tolipov et al. [41] also confirmed the effectiveness of this equation when estimating the thickness distribution during metal forming through their study on multi-point forming.

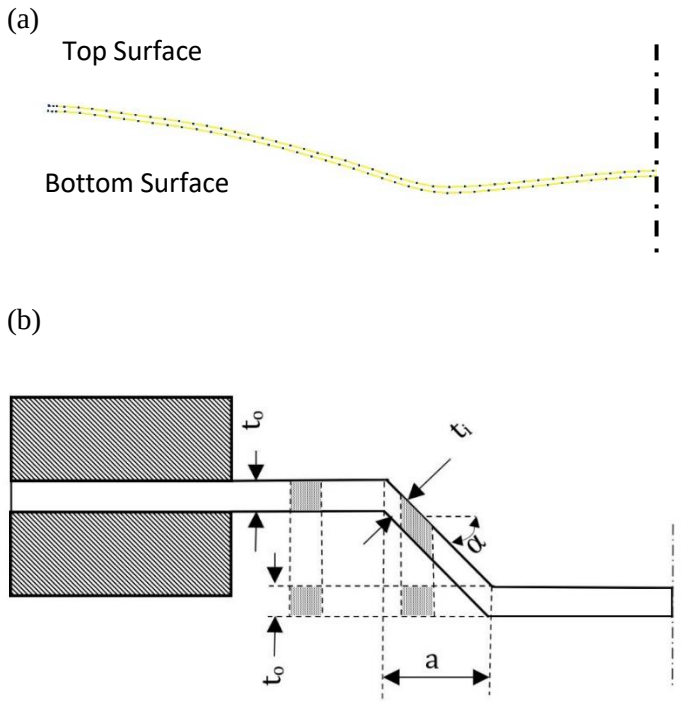

Figure 3-8 (a) Experimental thickness distribution between the top and bottom surfaces, (b) Schematic diagram of sine law.

Sheet thinning is a typical occurrence during incremental forming. The high levels of stress experienced during the process can result in local thinning of the sheet, which can cause an uneven distribution of thickness across the workpiece. This can negatively impact the mechanical properties and performance of the final product. To mitigate this effect, it is crucial to have an understanding of sheet thinning and be able to predict it during the design and development stages of incremental forming. Predictive models and numerical simulations can be utilised to estimate sheet thinning and optimise the forming process for minimal impact.

According to **Equation 3.2**, sheet thinning is related to the geometry depth. For a wall angle of 11.31°, the sine law predicted 0.73543 mm of sheet thinning in X along the pyramid wall. The experimental study found an average thickness of 0.745 mm with a thinning rate of 0.6%. The comparison of the measured and theoretical thickness distributions revealed a good agreement, as shown in **Figure** 3-9**a**. The results of the experiment indicated that the thickness of the wall decreases with an increase in forming depth, with a minimum calculated thinning of 0.73543 mm using the sine law equation and 0.7 mm from the experimental measurements.

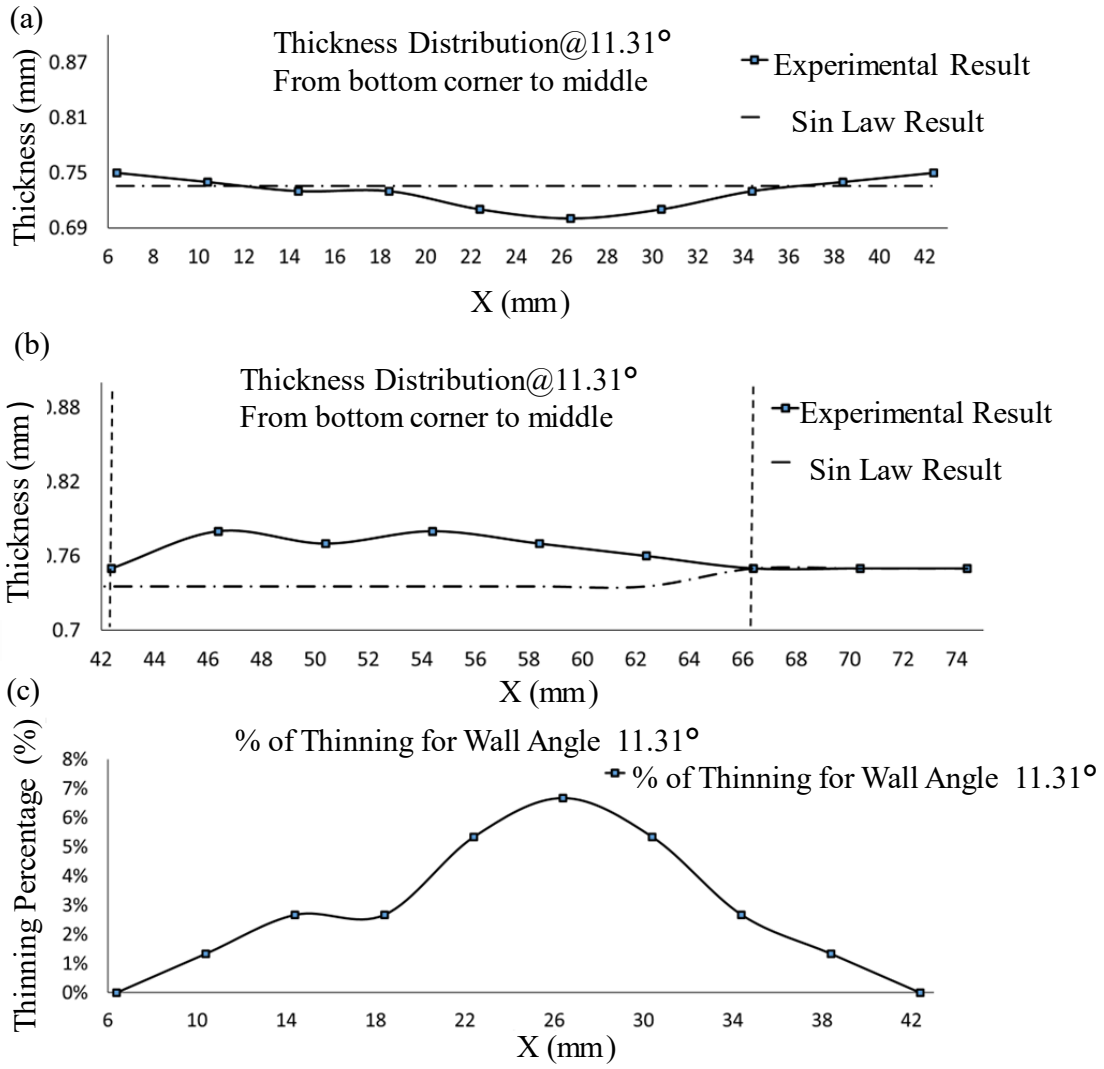

Figure 3-9 Thickness distribution using the experimental and theoretical calculations showing (a) sheet thinning, (b) materials building up, and (c) thinning percentage.

It is worth noting that in addition to sheet thinning, material buildup is also a phenomenon that can occur during incremental forming, see **Figure** 3-9**b**. The maximum material buildup in the sample was found to be around the pyramid corner of the workpiece. This may be due to the heating and pushing process causing the material to accumulate in the bottom corner of the sheet, resulting in an increase in wall thickness by approximately 3% before returning to its initial thickness, which is also in agreement with SPIF as in [42]. **Figure** 3-9**c** shows how much the workpiece thinned in the new CSPIF when the wall angles were 11.31 degrees. The results showed that 6% was the most thinning that could happen.

3.4.4 Surface Roughness

Surface roughness is a critical property for determining the quality of a formed part's surface. A Mitutoyo Formtracer Avant S-3000 Model Surface Roughness Tester with an accuracy of (0,05+0,001L) μm was used to assess the part's surface finish. The effect of the hot compressed air on the final part's quality was also assessed using the surface roughness characterisation [43]. In this study, four different roughness parameters were measured: the Average Roughness (Ra) value, which is an internationally recognized parameter for measuring surface roughness and the mean departure of a profile; the root mean square (Rq) value, determined as the square root of the mean squared roughness values over the evaluation length; Rz, calculated as the average of the five highest peaks and five deepest valleys within the evaluation length, offering insights into the height of surface irregularities by accounting for both peaks and valleys; and finally, Rt, which quantifies the total height discrepancy between the highest peak and lowest valley within the evaluation length, providing an assessment of the overall height variation across the surface. All values were measured five times at the same depth and perpendicular to

the forming tool movement using a 2.5 mm cut and a 12.5 mm sampling length.

The inner surface of the as received and experimental workpieces' surface roughness values are displayed in **Table** 3-3. The results show surface roughness Ra value increased by 0.3747 mm at the top layer, 0.0514 mm at the middle layer, and 0.1965 mm at the bottom layer when compared with the as-received surface roughness value. The minimum and maximum heights of the roughness profile Rz are obtained in the middle layer (0.5470 mm). At the bottom layer, the difference between the highest peak and the deepest valley is 0.65 mm. Wave format geometry was also noticed in the workspace due to the step size of the nozzle, see **Figure** 3-10. These wavy surfaces magnify the values of the surface roughness compared to the original values.

Table 3-3 Surface roughness values.

Sample no	Ra (µm)	Rq (µm)	Rz (µm)	Rt (µm)
As-received	0.0796	0.0846	0.1938	0.2441
Experimental (top)	0.4543	0.4722	0.5508	1.5403
Experimental (middle)	0.1310	0.1490	0.5470	1.5228
Experimental (bottom)	0.2761	0.3067	0.6521	1.3956
Average	0.2871	0.3093	0.5833	1.486

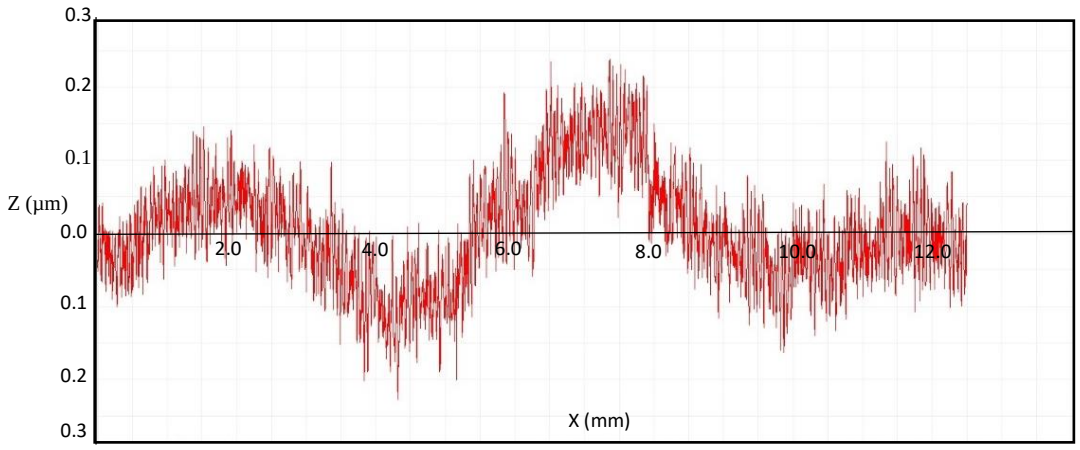

Figure 3-10 A sample of the surface roughness topography.

3.5 Conclusion

By eliminating the need for a rigid tool and replacing it with a contactless nozzle, a new design for CSPIF of polymers has been developed. Five key process parameters were identified, namely air temperature, air pressure, speed of the moving, initial gap, and step-down. The air flow from the compressed air nozzle was found to play a crucial role in the process as it creates a thrust to deform the PC sheet. The thrust force was measured by calculating the value of the air pressure and the affected area on the PC sheet. The precision and accuracy of the deformed workpiece were determined using a coordinate measuring machine (CMM) and were found to have high accuracy with only modest springback and pillow effects. However, deviation from the ideal profile was observed due to the bending effect at the starting point of the nozzle and it was highlighted that proper consideration of fixture design, nozzle placement, and starting position is crucial to minimise deviation. The results also showed that sheet thinning is proportional to pyramid depth and there was good agreement between the measured and theoretical thickness distributions. Material buildup was also observed and was found to be

around the pyramid corner of the workpiece. The surface roughness of the samples was also determined and found to have slightly but acceptably increased after the incremental forming due to the step-wise nature of the air nozzle. The study on the new HASPIF configuration opens up a new paradigm in sheet forming. It has shown success in deforming polycarbonate sheets and has the potential to be applied to other polymer materials and potentially metal as well. The results show that this method surpasses traditional SPIF in terms of surface quality and eliminates the need for tools and workpiece defects such as tearing and twisting.

3.6 References

1. Pratheesh Kumar, S.; Elangovan, S.; Mohanraj, R.; Naveen Anthuvan, R.; Nithin, V., Development of Flexible Mechanism for Two-Point Incremental Forming. In Advances in Forming, Machining and Automation: Select Proceedings of AIMTDR 2021, Springer: Berlin/Heidelberg, Germany, 2022; pp 37-46.

2. Zhou, C.; Zhang, F.; Wei, B.; Lin, Y.; He, K.; Du, R., Digital twin–based stamping system for incremental bending. The International Journal of Advanced Manufacturing Technology 2021, 116 (1-2), 389-401.

3. Leszak, E. Apparatus and Process for Incremental Dieless Forming. U.S. Patent No 3,342,051, 19 September 1967.

4. Mohanraj, R.; Elangovan, S., Incremental sheet metal forming of Ti–6Al–4V alloy for aerospace application. Transactions of the Canadian Society for Mechanical Engineering 2019, 44 (1), 56-64.

5. Li, W.; Attallah, M. M.; Essa, K., Experimental and numerical investigations on the process quality and microstructure during induction heating assisted incremental forming of Ti-6Al-4V sheet. Journal of Materials Processing Technology 2022, 299, 117323.

6. Pandre, S.; Morchhale, A.; Kotkunde, N.; Kurra, S., Processing of DP590 steel using single point incremental forming for automotive applications. Materials and Manufacturing Processes 2021, 36 (14), 1658-1666.

7. Cheng, Z.; Li, Y.; Xu, C.; Liu, Y.; Ghafoor, S.; Li, F., Incremental sheet forming towards biomedical implants: A review. Journal of Materials Research and Technology 2020, 9 (4), 7225-7251.

8. Essa, K.; Hartley, P., An assessment of various process strategies for improving precision in single point incremental forming. International journal of material forming 2011, 4 (4), 401-412.

9. Grimm, T. J.; Parvathy, G. V.; Mears, L. In Single Point Incremental Forming Springback Reduction Using Edge Stiffener, ASME International Mechanical Engineering Congress and Exposition, American Society of Mechanical Engineers: 2020; p V02AT02A022.

10. Van Viet, M.; Thinh, N. T.; Van Sy, L. In Effect of Lubrication on Deforming the Aluminum Sheet with Two Points Incremental Forming Technology, In Proceedings of the 2nd Annual International Conference on Material, Machines and Methods for

Sustainable Development (MMMS2020), Nha Trang, Vietnam, 12–15 November 2020; pp. 975–982.2.

11. Sieczkarek, P.; Wernicke, S.; Gies, S.; Tekkaya, A.; Krebs, E.; Wiederkehr, P.; Biermann, D.; Tillmann, W.; Stangier, D., Wear behavior of tribologically optimized tool surfaces for incremental forming processes. Tribology International 2016, 104, 64-72.

12. Murugesan, M.; Yu, J.-H.; Jung, K.-S.; Cho, S.-M.; Bhandari, K. S.; Lee, C.-W., Optimization of forming parameters in incremental sheet forming of AA3003-H18

sheets using Taguchi method. Materials 2022, 15 (4), 1458.

13. Zavala, J. M. D.; Martínez-Romero, O.; Elías-Zúñiga, A.; Gutiérrez, H. M. L.; Vega, A. E.-d. l.; Taha-Tijerina, J., Study of friction and wear effects in aluminum parts manufactured via single point incremental forming process using petroleum and vegetable oil-based lubricants. Materials 2021, 14 (14), 3973.

14. Li, W.; Essa, K.; Li, S., A novel tool to enhance the lubricant efficiency on induction heat-assisted incremental sheet forming of Ti-6Al-4 V sheets. The International Journal of Advanced Manufacturing Technology 2022, 120 (11-12), 8239-8257.

15. Li, W.; Shu, C.; Hassan, A.; Attallah, M. M.; Essa, K., Application of machine learning on tool path optimisation and cooling lubricant in induction heating-assisted single point incremental sheet forming of Ti-6Al-4V sheets. The International Journal of Advanced Manufacturing Technology 2022, 123 (3-4), 821-838.

16. Hassan, M.; Hussain, G.; Wei, H.; Qadeer, A.; AlKahtani, M., Progress on single-point incremental forming of polymers. The International Journal of Advanced Manufacturing Technology 2021, 114, 1-26.

17. Zhu, H.; Ou, H.; Popov, A., Incremental sheet forming of thermoplastics: a review. The International Journal of Advanced Manufacturing Technology 2020, 111, 565-587.

18. Roşca, N. A.; Oleksik, M., Simulation of the Single Point Incremental Forming of Polyamide and Polyethylene Sheets. MATEC Web Conf. 2019, 290, 03014.

19. Durante, M.; Formisano, A.; Lambiase, F., Formability of polycarbonate sheets in single-point incremental forming. The International Journal of Advanced

Manufacturing Technology 2019, 102, 2049-2062.

20. Li, W.; Li, S.; Li, X.; Xu, D.; Shao, Y.; Attallah, M. M.; Essa, K., Crystal plasticity model of induction heating-assisted incremental sheet forming with recrystallisation simulation in cellular automata. The International Journal of Advanced Manufacturing Technology 2022, 123 (3-4), 903-925.

21. Li, W.; Attallah, M. M.; Essa, K., Heat-assisted incremental sheet forming for high-strength materials—a review. The International Journal of Advanced Manufacturing Technology 2023, 124 (7-8), 2011-2036.

22. Ambrogio, G.; Gagliardi, F.; Conte, R.; Russo, P., Feasibility analysis of hot incremental sheet forming process on thermoplastics. The International Journal of Advanced Manufacturing Technology 2019, 102, 937-947.

23. Conte, R.; Gagliardi, F.; Ambrogio, G.; Filice, F.; Russo, P. In Performance analysis of the incremental sheet forming on PMMA using a combined chemical and mechanical approach. In Proceedings of the AIP Conference Proceedings, Dublin, Ireland, 26–28 April 2017.

24. Okada, M.; Kato, T.; Otsu, M.; Tanaka, H.; Miura, T., Development of optical-heating-assisted incremental forming method for carbon fiber reinforced thermoplastic sheet—Forming characteristics in simple spot-forming and two-dimensional sheet-fed forming. Journal of Materials Processing Technology 2018, 256, 145-153.

25. .Sridhar, R.; Rajenthirakumar, D., Polymer sheet hot incremental forming-an innovative polymer forming approach. Polymers and Polymer Composites 2016, 24 (7), 447-454.

26. Al-Ghamdi, K. A., Spring back analysis in incremental forming of polypropylene sheet: An experimental study. Journal of Mechanical Science and Technology 2018, 32, 4859-4869.

27. Bagudanch, I.; Lozano-Sánchez, L. M.; Puigpinós, L.; Sabater, M.; Elizalde, L. E.; Elías-Zúñiga, A.; Garcia-Romeu, M. L., Manufacturing of polymeric biocompatible cranial geometry by single point incremental forming. Procedia Engineering 2015, 132, 267-273.

28. Sabater, M.; Garcia-Romeu, M. L.; Vives-Mestres, M.; Ferrer, I.; Bagudanch, I., Process parameter effects on biocompatible thermoplastic sheets produced by incremental forming. Materials 2018, 11 (8), 1377.

29. Thangavel, K.; Duraiswamy, R.; Nagarajan, S.; Ramasamy, S., Influence of roller ball tool in single point incremental forming of polymers. Tehnički vjesnik 2019, 26 (1), 171-176.

30. Medina-Sánchez, G.; Torres-Jimenez, E.; Lopez-Garcia, R.; Dorado-Vicente, R.; Cazalla-Moral, R., Temperature influence on single point incremental forming of PVC parts. Procedia Manufacturing 2017, 13, 335-342.

31. Miroir, M.; Laniel, R.; Brient, A.; Kerbrat, O., Water jet incremental sheet metal forming: a critical state-of-the-art review and a proposal for technological windows. The International Journal of Advanced Manufacturing Technology 2022, 119 (7-8), 4159-4175.

32. Richeton, J.; Ahzi, S.; Vecchio, K. S.; Jiang, F. C.; Adharapurapu, R. R., Influence of

temperature and strain rate on the mechanical behavior of three amorphous polymers: Characterization and modeling of the compressive yield stress. International journal of solids and structures 2006, 43 (7-8), 2318-2335.

33. Dar, U. A.; Zhang, W.; Xu, Y.; Wang, J., Thermal and strain rate sensitive compressive behavior of polycarbonate polymer-experimental and constitutive analysis. Journal of Polymer Research 2014, 21, 1-10.

34. Kaessinger, J. C.; Kors, K. C.; Lum, J. S.; Dillon, H. E.; Mayer, S. K. In Utilizing Schlieren imaging to visualize heat transfer studies. In Proceedings of the ASME International Mechanical Engineering Congress and Exposition, Montreal, QC, Canada, 14–20 November 2014; p. V005T005A033.

35. Borboni, A.; De Santis, D., Large deflection of a non-linear, elastic, asymmetric Ludwick cantilever beam subjected to horizontal force, vertical force and bending torque at the free end. Meccanica 2014, 49 (6), 1327-1336.

36. Archansdran, S.; Shaari, M.; Rosly, M., Characterization of double layer IPMC bending actuation. ARPN J. Eng. Appl. Sci. 2016, 11 (10), 6536.

37. Cao, T.; Lu, B.; Xu, D.; Zhang, H.; Chen, J.; Long, H.; Cao, J., An efficient method for thickness prediction in multi-pass incremental sheet forming. The International Journal of Advanced Manufacturing Technology 2015, 77 (1), 469-483.

38. Limpadapun, K.; Kesvarakul, R., An investigation of thickness distribution in Single-Point incremental forming with different forming parameter in Hot-dipped zinc-coated cold-rolled steel. Materials Today: Proceedings 2020, 33, 1988-1992.

39. Hussain, G.; Gao, L., A novel method to test the thinning limits of sheet metals in negative incremental forming. International Journal of Machine Tools and Manufacture 2007, 47 (3), 419-435.

40. Lu, B.; Fang, Y.; Xu, D. K.; Chen, J.; Ai, S.; Long, H.; Ou, H.; Cao, J., Investigation of material deformation mechanism in double side incremental sheet forming. International Journal of Machine Tools and Manufacture 2015, 93, 37-48.

41. Tolipov, A.; Elghawail, A.; Abosaf, M.; Pham, D.; Hassanin, H.; Essa, K., Multipoint forming using mesh-type elastic cushion: modelling and experimentation. The International Journal of Advanced Manufacturing Technology 2019, 103 (5), 2079-2090.

42. Abe, Y.; Mori, K.-i.; Ito, T., Plate forging of drawn cup with flange including thickening of corners. Manufacturing Review 2014, 1, 16.

43. Abd Ali, R.; Chen, W.; Al-Furjan, M.; Jin, X.; Wang, Z., Experimental investigation and optimal prediction of maximum forming angle and surface roughness of an Al/SUS bimetal sheet in an incremental forming process using machine learning. Materials 2019, 12 (24), 4150.

4 Chapter Four: Single Point Incremental Forming: Experimental and Numerical Simulation

Mohammad Almadani [a,b], Ahmet Guner [a], Hany Hassanin[c] , Michele De Lisi [a], Khamis Essa[a]

[a] *Mechanical Engineering, University of Birmingham, Edgbaston, Birmingham, B15 2TT, UK*

[b] *Department of Mechanical Engineering Technology, Yanbu Industrial College, Yanbu Al-Sinaiyah City, 41912, Kingdom of Saudi Arabia.*

[c] *School of Engineering, Technology, and Design, Canterbury Christ Church University, B15 2TT, UK*

This research was published as a full-length research article in International Journal of Advanced Manufacturing Technology:

Mohammad Almadani, Ahmet Guner, Hany Hassanin, Michele De Lisi, and Khamis Essa, *Contactless Single Point Incremental Forming: Experimental and Numerical Simulation.* Accepted by International Journal of Advanced Manufacturing Technology.

Credit authorship contribution statement

Mohammad Almadani: Conceptualisation, Investigation, Methodology, Validation, Software, Formal analysis, Writing - original draft.

Ahmet Guner: Writing - review & editing, Software.

Hany Hassanin: Writing - review & editing, Supervision.

Michele De Lisi: Reviewing & editing, Software.

Khamis Essa: Writing - review & editing, Resources of lab equipment, Supervision, Project Administration**.**

Research contributions:

This chapter aims to complete the objective 3 and 4 which cover the following insights:

- A novel contactless single point incremental forming was developed for sheet forming.
- An FEM was developed combining CFD and structural calculations to predict deformation.
- Sheet thinning and material build-up observed, but does not significantly reduce the quality of the workpiece.
- Slight increase in surface roughness due to stepwise waviness of the nozzle path.

4.1 Abstract

The demand for small-batch manufacturing processes has increased considerably in recent years due to the need for personalized and customized products. Single Point Incremental Forming (SPIF) has emerged as a time-efficient approach that offers increased material formability when compared to conventional sheet metal forming techniques. However, the complexity of SPIF requires a complete understanding of the material deformation mechanism. In this study, a non-conventional contactless tool in the form of hot compressed air is employed to form a polycarbonate sheet. The influence of the contactless tool on the shaping process is modelled and analysed with a finite element modelling (FEM). Two different models were developed and coupled to estimate the resulting shape of the sheet. A CFD model was created to obtain pressure and temperature values of the air impacting the sheet, while a transient structural model was employed to study the deformation of the sheet. The research provides a working model that is able to predict the performance of this contactless incremental forming process of polymers with high accuracy. The comprehensive FE model developed in this work is able to forecast the final part geometries and dimensions in addition to the normal strain progression. It also revealed that the primary modes of deformation in SPIF were stretching, thinning and bending. The model was validated by experimental results, and the predicted sheet deformation was compared to the one generated experimentally, and the results obtained were in good agreement.

Keywords: Contactless; Finite Element Modelling; Single Point Incremental Forming; Polycarbonate; Formability.

4.2 Introduction

Advanced manufacturing processes require precise and efficient techniques to meet the demands of modern industries. Sheet forming manufacturing processes have gained popularity due to their flexibility, allowing for shorter lead times and reduced costs, making them ideal for small customized batch sizes. One particular technology that has been of significant interest in this field is Single Point Incremental Forming (SPIF). This method involves gradually deforming a sheet in a CNC unit using a forming tool that follows a pre-programmed trajectory to produce the final product shape [1, 2]. To ensure the reliability and accuracy of sheet forming manufacturing processes, it is crucial to use components that are free from any similarity. The use of similar raw materials or production techniques can compromise the quality of the final product, resulting in costly errors that can impact the success of the manufacturing process and customer satisfaction [3].

Single Point Incremental Forming has traditionally been employed for forming metals, including aluminum alloys and deep drawing grade steels. However, in recent years there has been a growing interest in the use of SPIF for forming polymers, which has led to increased attention and research in this area [4]. Polymers have gained attention in various fields despite being known for their difficulty in forming. SPIF presents a solution to overcome the challenges posed by traditional polymer processing methods like compression or injection molding. SPIF also eliminates the need for molds, making it a cost-effective alternative for producing small batches and unique parts [5]. In contrast, SPIF enables the creation of objects using localized deformations at room temperature, using a variety of commercial thermoplastics, including highly crystalline materials such as polyethylene,[6] to amorphous forms like polycarbonate [7].

To enhance the formability of polymers using SPIF, a range of approaches have been developed, including modifications to polymer properties, tool design, and process parameters. These approaches have been found to have a major effect on the formability of the polymer sheet during SPIF. Specifically, several SPIF process factors have been identified that can affect the formability of the polymer, such as tool geometry, feed rate, and step size. By understanding the influence of these factors, it is possible to optimise the SPIF process for polymer forming and improve the quality of the formed sheet. In a recent study, it was found that the formability of various polymers during SPIF is primarily influenced by sheet thickness, tool diameter, and material ductility. Increasing the thickness of the test specimen and the initial drawing angle was shown to result in increased spring back. Additionally, SPIF-induced strain has been observed to cause three distinct failure types in polymers, which are not typically seen in metal testing. Unlike metals, which tend to crack, these failures in polymers are more likely to manifest as tears in the material [8, 9]. Kulkarni [10] conducted a study on the effect of heat on the formability of various thermoplastic polymers. The results indicated that heating a material below its glass transition temperature can significantly enhance its formability, with the maximum achievable wall angle increasing from 27° to 46° and the required forming forces decreasing. This finding highlights the potential for improving the SPIF process for polymers by carefully controlling the heating conditions.

Finite element models have become increasingly important in manufacturing applications, providing valuable insights into the influence of the process parameters on a range of outputs including thickness distribution, geometrical accuracy, and surface roughness [11]. In order to advance our understanding of the Incremental Sheet Forming (ISF) technique, a study was carried out to explore the application of the Finite Element Method (FEM) in predicting thickness and stress distributions on the sheet during forming [12]. The process was applied to produce a highly intricate conical shape, and to make sure that the precision of the final product,

the FEM was employed for validation purposes, predicting the geometry limitations of the final product [13]. To investigate the impact of using a pre-formed blank in SPIF, a FEM was developed using ANSYS software. The model was utilised to determine the SPIF parameters used in the analysis, focusing on the strain and stress conditions in the region of contact where the plastic deformation occurs due to the activity of the forming tool [14-15].

Over the past decade, several studies have been conducted to enhance the modelling of the SPIF process with the aim of gaining a better understanding of the underlying mechanics and predicting the material behavior. As a result, a numerical simulation was developed in the LS-Dyna software and was experimentally validated using micro-squared copper steel sheets [13]. To simulate SPIF, researchers have introduced a non-linear algorithm based on the Lagrangian approach [16]. Large deformation and deformation of complex structures can be simulated using Lagamine, which employs a vast library of finite elements and constitutive laws. LS-Dyna with a dynamic explicit solver is commonly used in many studies. However, SPIF simulations are typically limited to small components due to the nonlinearities in the software, which make the simulation computationally expensive and time-consuming. Implicit solvers produce accurate results compared to explicit solvers, but they require longer computing time to solve the numerical models. As a result, various approaches, such as remeshing or adaptive meshing, can be used to simulate SPIF processes with less computing costs [17].

Recently, López et al. evaluated the capabilities of Solidworks® [18] in simulating SPIF processes. They discovered that the program could only model short pathways, and that a more robust solution was necessary. In particular, it was difficult to simulate medium-sized, full portions of basic geometries such as pyramids. To minimise the length of the tool to be analysed, only components with relatively small heights and unrealistic forming parameters could be modeled. Consequently, the authors decided to explore other general-purpose software

options and ultimately chose ANSYS Workbench due to its ability to handle large-scale deformations and its implicit solvers, which produce higher-quality results than explicit solvers.

The conventional SPIF process for polymers has faced persistent challenges such as accuracy, wrinkling, twisting, and rough surfaces, primarily due to the polymer sheet and the forming tool interaction. Additionally, adapting the SPIF process for metals to polymers has exacerbated these issues. To address these challenges and enhance the SPIF process for polymers, a novel technique has been introduced in this study. The contactless SPIF process employs hot compressed air as a deforming tool, eliminating physical contact with the polymer sheet. This innovative approach has the potential to significantly reduce defects, lower the cost of producing rigid tools, and eliminate the need for lubricants. To better understand the contactless SPIF technique, the deformation behavior of polymer sheets has been modeled using ANSYS 21 Workbench software, which incorporates both fluent and transient structural models. The simulation results provide valuable insights into the contactless SPIF process and its capabilities. To verify the accuracy of the model, an experimental truncated pyramid part has been produced using the contactless SPIF method, and the simulation results have been compared to the experimental data. The proposed contactless SPIF approach represents a distinct and innovative solution to enhance the SPIF process for polymer sheets. It offers exciting possibilities for further research and development, as well as a promising path to overcome the persistent challenges associated with conventional SPIF processes.

4.3 Experimental

The contactless SPIF process utilises pressurised hot air to deform a clamped workpiece, unlike the conventional SPIF which uses a rigid forming tool. For this study, a new setup was designed to incorporate essential components such as air compressors, an in-line air and gas heater pipe,

a PID temperature controller, and a 3D coordinate controller. The temperature controller is connected to a thermocouple and an SSR relay to maintain a consistent temperature. The flow of air and gas is regulated by a stainless-steel nozzle. **Figure** 4-1**a** depicts the entire new forming tool and experimental setup developed for this study. To form the workpiece, a 3D printed steel nozzle with an inlet diameter of 33 mm and an outlet diameter of 5 mm **Figure** 4-1**b** was developed and mounted on a 3D-axis CNC machine. A steel fixture was also designed to clamp the polymer sheet on the CNC machine (**Figure** 4-1**c**). The tool paths were generated using Excel software with the help of the parallel loop visible on the exterior.

In this study, experimental work was conducted on a truncated pyramid which was manufactured using a high-quality material polycarbonate (PC) sheet with a trade name of Lexan® 9030. The material was chosen for its exceptional properties including strong impact resistance, high modulus of elasticity, and excellent heat resistance. Due to its remarkable stress absorption and low density, PC is widely used in various industries such as automotive and electronics. The selection of this material was based on its properties, which make it suitable for low forming force and heating impact. The material properties of the PC material were extracted from previously published literature across different temperatures which was used during the modelling stage [19, 20]. **Table** 4-1 provides a comprehensive overview of the material properties that were utilised in the finite element software employed for the process simulations. During the experiments, the temperature control range spanned from 23 °C to 160 °C. This precise temperature control was crucial for investigating how polycarbonate behaves mechanically. The storage modulus, as described by Fisher and colleagues [21], played a central role in assessing the material's response to applied stress and deformation within this thermal spectrum. Consequently, polycarbonate undergoes a transition from its glassy form to a rubbery form at temperatures above 147°C, as the storage modulus drops to zero at that temperature. This implies that polycarbonate remains elastic up to that temperature but

undergoes plastic deformation beyond it. A polycarbonate sheet with dimensions of 205×170×0.75 mm^3 was prepared to perform the contactless SPIF experimental tests.

The forming operations were conducted at a tool speed of 0.75 m/min in the X and Z directions and 10 m/min in the Y direction for the step-down movement (transition point). The initial distance between the nozzle and the sheet was 6 mm. Moreover, the truncated pyramid shape was generated so that 10 full loops were conducted, starting from a 152×120 mm^2 rectangle at the first loop and ending with a 62×30 mm^2 one in the last loop. The step down between consecutive loops was set to 0.75 mm for each step, with a total depth of 7.5 mm.

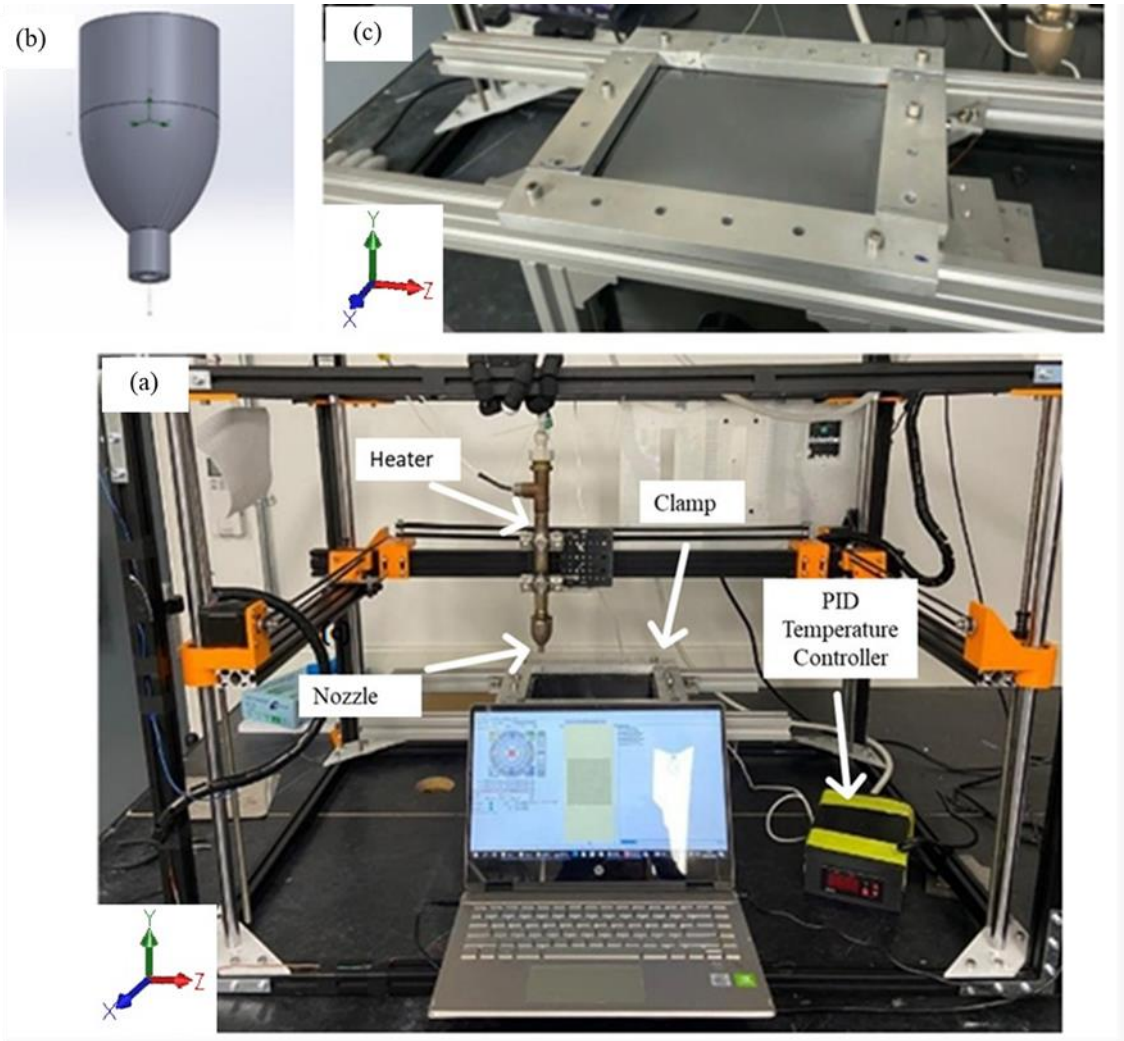

Figure 4-1 (a) Full setup, (b) The forming tool, and (c) Fixture for the PC sheet.

Video: https://www.dropbox.com/s/w0n4n3narl0dgvi/Contact-less%20SPIF.mp4?dl=0

Table 4-1 Material properties of LEXAN® 9030 polycarbonate.

Property	**Value**
Thickness	0.75 mm
Density	1.2 g/cc
Young's Modulus	2.3 GPa
Yield stress	60 MPa
Poisson's Ratio	0.38
Maximum Elongation	110%
Thermal Conductivity	0.2 W/m. °C

4.4 Simulation

To carry out the numerical simulation of the contactless SPIF method, ANSYS 21 Workbench software was employed in this study. In order to simplify the simulation for long tool paths, the sheet was treated as an isolated element, which entailed removing the frame used to secure the

sheet. Additionally, a fixed support mechanical boundary condition was applied to the extremes of the sheet to maintain stability during the simulation. Notably, the support mesh results were not calculated to minimise the simulation time. A multilinear isotropic hardening material's engineering data were developed by defining the true stress and strain curves. Specifically, critical mechanical properties like the yield stress point were derived from literature [19, 20]. It is worth highlighting that changes in the tool used to conduct the process resulted in the integration of two different models into the software for the calculations. These two models will be explained in detail in the following subsections to provide a comprehensive understanding of the numerical simulation process.

4.4.1 Computational Fluid Dynamics

To investigate the compressed air pressure and temperature distributions and values produced by the nozzle design in the contactless SPIF process, a computational fluid dynamic model (CFD) using fluent from ANSYS software was utilised. As depicted in **Figure** 4-2**a**, the simulation model consisted of three main parts: a reducer, a sheet, and a closed environmental box. The reducer was designed with a 33 mm inlet diameter, a 5 mm outlet diameter, and a height of 55 mm to control the temperature and pressure of the air flowing out from the heater. The temperature, pressure, flow rate and of the air flowing towards the sheet were also analysed. To model a deformed sheet, a polycarbonate sheet was included in the simulation under the nozzle outlet, positioned 6 mm away from the reducer nozzle. This allowed for the prediction of the pressure and temperature values reached on the top surface of the sheet during the forming process. Finally, a closed box was incorporated into the model to establish a closed environmental boundary, as depicted in **Figure** 4-2**a**. This was essential to account for the effects of the surrounding environment during the forming process. The use of the fluent model allowed for a more in-depth analysis of the process and provided valuable insights into the

performance of the new reducer design concept.

Regarding the meshing strategy for the CFD simulation, a hybrid mesh was created using a combination of structured and unstructured meshing techniques. The areas surrounding the nozzle and sheet were meshed with a relatively coarse element size of 1×10^{-3} m to minimise computational expense while still providing sufficient resolution to capture the overall flow behavior. However, in regions of high flow complexity, a finer mesh was necessary to accurately capture the details of the flow field. Therefore, a fine inflation mesh with 5 layers was implemented on the wall inside the nozzle and in the area between the nozzle and the sheet, with an element size of 1.5×10^{-6} m. This technique allows for a smooth transition between the coarse and fine meshes, ensuring that the numerical solution is accurately resolved across the entire domain. The mesh was created using a combination of commercial software tools and manual refinement to ensure optimal mesh quality and resolution. To provide a better understanding of the mesh employed in the study, a detailed figure (**Figure** 4-2**b**) is included that shows the mesh structure and layout. The figure highlights the regions where the fine inflation mesh was used and demonstrates the smooth transition from the coarse to the fine mesh.

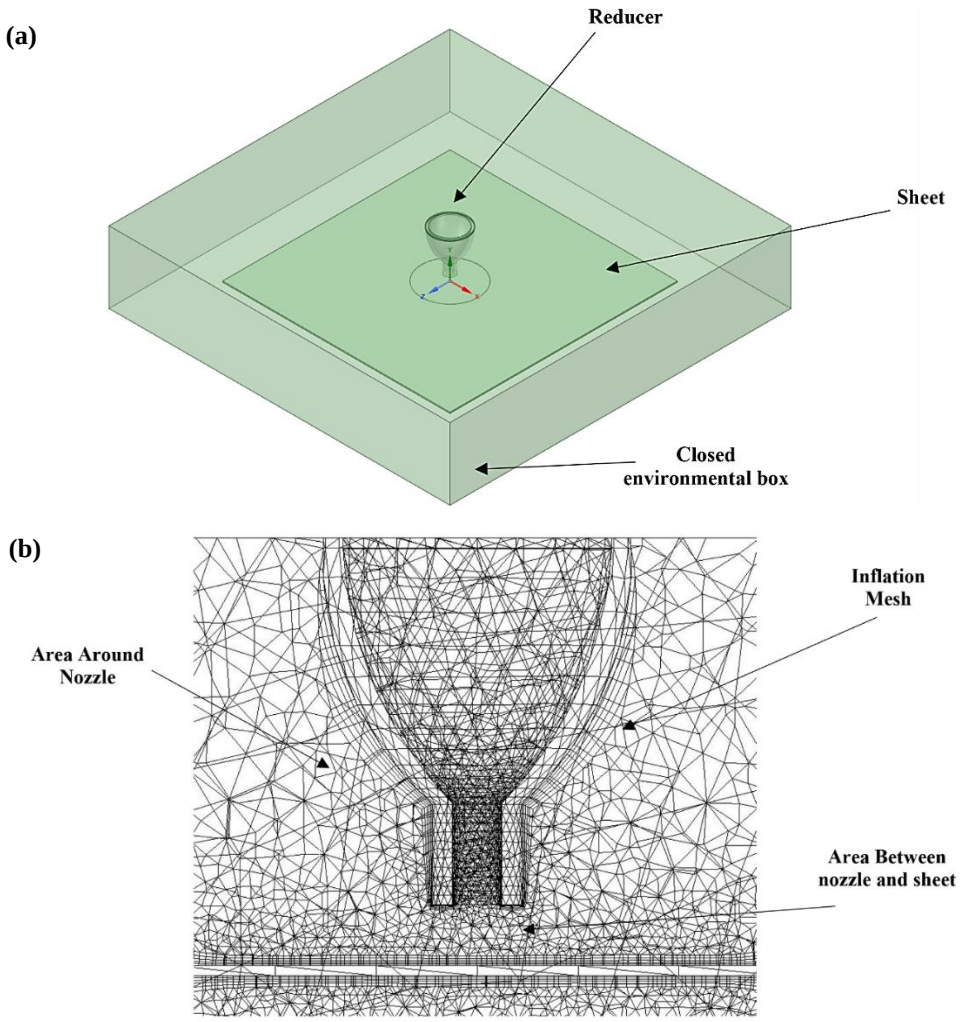

Figure 4-2 (a) The three main components employed for the simulation of the CFD model, (b) the created mesh for the CFD model.

The viscous turbulence model k-ε is a widely used model in the field of computational fluid dynamics (CFD) that is designed to simulate turbulent flows. This model was employed in the analysis, with the aim of accurately predicting the behavior of the fluid being studied. The model is based on two transport equations, one for the turbulent kinetic energy k (see **Equation 4.1**) and one for the turbulent dissipation rate ε (see **Equation 4.2**). These equations are used to derive the rate of dissipation and kinetic energy of turbulence.

The use of the k-ε model in FLUENT was first suggested by Launder and Spalding [22] and has since become a fundamental tool for actual engineering flow computations. Its accuracy and ability to provide reliable results for a wide range of turbulent flows make it an essential tool for engineers and scientists in many fields.

It is important to note, however, that the typical k-ε model is only applicable for completely turbulent flows. In other words, it may not be suitable for certain types of flows, such as laminar or transitional flows, and other turbulence models may need to be used in those cases. To simulate the behavior of the fluid accurately, the SIMPLEC algorithm was used in the simulation. This is a numerical method for solving the Navier-Stokes equations that is often used in CFD simulations. It is designed to provide accurate and reliable results while minimising computational costs. The combination of the k-ε model and the SIMPLEC algorithm provided a powerful tool for analysing and simulating turbulent flows. The equations governing the k-ε model, namely **Equation 4.1** and **Equation 4.2**, played a crucial role in accurately predicting the behavior of the fluid and ensuring the reliability of the results obtained [23, 24].

$$\frac{\partial}{\partial t}(\rho k) + \frac{\partial}{\partial xi}(\rho k ui) = \frac{\partial}{\partial xj}[(\mu + \frac{\mu t}{\sigma k})\ \frac{\partial k}{\partial xj})] + Gk + Gb - \rho\varepsilon - YM + Sk \qquad \textbf{(4.1)}$$

And

$$\frac{\partial}{\partial t}(\rho\varepsilon) + \frac{\partial}{\partial xi}(\rho\varepsilon ui) = \frac{\partial}{\partial xj}[(\mu + \frac{\mu t}{\sigma\varepsilon})\ \frac{\partial\varepsilon}{\partial xj})] + C1\varepsilon\varepsilon k(Gk + C3\varepsilon Gb) + C2\varepsilon\rho\varepsilon 2k + S\varepsilon \qquad \textbf{(4.2)}$$

where Gk is the kinetic energy of turbulence that is made by mean velocity gradients. Gb is the amount of kinetic energy that is added to turbulence because of buoyancy. YM is the amount that fluctuating dilatation in compressible turbulence adds to the overall rate of dissipation. C1,

C2, and C3 are constants. σk and $\sigma \varepsilon$ and are the turbulent Prandtl numbers for k and ε, respectively. Sk and Sε are source terms that were made by users.

In the simulation, time step increments were set to be steady, meaning that the time between each step remained constant throughout the simulation. This was done to ensure accurate and consistent results. To model the behavior of the air in the simulation, ideal gas properties were chosen for the air. The inlet air pressure was set to 1 bar, which is a measure of the air pressure at the inlet boundary. Additionally, the inlet temperature was set to 160℃, which is the temperature at the inlet boundary.

4.4.2 Forming Model

The second model aimed to analyse the deformation of the polycarbonate sheet. This was an important aspect to consider, as the final product needed to maintain its structural integrity under various conditions and achieve high quality geometrical precision. The model was created using ANSYS Parametric Design Language (APDL), which proved to be the most efficient way to represent the deforming tool, in this case, hot compressed air. The thermal element type SOLID226 was defined in the geometry section at the beginning of the model creation to allow the model to read the heat on the sheet. To simulate the path-moving design for the deformation, forty different coordinates in the X, Y, and Z directions were defined. An example of the tool path programmed for one experimental trial, see **Figure** 4-3**(a-b)**. The sheet was meshed with a total of 12,141 elements to ensure accurate representation, see **Figure** 4-3**c**. The movement of the hot pressure air over the plate occurred along the X and Z directions, while the step-down motion occurred along the Y direction, see **Figure** 4-3**e**. In order to obtain accurate results, temperature-dependent polycarbonate material data were considered and assigned to the sheet.

According to the boundary condition, the sheet was assumed to be fixed at the edges, while the middle was free to deform. Additionally, the gravity force was taken into account and applied to the sheet to make it closer to the real case. The results of the hot compressed air from the fluent model were applied to the APDL commands. The pressure and temperature values obtained were displayed along the defined circle source. Furthermore, the specific path followed by the air source and nozzle was added to the model as a code following the coordinates previously determined. The air source, which had a diameter of 6 mm, was moved in the X and Z directions at a speed of 0.75 m/min. After one complete revolution, the step-down motion was simulated at a speed of 10 m/min in the X, Y, and Z directions to move the air source to the next step. After ten full paths with their corresponding steps were completed, the final shape of the sheet was calculated. This process was crucial in ensuring that the sheet would maintain its desired shape even under different conditions, and the model created allowed for accurate representation and analysis of the deformation process.

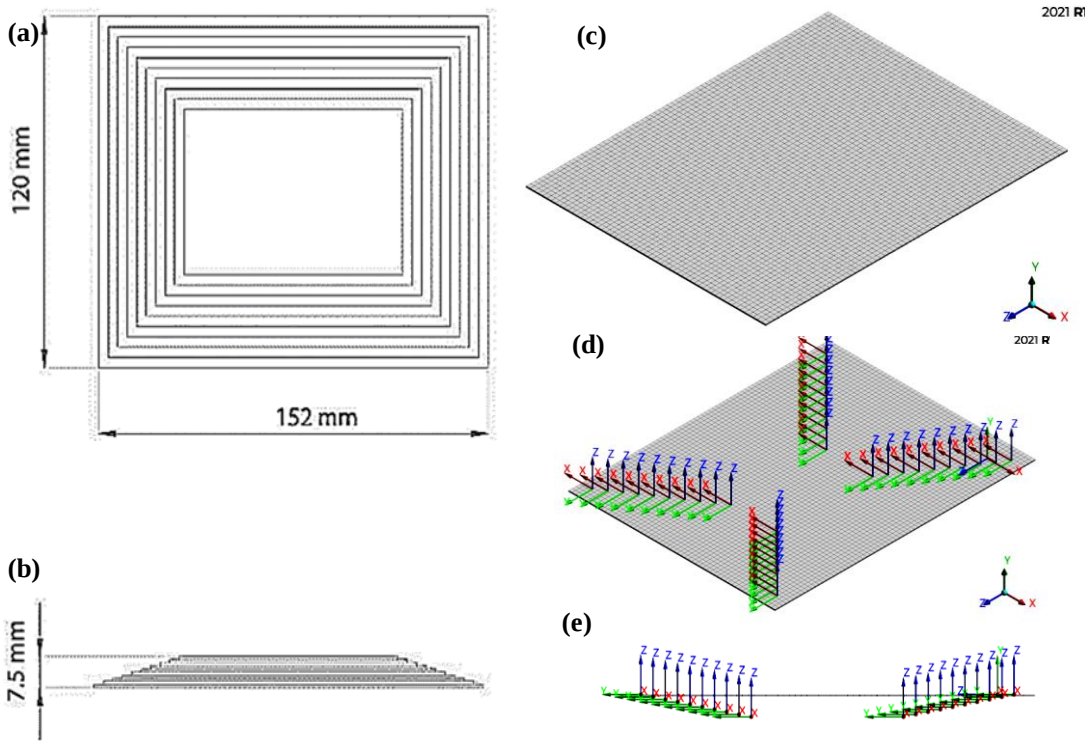

Figure 4-3 (a) top view showing the tool tracks on the XZ plane and (b) side view showing the step downs in the Y direction, (c) the developed mesh (d) the sheet X and Z Coordinates, (e) sheet Y direction.

4.5 Results and discussion

4.5.1 Forming Hot Air Motion

Figure 4-4 provides the CFD simulation of a detailed visualization of the compressed air pressure and temperature distributions along the radial direction on the polymer sheet as the air flows through the reducer channel and hits the polycarbonate sheet. The figure clearly shows the variations in pressure and temperature along the radial direction, providing important insights into the behavior of the fluid and the overall outcome of the simulation.

The pressure and temperature distributions are critical parameters to consider when analysing the behavior of pressured hot air when passing over the polycarbonate sheet. The pressure distribution can influence the velocity and direction of hot air, while the temperature distribution can affect the thermodynamic properties of the air, such as density and viscosity, which in turn can impact the polycarbonate. As presented in **Figure** 4-4**(a,b)**, the upper surface of the sheet reaches a pressure value of 0.078 MPa and a temperature of 154℃. These values were employed as input for the second structural model utilised in this study.

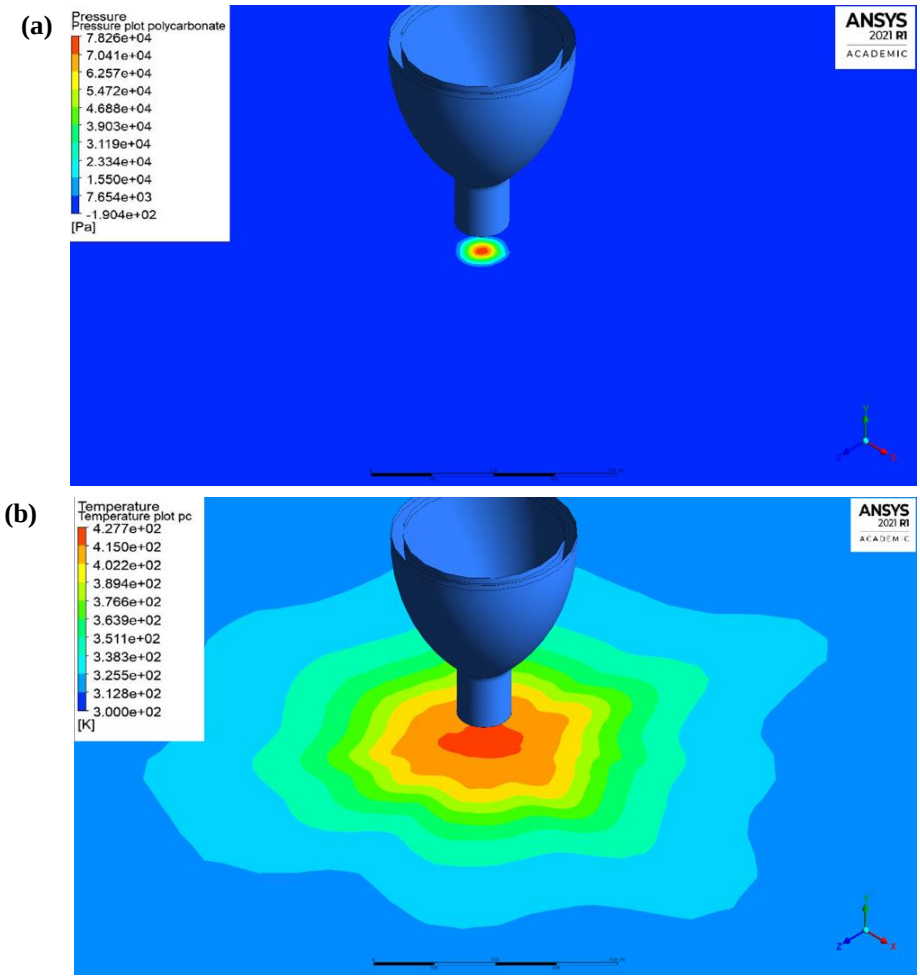

Figure 4-4 (a) Pressure distribution, (b) Temperature distribution.

4.5.2 Mesh sensitivity

The employed mesh sensitivity utilised elemental nodal forces to calculate the equivalent stress. To obtain a more stable model, a range number of elements was used to assess the effect of the elements number on the developed stresses and computing time, see **Figure** 4-5**a**. The CPU time increased from 27 minutes to 426 minutes when the number of elements increased from 2160 (coarse mesh) to 15600 (fine mesh), respectively.

Despite the increase in CPU time, the accuracy of the equivalent stress calculation also improved with the increasing number of elements (**Figure** 4-5**a**). This demonstrates the

importance of mesh sensitivity studies in accurately capturing the deformation behavior of the sheet and highlights the trade-off between computational efficiency and accuracy in FEM simulations.

As a result, it was determined that equivalent stress did not change significantly after 6450 elements and reached a stable mode at the 12141 elements count. Since the mesh composed of 12141 elements produced a stable result and increasing the number of elements over 12141 increased the computational time without improving the precision of the model, the 12141 elements mesh was chosen to be employed for evaluating the simulation results. Figure 5b illustrates a comparison between the predicted deformation values generated by the FEM and the actual deformation values measured from the experimentally formed sheet. By analysing the agreement between the predicted and measured values, the accuracy of the simulation model can be evaluated.

To ensure that the results obtained from the Finite Element Method (FEM) simulation accurately represent the experimental sheet profiles, the clamped workpiece was measured using a Mitutoyo Coordinate Measuring Machine Euro-CA776 (CMM). This allowed for the displacement boundary conditions specified in the FEM simulation to be replicated and matched to the displacement boundary requirements specified in the model and design drawing. The use of the CMM also eliminated any inaccuracies that may have occurred during unclamping and cooling, thereby enabling the effects of the new system to be seen more clearly. However, it was observed that the experimental profile shapes were significantly different from the simulated profiles when a coarse mesh was used (**Figure** 4-5**b**). This discrepancy can be attributed to the fact that a coarse mesh cannot accurately capture the complex deformation behavior of the sheet.

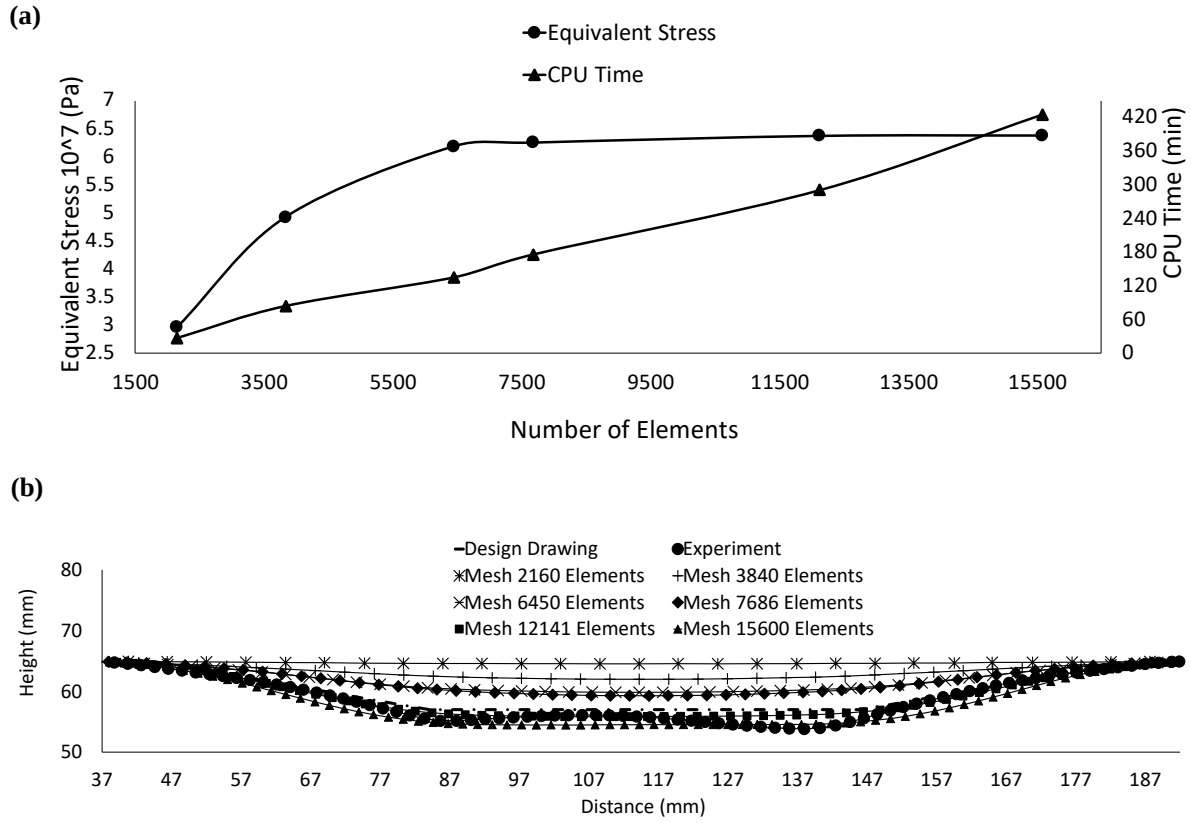

Figure 4-5 Mesh Sensitivity (a) equivalent stress vs number of elements (b) comparison between FEM and experimental sheet profile.

4.5.3 Geometric Profile

The model-predicted sheet final shape is seen in **Figure** 4-6**a**. The simulation shows that successful sheet deformation can be achieved by employing the new contactless technique described in this study. Furthermore, **Figure** 4-6**(b-d)** depicts a truncated pyramid part produced using the innovative contactless contactless SPIF process. As shown, the profile obtained at 160°C closely resembled the CAD design drawing profile, which demonstrates the effectiveness of the proposed technology. The contactless nature of the CSPIF system ensures that there is no tool-to-sheet contact, which reduces the risk of damage to the sheet and extends the life of the tool. The figure also demonstrates visible surface texture differences and

waviness. This illustrates the influence of the forming path on the part's surface and provides insight into the quality and accuracy of the formed part.

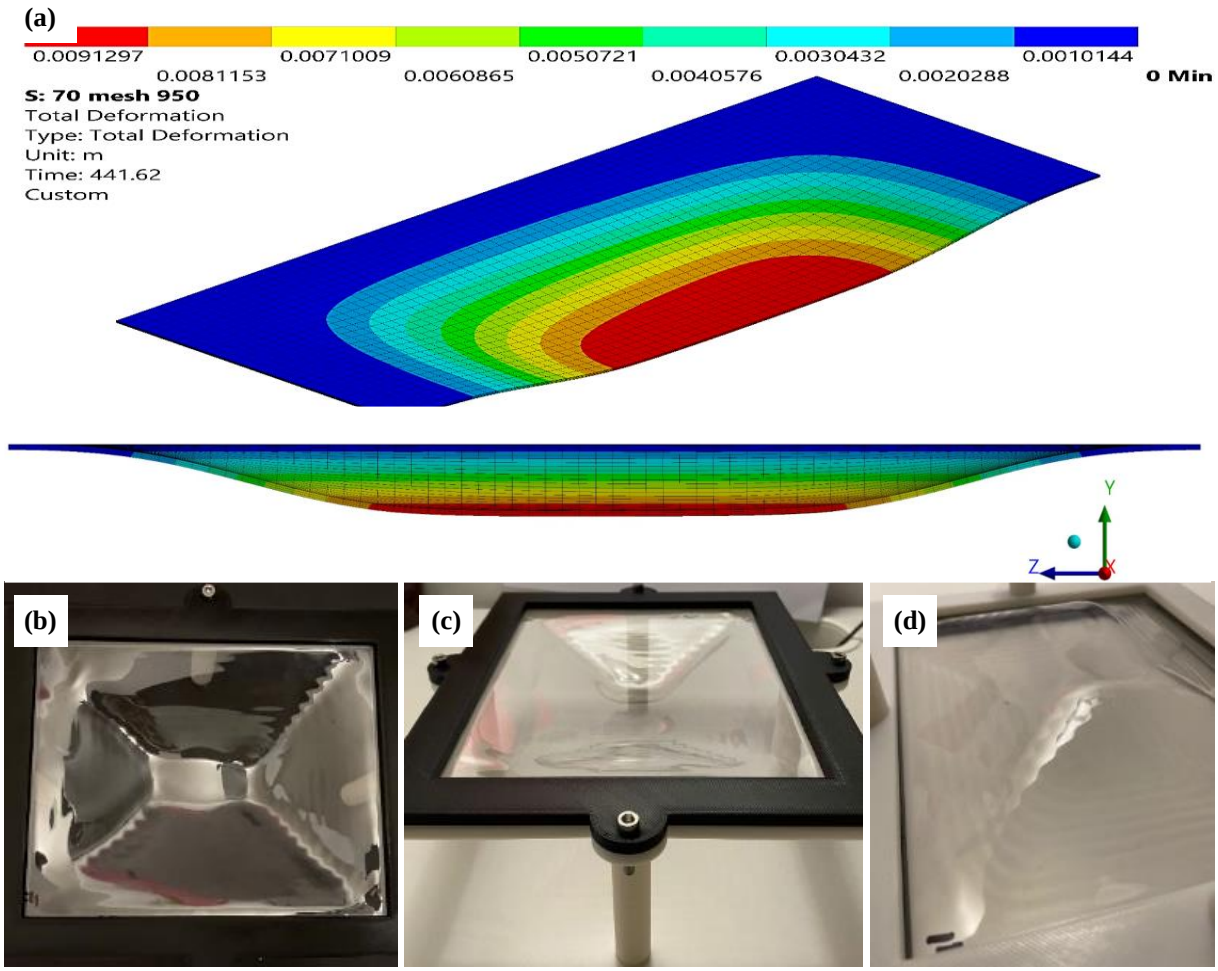

Figure 4-6 (a) Sheet deformation results obtained by the model. (b-d) Images of the truncated pyramid part created in this work by using the contactless contactless SPIF process.

Validation of simulation results was carried to ensure that the model accurately represents the physical system under investigation. In this study, CMM was used to measure the profile of the experimental result and compare it with the simulated and designed profiles. The CMM collected the "points cloud" of the formed truncated pyramid shape part that indicates the geometry of the workpiece. This allows for the computation of the profile and thickness of the deformed part, which can be compared with the simulation and design drawing data.

Figure 4-7 presents a comparison of the model-obtained profile, the experimentally measured profile, and the designed profile of the workpiece manufactured at 160°C. To represent the model outcome, a cut section from the middle of the sheet was used, and the path from the workpiece edge to the centre was determined using Ansys software. SolidWorks software was used to obtain the design drawing profile data, which included a path from the workpiece edge to the centre.

The comparison of the profiles allows for a comprehensive analysis of the accuracy of the model. As presented in **Figure** 4-7**i**, the FEM results is in a good agreement with the measured profile of the polycarbonate sheet. However, there are few areas (a-c) in the figure that shows discrepancies between the simulated and measured data, and the model can be improved upon to better represent the physical system.

In Single Point Incremental Forming (SPIF), the distance between the forming region and the sheet flange plays a critical role in determining the quality of the formed part. A narrow distance is preferred as it helps to minimise the bending impact at the major [25]. However, due to geometric limitations, the nozzle movement cannot be initiated from the sheet's original location, which generates a bending effect. This bending effect can impact the quality of the formed part, and therefore, it is essential to understand and minimise this effect. To better understand the bending effect, the horizontal and vertical displacements in deflection for a plastic sheet deformed by pressurised hot air and subjected to a vertical constant force and constant bending at the starting point of the nozzle was determined as (**Figure** 4-7**ii**) [20, 22]. It was suggested that the distance between the fixed edge and the initial location of the nozzle should be minimised to reduce the bending effect. Additionally, other factors such as the sheet material properties, toolpath, and process parameters can also be optimised to minimise the bending effect and improve the quality of the formed part [26, 27]. The deformation between

points (a) and (b) in **Figure** 4-7**i**, follows a similar trend for the measured profile results in **Figure** 4-7**i**. However, at the bottom corner in (b), the deformation for the model and the experiment profiles is greater than the designed one due to the high heating generated by the short path length, which causes the heat tail to overlap and the cooling to be extremely slow. The temperature distribution was measured using an RS T-10 smart thermal camera with 5% accuracy, and it was found that the temperature was eventually reaching 205 °C, see **Figure** 4-8.

The study also observed minimal springback at the base of the pyramid, indicating that the process was able to accurately deform the polycarbonate sheet. However, a pillow effect was observed in the centre as shown in (c) **Figure** 4-7**i**, which could be attributed to the local heating of the sheet during the forming process [28]. The successful application of a hot compressed air tool has continued to improve the deformation process, and the developed numerical model is able to predict the deformations and the final shape of the PC sheet with very low mismatch. In fact, the acquired profile at 160 °C appears acceptably similar to the predicted and designed profiles.

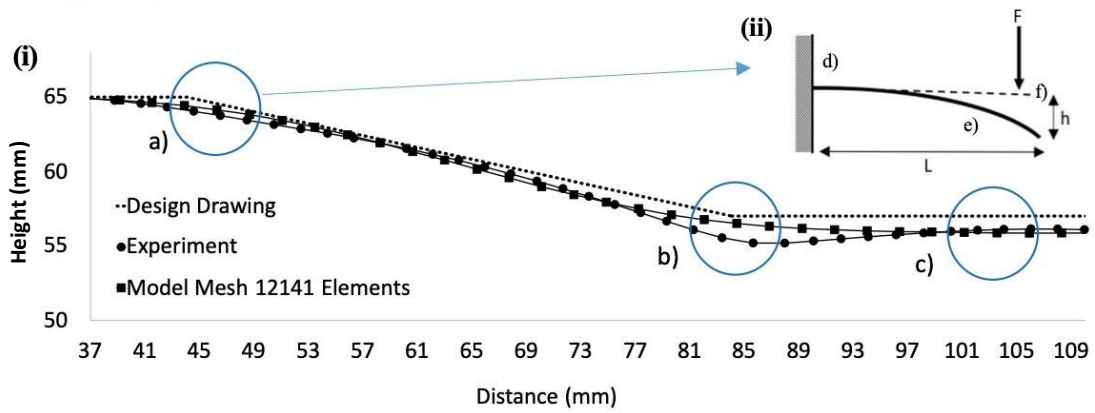

Figure 4-7 (i) Comparison between model output, design drawing and experimental profile,

(ii) bending effect at (d) edge of the sheet; (f) sheet before applying force; (e) sheet after applying force; (L) length from edge to starting point; (h) displacement from bending effect; (F) nozzle force position.

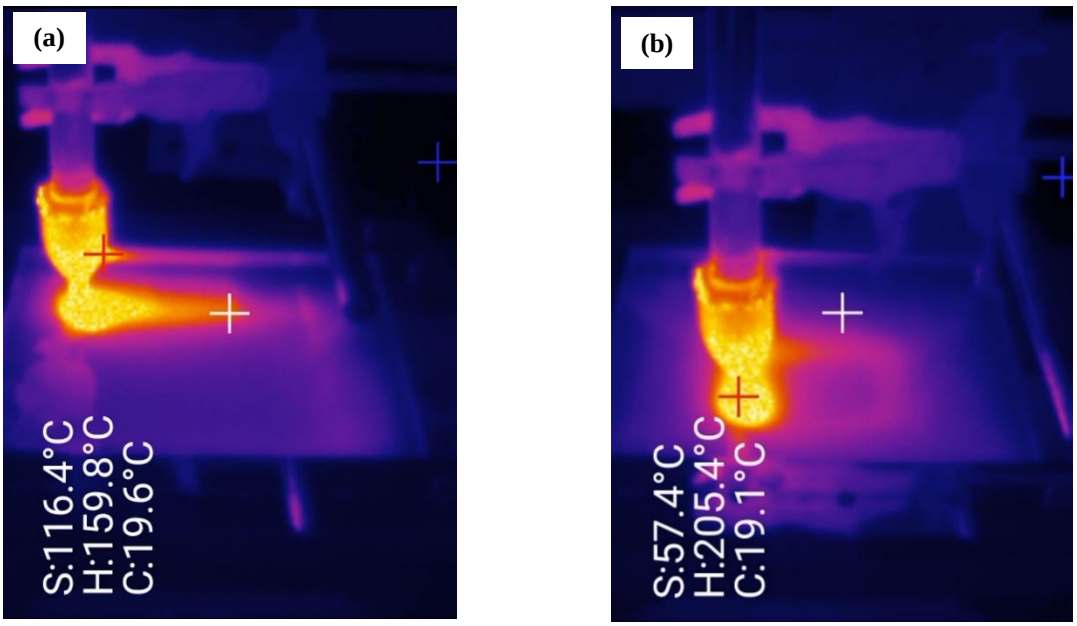

Figure 4-8 Temperature tail at the (a) first path and (b) last path with tail overlapping. S, H and C are representing surrounding, hot and cold spots, respectively.

4.5.4 Stretching and Thinning

To investigate stretching and thinning of the polycarbonate sheet during the forming process, the history of the strain component of two control elements are chosen from the pyramid's upper surface was carried out **(Figure** 4-9**a**): the former is situated in the middle, higher section of profile wall, while the latter is situated in the lower region, close to the pyramid's base. A local coordinate system is used to measure the strain components. It is important to note that **Figure** 4-9**b** shows that element 1 and element 2 were on the fourth and the last path of the heating source, respectively.

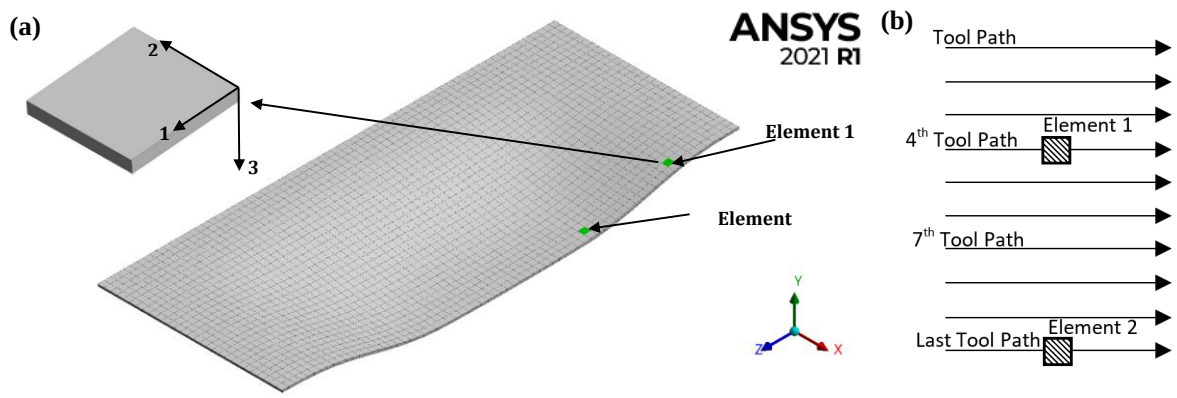

Figure 4-9 (a) Selected elements along the cut profile wall, (b) Location of the selected elements in regard to the path number.

The equivalent plastic strain analysis depicted in **Figure** 4-10 provides insights into the stretching and thinning of the polycarbonate sheet during the forming process. The figure illustrates the strain components for directions 1 and 3, namely ε11 and ε33, respectively, which have significant values in the 1-3 plane. As the heat source began to move, the sheet started to deform gradually, leading to the deformation process, which is explained in detail as follows:

At point (a), the heat source is on the second path and two steps-down from the first control element, causing a slight increase in temperature and strain. This trend continues as the source moves to the third path and one step-down from the first element at point (b), leading to a larger deformation compared to point (a).

At point (c), the source is on the same path as the first control element, resulting in a further increase in strain. However, after this point, the strain value decreases due to springback. At point (d), the source is one step further from the first element and heats it to 73.4 °C, causing it to reshape again. Although the temperature changes slowly in the range of ±4°C, it does not affect the equivalent strain of Element 1. The same effect can be seen at point (e), where the

temperature increases by only 0.2 °C, causing a change in the equivalent strain at the second control element. However, the amount of strain change is less than that observed at point (a).

At point (f), the source is one path before the second control element, and the strain amount is lower than that observed at point (b) due to material built-up at the bottom corner of the tool path, which reduces the strain of the element. At point (g), the source is on the same path as the second control element, and the strain value rises as shown at point (c) for Element 1. However, there is no drop in strain as observed at point (d) since this is the last path of the tool, and the element is not heated with the air source again.

The strain grows gradually with the deformation of the elements. The major types of deformation during the proposed process are sheet stretching associated with ε11, sheet thinning associated with ε33, and sheet bending in the region adjacent to the sheet flange, as demonstrated in **Figure** 4-11. These findings are consistent with previous studies by Hirt et al. [29] and Ambrogio et al. [30], which also reported the dominance of these deformation modes in SPIF. However, the employment of only two elements across the sheet is insufficient to acquire precise results on through-thickness shear strains. Several studies have aimed to tackle this problem by employing different methods of measuring strain, such as FEM, strain gauges, and digital image correlation. For instance, Mirnia et al. [31] used digital image correlation to measure the strain field during the SPIF process and reported that the maximum shear strain occurs in the flange region, which is consistent with the bending behavior observed in **Figure** 4-11.

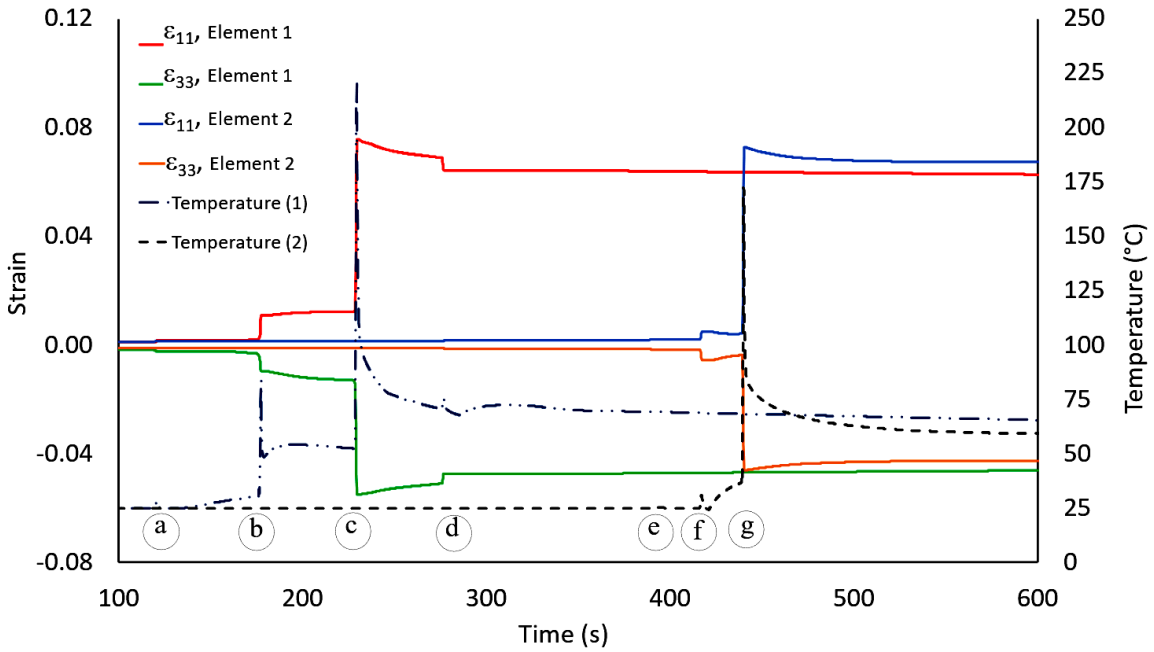

Figure 4-10 Strain history on the Element 1 and Element 2.

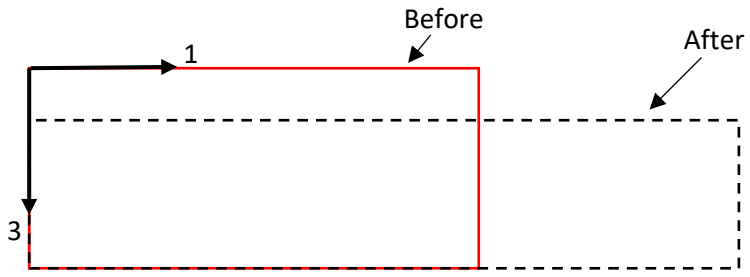

Figure 4-11 Stretching and thinning phenomena on the elements.

4.6 Conclusion and Future Work

In the present study, a novel contactless single point incremental forming (SPIF) process is presented, which utilises innovative pressured hot air nozzle as a deforming tool for polymers forming. A finite element models was developed and implemented combine CFD and transient structural calculations to predict the deformation of a sheet under specific air pressure and temperature conditions. The CFD model is used to calculate the local distribution of the

temperature and pressure of the air that hits the polycarbonate sheet, while the transient structural simulation is employed to calculate the deformation on the sheet. A truncated pyramid tool path is set, and an overall 7.5 mm depth track is simulated in 10 steps. To validate the model, the predicted sheet deformation is compared to the one generated experimentally, and the results obtained are in good agreement. The comprehensive FE model is able to predict the formed part geometries in addition to the normal strain progression. Moreover, it reveals that the primary modes of deformation in SPIF are stretching, thinning, and bending. Based on the results obtained, it can be stated that the model developed in this work is able to accurately predict sheet deformation generated through the contactless SPIF method proposed. The results of this study establish a solid groundwork for advancing and refining the contactless SPIF process. Furthermore, the use of additional polymer or low melting point metal materials could further enhance the process's potential for diverse applications in fields like automotive, aerospace, and biomedical engineering. This study's findings open up new avenues for exploring innovative designs and optimizing the contactless SPIF process to achieve superior outcomes in various applications.

4.7 References

1. Dewang Y., Sharma V.Sheet (2023) metal shrink flanging process: a critical review of current scenario and future prospects, Mater. Manuf ., 38, 629-658.DOI: 10.1080/10426914.2022.2149779.

2. Kopac J., Kampus Z. (2005) Incremental sheet metal forming on CNC milling machine-tool, J. Mater. Process. Technol. 162-163, 622-628.DOI: https://doi.org/10.1016/j.jmatprotec.2005.02.160.

3. Chenghui Z., Feifei Z., Bo W., Yangjun L., Kai H., Ruxu D. (2021) Digital twin-based stamping system for incremental bending, Int. J. Adv. Manuf. Technol. 116, 389-401.DOI: 10.1007/s00170-021-07422-7.

4. Edwards W. L., Grimm T. J., Ragai I., Roth J. T.(2017) Optimum process parameters for springback reduction of single point incrementally formed polycarbonate, Procedia Manuf. 10, 329-338.

5. Zhu, H., Ou, H., and Popov, A. (2020) Incremental sheet forming of thermoplastics: a review, Int. J. Adv. Manuf. Technol. 111, 565-587.DOI: 10.1007/s00170-020-06056-5.

6. Silva M. B., Martinho T. M.,Martins P. A. F. (2013) Incremental Forming of Hole-Flanges in Polymer Sheets, Mater. Manuf 28, 330-335.DOI: 10.1080/10426914.2012.682488.

7. Durante M., Formisano A., Lambiase F. (2019) Formability of polycarbonate sheets in single-point incremental forming, Int. J. Adv. Manuf. Technol. 102, 2049-

2062.DOI: 10.1007/s00170-019-03298-w.

8. Martins P. A. F., Kwiatkowski L., Franzen V., Tekkaya A. E., Kleiner, M. (2009) Single point incremental forming of polymers, CIRP Annals 58, 229-232.DOI: https://doi.org/10.1016/j.cirp.2009.03.095.

9. Franzen V., Kwiatkowski L., Martins P. A. F., Tekkaya, A. E. (2009) Single point incremental forming of PVC, J. Mater. Process. Technol. 209, 462-469.DOI: https://doi.org/10.1016/j.jmatprotec.2008.02.013.

10. Kulkarni S. (2016) Heat Assisted Single Point Forming of Polymer Sheets, 10. Kulkarni, S.Heat Assisted Single Point Forming of Polymer Sheets, 2016, Proceedings of the ASME 2016 International Design Engineering Technical Conferences and Computers and Information in Engineering Conference. Charlotte, North Carolina, USA. August 21–24, 2016. V004T05A006. ASME. https://doi.org/10.1115/DETC2016-6003.

11. Fontanari V., Benedetti M., Bruschi S., Fuganti A. (2012) Numerical and experimental analysis of the single point sheets incremental forming process, 15th International Conference on Experimental Mechanics, Porto/Portugal, 22-27.

12. Eksteen P., Van der Merwe, A. (2012) Incremental sheet forming (ISF) in the manufacturing of titanium based plate implants in the bio-medical sector, Proceedings of 42nd computers and industrial engineering, 15-18.

13. Thibaud S., Hmida R. B., Richard F., Malecot P. (2012) A fully parametric toolbox for the simulation of single point incremental sheet forming process: Numerical

feasibility and experimental validation, Simul Model Pract Theory 29, 32-43.

14. Abass K. (2016) A study on using pre-forming blank in single point incremental forming process by finite element analysis, IOP Conference Series: Materials Science and Engineering 161, 012031.

15. Neto D., Martins J., Oliveira M., Menezes L., and Alves, J. (2016) Evaluation of strain and stress states in the single point incremental forming process, Int. J. Adv. Manuf. Technol. 85, 521-534.

16. Guzmán C. F., Gu J., Duflou J., Vanhove H., Flores P., Habraken A. M. (2012) Study of the geometrical inaccuracy on a SPIF two-slope pyramid by finite element simulations, Int. J. Solids Struct. 49, 3594-3604.

17. Araghi B. T., Manco G., Bambach M., Hirt, G. (2009) Investigation into a new hybrid forming process: Incremental sheet forming combined with stretch forming,CIRP annals 58, 225-228.

18. Gómez-López L., Miguel V., Martínez A., Coello J., Calatayud, A. (2013) Simulation and modeling of single point incremental forming processes within a solidworks environment, 2013, Procedia Eng. 63, 632-641.

19. Richeton J., Ahzi S., Vecchio K. S., Jiang F. C., Adharapurapu R. R. (2006) Influence of temperature and strain rate on the mechanical behavior of three amorphous polymers: Characterization and modeling of the compressive yield stress, Int. J. Solids Struct. 43, 2318-2335.

20. Dar U. A., Zhang W., Xu Y., Wang J. (2014) Thermal and strain rate sensitive

compressive behavior of polycarbonate polymer-experimental and constitutive analysis, J. Polym. Res. 21, 1-10.

21. Fisher, F. and L.C. Brinson. Macroscale experimental evidence of a reduced-mobility non-bulk polymer phase in nanotube-reinforced polymers. in 44th AIAA/ASME/ASCE/AHS/ASC Structures, Structural Dynamics, and Materials Conference. 2003.

22. Launder B., Spalding D.The numerical computation of turbulent flows (1974). Comput. Methods Appl. Mech. Eng, 3, 269–289.

23. Adanta D., Fattah I. R., Muhammad N. M. (2020) Comparison of standard k-epsilon and sst k-omega turbulence model for breastshot waterwheel simulation, J. Mech. Eng. Sci. 7, 039-044.

24. Muralha, A., Melo, J. F., and Ramos, H. M.Assessment of CFD solvers and turbulent models for water free jets in spillways, 2020,Fluids 5, 104.

25. Micari, F., Ambrogio, G., and Filice, L.Shape and dimensional accuracy in single point incremental forming: state of the art and future trends, 2007,Journal of Materials Processing Technology 191, 390-395.

26. Borboni, A., and De Santis, D.Large deflection of a non-linear, elastic, asymmetric Ludwick cantilever beam subjected to horizontal force, vertical force and bending torque at the free end, 2014,Meccanica 49, 1327-1336.

27. Archansdran, S., Shaari, M., and Rosly, M.Characterization of double layer IPMC bending actuation, 2016,ARPN J. Eng. Appl. Sci. 11, 6536.

28. Mohanraj Murugesan M. S., Jung D. W. 2020 Experimental Investigations on Incremental Sheet Forming of Commercial Aluminum Alloys for Maximum Production Quality, Int. J. Mech. Eng. Robot. Res. 9, 1264-1270.

29. Hirt G., Bambach M., Junk S. (2003) Modelling of the incremental CNC sheet metal forming process, Proceedings of the 10th International Conference on Sheet Metal, 495-502.

30. Ambrogio G., Filice L., Fratini L., Micari F. (2004) Process mechanics analysis in single point incremental forming, AIP Conference Proceedings 712, 922-927.

31. Mirnia M. J., Shamsari M. (2017) Numerical prediction of failure in single point incremental forming using a phenomenological ductile fracture criterion, J. Mater. Process. Technol. 244, 17-43.DOI: https://doi.org/10.1016/j.jmatprotec.2017.01.029.

5 Optimisation of A Novel Hot Air Contactless Single Incremental Point Forming of Polymers

Mohammad Almadani [a,b], Ahmet Guner [a], Hany Hassanin[c] , Khamis Essa [a]

[a] *Mechanical Engineering, University of Birmingham, Edgbaston, Birmingham, B15 2TT, UK*

[b] *Department of Mechanical Engineering Technology, Yanbu Industrial College, Yanbu Al-Sinaiyah City, 41912, Kingdom of Saudi Arabia.*

[c] *School of Engineering, Technology, and Design, Canterbury Christ Church University, B15 2TT, UK*

This research was published as a full-length research article in Journal of Manufacturing Processes:

Mohammad Almadani, Ahmet Guner, Hany Hassanin, and Khamis Essa, *Optimisation of A Novel Hot Air Contactless Single Incremental Point Forming of Polymers.* Under review by Journal of Manufacturing Processes.

Credit authorship contribution statement

Mohammad Almadani: Conceptualisation, Investigation, Methodology, Validation, Software Formal analysis, Writing - original draft.

Ahmet Guner: Reviewing & editing, Supervision.

Hany Hassanin: Writing - review & editing, Supervision.

Khamis Essa: Writing - review & editing, Resources of lab equipment, Supervision, Project Administration**.**

Research contributions:

This chapter aims to complete the objective 5 and 6 which cover the following insights:

- A novel sheet forming process was developed and called Hot Air contactless Single Point Incremental Forming using a commercial 3D printer equipped with a hot air nozzle as a deforming tool.

- The new deforming method eliminates physical contact between the forming tool and the polymer sheet, reducing costs and eliminating the need for a rigid tool.

- 54 different forming conditions evaluated using DoE methodology and response surface Method.

- The DOE results show that air pressure, air temperature, and feed rate identified as significant variables, whereas Tool offset had no discernible effect.

- Increasing feed rate decreased profile variation, thickness variation, and surface roughness.

- A prediction model was developed and used to optimise the process conditions.

5.1 Abstract

This study presents a new contactless sheet forming method that utilises hot air as a forming tool to address tool wear challenges in single-point incremental forming. Experiments were conducted on a 3-axis CNC machine equipped with a hot air nozzle on a polycarbonate sheet. A design of experiment (DOE) approach was employed, evaluating five control factors: air pressure, air temperature, feed rate, tool offset, and step down. The evaluation criteria for the formed sheets are profile variation, thickness variation, and surface roughness. The results indicate that air temperature and feed rate have the most significant influence on the deformation process. Additionally, air pressure and feed rate substantially impact both thickness variation and surface roughness of the formed material. To optimise the process parameters for high-quality forming, a prediction model is developed. The optimised process shows good agreement with the predicted model regarding profile and thickness variations. However, it does not align with surface roughness due to the stepwise nature and inherent waviness of the contactless forming technique. This study offers a promising approach for developing innovative contactless forming techniques using hot pressurised air as a forming tool. The proposed technique has the potential to significantly reduce tool wear and lubrication requirements.

Keywords: Sheet forming, Response surface methodology, contactless incremental forming, formability, design of experiment.

5.2 Introduction

Single Point Incremental Forming (SPIF) is an efficient and versatile alternative to conventional forming techniques, particularly for low-volume batches, prototypes, and specialised parts. Unlike traditional forming methods, SPIF doesn't necessitate expensive or specialised tools. Instead, a rigid tool follows a series of planar shapes or a single spiral contour to create parts. This recent process has unlocked new possibilities for sheet forming, eliminating the need for a specific die. It's a manufacturing technique that employs a customisable tool to shape sheets into specific configurations. Through the utilisation of computer numerically controlled (CNC) technology, SPIF can achieve high precision and accuracy, allowing for the creation of complex shapes with minimal lead time and low forming forces. These advantages make SPIF an exceptionally adaptable and flexible manufacturing process that harmonises with the demands of Industry 4.0 [1-3].

In the aerospace industry, SPIF is employed to manufacture lightweight components with intricate shapes, including aircraft panels and engine components. SPIF offers the advantage of reducing material waste while ensuring high precision, rendering it a highly suitable manufacturing process for the aerospace industry [4, 5]. The automotive industry also reaps the benefits of SPIF, particularly in the production of low-volume components with complex geometries, like exhaust systems and car body parts. SPIF's capability to achieve high formability with minimal tooling costs positions it as an ideal solution for the automotive industry [6-8]. In the biomedical industry, SPIF has found application in the manufacturing of implants, including orthopedic implants and dental prostheses. SPIF's precise and customisable forming capabilities have rendered it an appealing alternative to traditional manufacturing processes [9].

The single-point incremental forming process has garnered researchers' attention for improving its forming results and eliminating defects. Several investigations have focused on the process elements that significantly impact the performance of Single Point Incremental Forming (SPIF). These factors include the thickness of the sheet, the depth of vertical steps, the size and speed of the forming tool, the use of lubrication, and the quality of the material. For instance, a study by Kim et al. found that using a roller end tool provides better formability than a hemispherical tool when deforming an aluminum alloy sheet [4]. Meanwhile, another study by Azevedo et al. investigated the effects of lubricants on the surface finish of steel (DP780) and aluminum (AA1050-T4) sheets [5]. The authors applied various types of lubricants, including Total Finaro LB5746, Repsol SAE 30, Moly Slip AS 40, Moly Slip HSB, and Weicon AL-M. The study demonstrated that selecting the appropriate lubricant viscosity depends on the hardness of the material being formed to achieve optimal performance. The findings indicated that SAE 30 lubricant produced a smoother surface finish when applied to AA1050-T4, while AS-40 grease resulted in a rougher surface finish. Conversely, AS-40 grease provided a smoother surface finish for steel, while SAE-30 gave a rougher surface finish. Consequently, low-viscosity lubricant is needed for materials with high hardness, whereas high-viscosity lubricant is necessary for materials with low hardness.

While the SPIF process was initially developed for metal materials, it has also been applied to polymeric sheets, thermoplastics, and composite materials. The SPIF process for polymers is a cost-effective method for producing customised product parts from a wide range of materials, including metals, polymers, and composites [10]. The process has been refined over the years through research focused on factors such as sheet thickness, tool size, lubrication, and material properties [11]. The material properties of polymers play a crucial role in determining their suitability for the SPIF process, with factors such as ductility and colour stability impacting the final product's quality. However, achieving successful polymer material formation requires a

thorough understanding of these properties. To address this, Martins and colleagues [8] conducted a comprehensive study to assess the formability of five different types of polymers using SPIF. The study utilised a rigid tool with diameters of 10 and 15 mm and sheet thicknesses of 2 and 3 mm. Each polymer material exhibited unique properties that influenced its suitability for SPIF. For instance, PE and PA showed higher ductility, making them suitable for components with significant wall angles. Conversely, PVC displayed lower springback, making it the ideal choice when high accuracy is required. PC proved excellent for applications demanding high surface quality, as it retained its colour during the incremental cold forming technique. However, POM performed the poorest among all the investigated polymers due to its limited ductility. Additionally, the study revealed colour changes in the polymer materials after the SPIF process, emphasising the importance of considering colour stability when selecting the polymer material for the process.

The SPIF process is influenced by several parameters, including tool size, step size, feed rate, and spindle speed, all of which can significantly impact the final shape of the polymer sheet. A study by Le et al. [12] on the effects of these parameters on forming polypropylene sheets revealed that using a small tool radius reduces the formability of the polypropylene sheet, while an increase in step size decreases the formability and can lead to defects such as final shape wrinkles. The study also found that elevating the spindle speed of the tool increases formability, and using high spindle speeds with small step sizes and large tool sizes can further improve the formability rate of PP sheets. However, despite the success in optimising these parameters, the rigid tool used in SPIF can still lead to several drawbacks and needs to be eliminated from the process. In addition to the effects of traditional SPIF parameters, alternative tools have been explored to improve the process. For example, Jurisevic et al. [13] have suggested using a waterjet nozzle instead of a rigid tool. In their study, it was found that the surface finish of the sheet was notably smoother, and no wear was detected on the tool. Moreover, the equipment

cost was considerably lower, and the entire process was deemed to have a more environmentally friendly impact. The use of a waterjet nozzle was successful in deforming a brass sheet, and the accuracy, energy efficiency, and forming time were better than those achieved with conventional methods. To achieve the best possible results, the researchers conducted a thorough examination of various parameters such as water pressure, stand-off distance, nozzle geometry, and forces at the interface of the tool and the workpiece. After careful analysis, they made necessary adjustments to these parameters to optimise the process [13, 14].

Design of Experiments (DOE) and statistical analysis have been established as effective methods for studying the influence of operating parameters on sheet forming processes. These techniques have been proven to be particularly useful in understanding the effects of various parameters on the forming process, which, in turn, helps optimise the process for superior performance. Statistical methods can provide valuable insights into the process, including identifying the most significant parameters, evaluating the effect of interactions between parameters, and predicting optimal settings for improved performance. Therefore, the use of DOE and statistical analysis has become increasingly popular in various manufacturing processes to enhance the quality of the final product while minimising the cost and time required for production. Yang et al. [15] employed the Taguchi approach to ascertain the optimal working parameters for cutting glass fiber, while Bacchewar et al. [16] utilised response surface Design of Experiments (DOE) and ANOVA methodologies to analyse the pertinent process variables in selective laser sintering. Similarly, Hussain et al. [17] Ham and Jeswiet [18] and Filice et al. [19] all employed DOE methodologies to study the influence of processing parameters, including feed rate, rotational speed, and sheet thickness, on formability in incremental sheet forming.

Ham and Jeswiet [20] conducted two Design of Experiments (DOEs) to identify key factors affecting the SPIF process to achieve effective deformation without defects like tears or cracks. They investigated how these key variables influenced the process's formability. In another study, Ambrogio et al. [21] employed a modeling approach to link process parameters to geometrical inaccuracies in SPIF using statistical analytical techniques, including DOE and ANOVA. Similarly, Essa et al. [10] utilised DOE to optimise process parameters for both sheet metal spinning and single-point incremental forming [17]. Majagi et al. [11] employed a Box-Behnken experimental design and response surface methodology to assess the effects of speed, feed rate, and coolant on the surface roughness, thickness reduction, and hardness of aluminum sheets Furthermore, Elgahwail et al. [22] used response surface DOE and analysis of variance to determine optimal process parameters for the MPF process, particularly regarding springback amount. These studies collectively demonstrate that DOE and statistical analysis are effective tools for identifying and optimizing critical process parameters in various sheet forming processes, including cutting glass fiber, selective laser sintering, sheet metal spinning, and incremental sheet forming.

The SPIF process for polymers still encounters challenges such as issues with geometric precision, thickness variation, wrinkling, and rough surface finishes. These issues arise due to the physical interaction between the tool and the polymer sheet [7]. To address these challenges, a recent study has introduced an innovative method known as Contactless Single Point Incremental Forming (CSPIF). CSPIF revolutionises the process by employing hot compressed air as the shaping tool, completely eliminating physical contact between the tool and the polymer sheet. This groundbreaking approach not only eliminates the need for a rigid tool but also results in substantial cost savings. It reduces process costs by lowering tool expenses and mitigating factors such as tool wear, all while eliminating the necessity for lubrication. Furthermore, CSPIF enhances surface finish by avoiding direct contact, and it improves the

shaping of less malleable polymer materials. This enhancement extends to quality aspects related to springback and geometric precision. Since this deformation process involves no friction forces, there is no risk of wrinkling or twisting. In this research, the novel CSPIF process was developed and optimised using Design of Experiments (DOE) to address the geometric defects commonly encountered in the SPIF process for polymers. The primary focus was on identifying the most suitable combination of various parameters to enhance the final product's quality. The study employed DOE techniques to identify key parameters and their impact on profile variation, thickness variation, and surface roughness during the production of a truncated pyramid. The research also determined the ideal operating parameter settings for achieving the best quality features using a min-max optimisation method.

5.3 Method and Experimental

The novel process called Contactless Single Point Incremental Forming (CSPIF) is an innovative sheet-forming technique that involves the gradual deformation of a sheet workpiece using a non-contact heated compressed air tool. This tool employs pressurised hot air instead of a solid tool. The newly designed setup comprises essential components, including a nozzle, an in-line air and gas heater pipe, a temperature controller, an air compressor, an air tube, and a seamlessly integrated computer numerical control system with a clamped frame.

The nozzle is a crucial part of the setup and controls the flow of hot pressurised air, producing a force on the polymer material while avoiding direct contact. The nozzle was designed using SolidWorks, and a metal laser powder bed fusion printer was used to produce the alloy steel nozzle. The design allows for the measurement and management of the temperature and pressure of the hot air at the inlet of the nozzle. The contactless process is illustrated in **Figure** 5-1**a** through the schematic diagram shown. It depicts the various components and their

interactions during the process. **Figure** 5-1**b** depicts the setup before forming, while **Figure** 5-1**c** shows the setup after the forming stage.

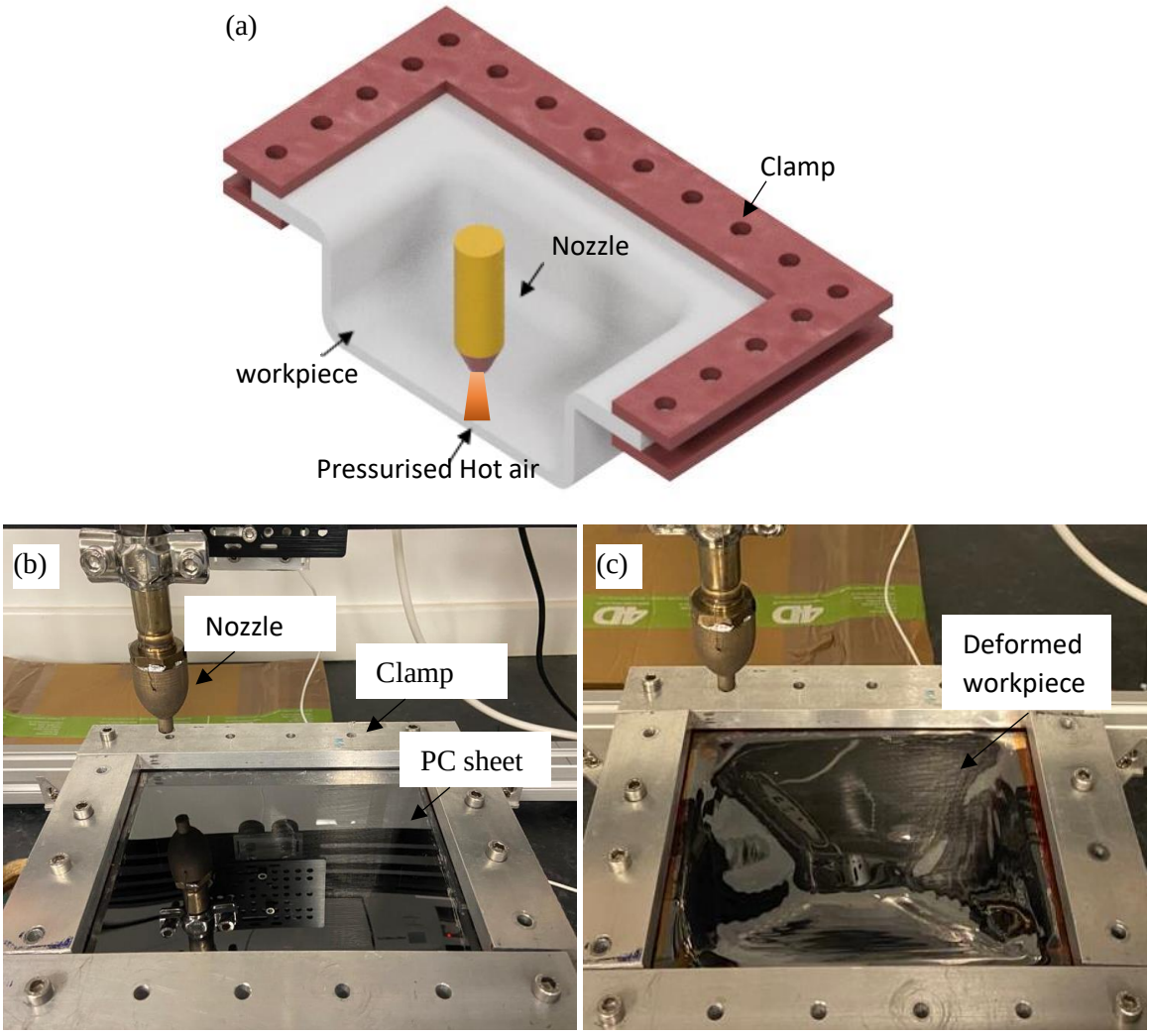

Figure 5-1 (a) A schematic of the process, (b) the experimental setup before forming, (c) after deformation. A video of the process: **https://cccu-my.sharepoint.com/:v:/g/personal/hh36_canterbury_ac_uk/EY4dqyhotrVJomEFsv1JP94B1DUkkwWKT75Zeqpg-J00mg?e=5VIkT3**

The mechanics of this novel process closely resemble those of conventional SPIF, with the key difference being that the deformation is applied to the sheet using a contactless hot compressed air tool, thus eliminating friction. The process begins by securing the polycarbonate sheet at its

edges to prevent uncontrolled distortions. The contactless tool is mounted on a 3D printer machine, which controls the tool's movement through CNC programming and G-code-defined paths, as seen in **Figure** 5-2**a**. The force of the deformation is generated by adjusting the air pressure, regulated by the air compressor, and the air temperature, which is controlled by a PID temperature controller.

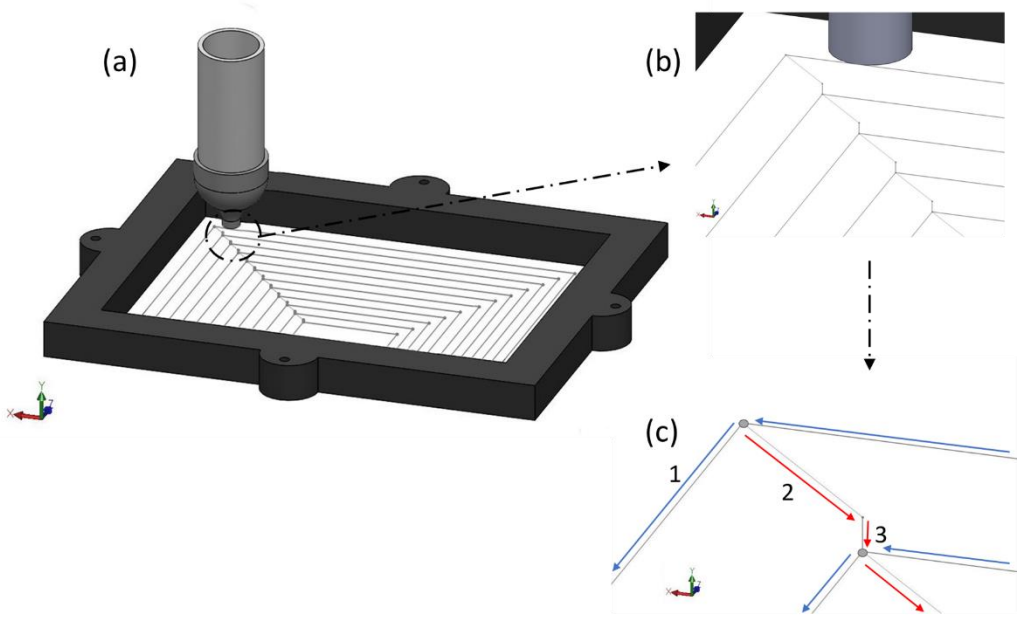

Figure 5-2 The nozzle trajectory (a) Completed path, (b) location of the nozzle over the sheet, and (c) Movement along the path.

The deformation process was initiated by positioning the nozzle at its initial location with a predetermined gap, as programmed in the G-code of the 3D printer machine, as illustrated in **Figure** 5-2**b**. Subsequently, the nozzle began to follow the predefined path outlined in the G-code. In this study, this path assumed a truncated pyramid shape, as shown in **Figure** 5-3.

Initially, as can be seen in **Figure** 5-2**c**, the nozzle moved along the -z axis at a specific feed rate and distance of 152 mm, and then proceeded to move along the -x axis with a specific feed rate and distance of 120 mm, forming a rectangular shape. Upon completing this initial

trajectory, the nozzle descended along both the -x and -z axes, before shifting along the -y axis with a specified step-down gap to initiate the second path. This process continued until the final path was attained, covering an area of 62 × 30 mm², marking the conclusion of the code. The step-down between each step was set to range between 0.5, 0.75, and 1 mm, in a total depth of 5, 7.5, and 10 mm.

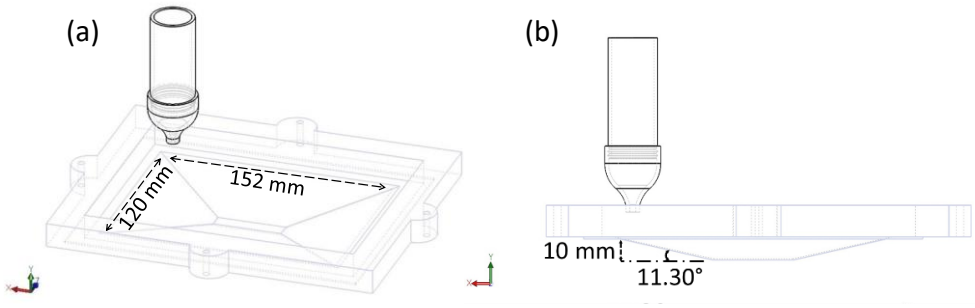

Figure 5-3 The final Shape geometry (a) 3D view, and (b) Side view.

Preliminary studies have been conducted to assess the impact of specific parameters on the final shape of the samples. As shown in **Figure** 5-4 and **Figure** 5-5, comprehensive investigations were carried out using Computational Fluid Dynamics (CFD) and Finite Element Analysis (FEM) to predict the final shape of the deformed component, and these predictions were subsequently validated through experimental trials.

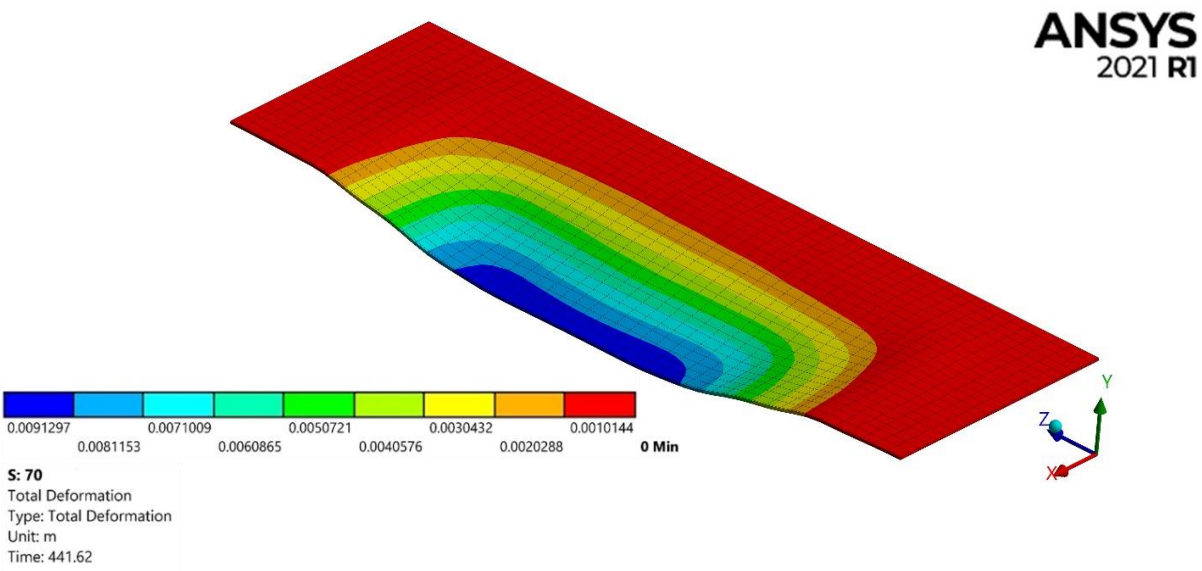

Figure 5-4 The finite element analysis (FEM) result.

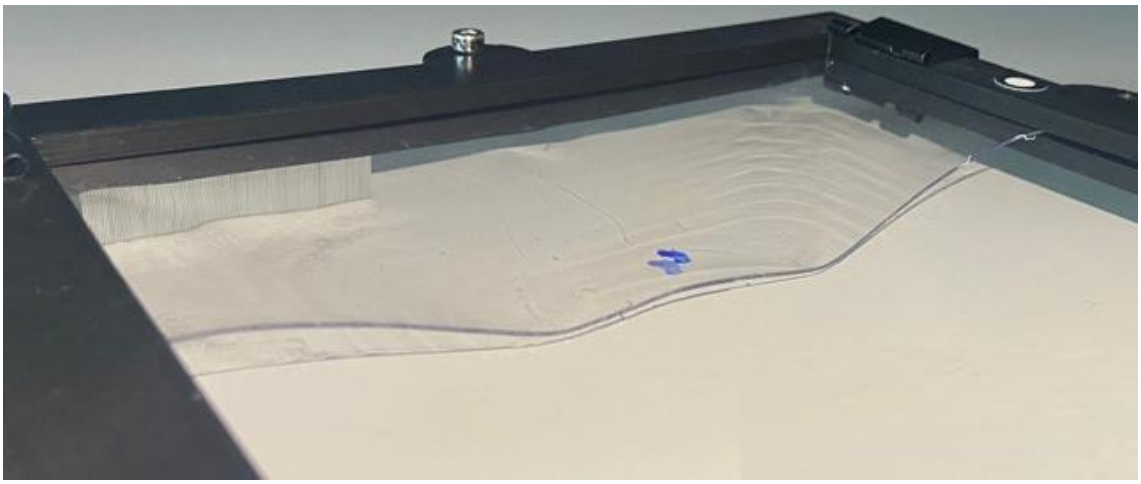

Figure 5-5 The experimental result.

As a result, five distinct parameters were identified as the main key factors influencing the final geometrical features. These parameters include air pressure, air temperature, feed rate, the initial gap between the nozzle and the polymer sheet, and step-down thickness. The air pressure and temperature are critical parameters that are controlled using an air heater and controller. The air compressor is used to deliver pressurised air through a plastic hose, which is connected

to the air heater on one end and the air compressor on the other. The compressed air is heated to the required temperature as it passes through the heating element in the heater. After reaching the desired temperature, the heated compressed air is directed to the nozzle, located at the exit of the heater. The nozzle is an essential component of the process, as it increases the air velocity, enhancing the forming force and pressure concentration in a specific area of the polycarbonate sheet. The nozzle speed, the distance between the nozzle and the polymer sheet, and step-down thickness are also crucial parameters carefully controlled to achieve the desired result.

The process begins with the startup of the air heater and the temperature adjustment set by the controller. Temperature adjustment is critical as it determines the heating temperature of the compressed air, which is essential for the successful deformation of the polymer sheet. Once the temperature is set, the air compressor is started, and the pressurised air is delivered through the plastic hose to the air heater with a certian pressure that is adjusted using the regulator. The nozzle has been specifically designed to incorporate a thermocouple, facilitating precise measurement of the high-temperature compressed air passing through it. Additionally, a thermal camera was utilised to visualise and analyse the temperature distribution within the nozzle.

For this study, a Lexan® 9030 workpiece made of polycarbonate (PC) sheet, measuring 170 mm by 205 mm and with a thickness of 0.75 mm, was selected. The material properties of the PC sheet are outlined in **Table** 5-1. To obtain a comprehensive understanding of the PC sheet's behavior at different temperatures, stress and strain curves were analysed at elevated temperatures. These curves illustrate the relationship between temperature and the mechanical properties of PC sheets and were obtained from previous research as low-strain rate of tensile test curves [23].

Table 5-1 Properties of the Lexan® 9030 polycarbonate (PC) sheet.

Thickness	0.75 (mm)
Density	1.2 (g/cm)
Young's modulus	2.3 (Gpa)
Yield stress	60 (Mpa)
Poisson's Ratio	0.38
Maximum elongation	110 (%)
Thermal conductivity	0.2 (W/m.°C)

The commercial software Minitab 20 was chosen as the analytical tool for this study because it is a powerful statistical software package widely used in the industry for data analysis. The purpose of the Design of Experiments (DOE) was to evaluate the effects of the experimental factors on profile variation, thickness variation, and surface roughness, which are crucial parameters in the manufacturing process. These factors included air pressure, air temperature, feed rate, tool offset, and step down, which were chosen based on their relevance to the conventional SPIF manufacturing process and their association with the new tool. Furthermore, new parameters were introduced to complement the new hot compressed air tool, which were tested and selected for their potential impact on the product's quality.

The primary objective of this study was to develop an empirical model capable of predicting

the responses of the aforementioned experimental factors for any combination of operating conditions. By doing so, the model could aid in the optimisation of the novel contactless SPIF manufacturing process and the production of a high-quality end product. To achieve this goal, a response surface design was employed to construct a series of experiments using only the five selected components. This approach allowed for a more detailed analysis of the interaction between the various factors, identification of the optimal levels for each factor, and their impact on the product's quality.

In this Design of Experiments (DOE), quantitative quality parameters included variances in profile, thickness, and surface roughness, were utilised as critical factors in determining the overall quality of the formed sheet. To measure the average surface roughness (Ra) of each part, a Mitutoyo Formtracer Avant S-3000 Model Surface Roughness Tester was employed. The coordinate measurement machine (CMM) was used to measure the profile and thickness of the pyramid across the entire cross-section of each experiment. **Equation 5.1** was utilised to calculate the profile and thickness variation of the deformed parts [22].

$$\text{Thickness variation} = \sqrt{\frac{1}{N}\sum_{i=1}^{N}(xi - \bar{x})^2} \quad \textbf{(5.1)}$$

Here, N represents the number of points where the workpiece thickness was measured, xi is the thickness at a given point i, and x¯is the average thickness value for all points.

Three levels of the method were used to generate data. The levels of factor control are presented in detail in **Table** 5-2, providing information about the high, medium, and low levels of the SPIF contactless process parameters. To create the truncated pyramid-shaped product, a total of 54 trials were conducted using the experimental surface response method's design.

Table 5-2 Propose control factors and their levels.

Factor	Parameter	Level 1	Level 2	Level 3
A	Air Pressure	0.75 (bar)	1 (bar)	1.25 (bar)
B	Air Temperature	140 (°C)	160 (°C)	180 (°C)
C	Feed Rate	500 (mm/min)	750 (mm/min)	1000 (mm/min)
D	Tool Offset	4 (mm)	6 (mm)	8 (mm)
E	Step Down	0.5 (mm)	0.75 (mm)	1 (mm)

To analyse the compressed air pressure and temperature distributions and values produced by the nozzle design in the contactless SPIF process, a Computational Fluid Dynamics (CFD) model was created using ANSYS Fluent software. The model consisted of a reducer, a sheet, and a closed environmental box. The reducer had a 33 mm inlet diameter, a 5 mm outlet diameter, and a height of 55 mm to control the pressure and temperature of the air flowing out from the heater. A polycarbonate sheet was included in the simulation under the nozzle outlet, positioned 6 mm away from the reducer nozzle, to model a deformed sheet and predict the pressure and temperature values on the surface of the sheet during the forming process.

A hybrid mesh was created using a combination of structured and unstructured meshing techniques, with a fine inflation mesh of 5 layers in regions of high flow complexity, as shown in **Figure** 5-6. The k-ε model was employed to simulate turbulent flows, with the SIMPLC algorithm used in the simulation to provide accurate and reliable results while minimising

computational costs. In the simulation, time step increments were set to be steady, meaning that the time between each step remained constant throughout the simulation.

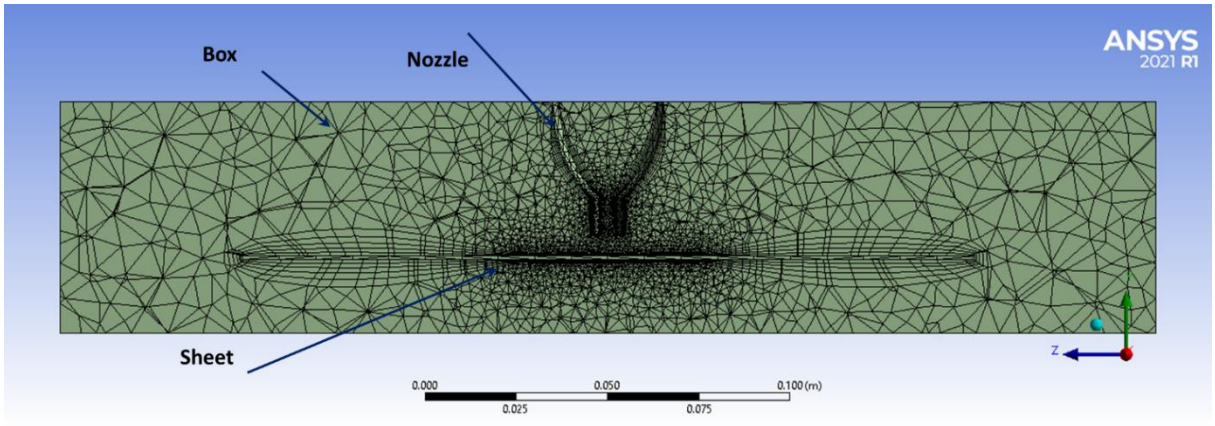

Figure 5-6 Mesh in a CFD model.

5.4 Results and Discussions

5.4.1 DOE Results

The measured findings for the variations in profile, thickness, and surface roughness from 54 experiments are presented in **Table** 5-3. The table reveals that using trial 22 produced the lowest profile variation of 0.48 mm, whereas trial 50 yielded the lowest thickness variation of 0.04 mm, Additionally, trial 39 resulted the lowest surface roughness of 0.15 µm.

The calculated P-value is a statistical measure that indicates the probability of obtaining an observed effect due to chance alone in the context of hypothesis testing. A commonly accepted criterion for statistical significance is a P-value of 0.05 or less. This indicates that the observed effect is highly unlikely to be a result of chance and instead suggests a strong correlation between the variables being tested [24, 25].

Table 5-3 The surface response design and measured Results.

Run	Air Pressure (bar)	Air Temp. (°C)	Feed Rate (mm/min)	Tool Offset (mm)	Step Down (mm)	Profile variation (mm)	Thickness variation (mm)	Surface Roughness (Ra) µm
1	1.25	140	1000	8	0.5	1.18173089	0.080660679	0.2509
2	1.25	140	1000	4	0.5	1.36918601	0.110775138	0.3041
3	1.25	140	500	4	1	2.91786758	0.266528666	0.5859
4	1.25	140	1000	4	1	2.92377492	0.103916393	0.2293
5	1.25	180	1000	8	1	1.07406486	0.116801641	0.2259
6	0.75	140	500	8	0.5	2.87817489	0.147613758	0.7908
7	1.25	180	1000	4	0.5	0.94335312	0.06609622	0.4179
8	1	160	750	6	0.75	1.35066503	0.062230035	0.1579
9	0.75	180	500	8	1	2.38957227	0.374885932	0.812
10	1.25	140	500	4	0.5	4.42109651	0.444866487	0.3837
11	0.75	180	1000	4	0.5	1.39566105	0.132027581	0.2281

12	0.75	140	1000	8	1	1.63905205	0.166044773	0.4673
13	0.75	140	500	4	1	1.55753048	0.269056784	0.8952
14	1.25	180	500	4	1	0.74587662	0.067873153	0.384
15	0.75	180	500	8	0.5	3.11889094	0.284992513	0.6153
16	0.75	180	500	4	0.5	2.83054680	1.007566212	0.7979
17	0.75	140	500	8	1	3.53369790	0.482266192	0.389
18	1.25	180	1000	4	1	2.26090692	0.0659259	0.2753
19	1	160	750	6	0.75	1.35066503	0.062230035	0.1562
20	0.75	180	1000	8	0.5	1.53602408	0.102400875	0.3512
21	1.25	140	1000	8	1	1.10514159	0.085817972	0.3334
22	1.25	180	500	8	1	0.48294997	0.096642375	0.3001
23	1.25	180	1000	8	0.5	0.97473999	0.067375542	0.341
24	0.75	180	1000	8	1	0.99575201	0.148474341	0.1737
25	0.75	140	500	4	0.5	4.14795425	0.184999393	0.5255

26	0.75	140	1000	4	1	2.02913008	0.0680572	0.8828
27	1	160	750	6	0.75	1.35066503	0.062230035	0.1549
28	1	160	750	6	0.75	1.35066503	0.062230035	0.1596
29	1	160	750	6	0.75	1.35066503	0.062230035	0.1547
30	0.75	180	500	4	1	1.48622536	0.333550099	0.992
31	1	160	750	6	0.75	1.35066503	0.062230035	0.1498
32	1.25	180	500	8	0.5	0.74961974	0.119102436	0.2934
33	1.25	140	500	8	0.5	4.17303030	0.413982694	0.3509
34	0.75	140	1000	8	0.5	1.60015426	0.140699758	0.3749
35	0.75	140	1000	4	0.5	2.38173701	0.143004906	0.3809
36	1.25	180	500	4	0.5	1.78483941	0.167494402	0.2545
37	0.75	180	1000	4	1	1.93005499	0.187087086	0.6132
38	1.25	140	500	8	1	2.28401224	0.199127946	0.6349
39	1	160	750	6	0.75	1.35066503	0.062230035	0.1532

40	1	160	750	6	0.75	1.35066503	0.062230035	0.1549
41	1	160	750	8	0.75	1.33369375	0.048012798	0.3608
42	1	140	750	6	0.75	3.49140900	0.217348263	0.9107
43	1	160	750	6	0.75	1.35066503	0.062230035	0.1559
44	1.25	160	750	6	0.75	2.73339520	0.229150227	0.3944
45	1	160	750	6	0.75	1.35066503	0.062230035	0.1562
46	1	160	500	6	0.75	2.16994734	0.166578688	0.4593
47	1	160	750	6	0.75	1.35066503	0.062230035	0.1533
48	1	160	1000	6	0.75	1.57316175	0.064524773	0.3692
49	1	180	750	6	0.75	4.21451457	0.3913118	0.47
50	1	160	750	4	0.75	1.16652001	0.040887112	0.2971
51	1	160	750	6	0.5	0.53106607	0.073992727	0.3775
52	0.75	160	750	6	0.75	3.58870995	0.33654152	0.3741
53	1	160	750	6	1	1.79598464	0.060570038	0.4058

54	1	160	750	6	0.75	1.35066503	0.062230035	0.1537

In this study, the P-values of the important factors and their interactions were calculated and are presented in **Table** 5-4. Factors with P-values less than or equal to 0.05 were considered statistically significant, indicating their influence on the response. These results were then used to develop a predictive model that can aid in optimising the process parameters and ensuring high-quality products.

Table 5-4 presents the results of an experiment on the impact of various parameters on the forming process. The data clearly shows that the forming feed rate is a significant factor affecting profile variation, thickness variation, and surface roughness. Additionally, air pressure also significantly impacts thickness variation and surface roughness. However, the impact of air pressure on profile variation is not significant. The air temperature of the pressurised air is also an important factor that affecting profile variation, but its impact on the thickness variation and surface roughness is not significant.

Interestingly, the interactions between various parameters also have a significant impact on the forming process. Specifically, the interaction between air pressure and air temperature, air temperature and feed rate, and feed rate and step-down all have a significant impact on the product's profile variation. The thickness variation is also significantly affected by the interaction between air pressure and temperature.

Table 5-4 The P-values of the important factors and interactions.

	Profile variation	Thickness variation	Surface Roughness (Ra)
Air Pressure (A)	-	0.01403	0.00020
Air Temperature (B)	0.00027	-	-
Feed Rate (C)	0.00026	0.00007	0.00086
Tool Offset (D)	-	-	-
Step Down (E)	-	-	-
Important Interactions	(A*B) 0.04523 (B*C) 0.01280 (C*E) 0.00285	(A*B) 0.00802	-

5.4.2 Profile Variation

The thermocouple recorded the measured temperature, while the RS T-10 smart camera was utilised to monitor the temperature distribution during the deformation process. **Figure** 5-7**a,** and the accompanying video show a recording from the thermal camera during the forming process.

Additionally, the significance of air temperature during the DOE study is depicted in **Figure** 5-7**b**, which presents a typical parabolic curve representing the effect of air temperature on profile variation. The data revealed that the minimum profile variation was achieved at a temperature near 160°C. Deviation in profile variation increased when the temperature exceeded or fell below 160°C.

If the air temperature during the forming of the PC sheet is less than 160°C, it affects the sheet deformation, causing the total deformation to be less than the target profile. The pressure applied at the same temperature to the nozzle may not be sufficient to deform the sheet properly. Similarly, an increase in the profile variation was also observed at temperatures higher than 160°C, as the sheet becomes overly deformed due to the exposure to higher temperatures.

The lowest profile variation and closest match to the CAD drawing were achieved at the smallest valley of the U-shaped curve around 160°C. This indicates that the profile is more uniform at this temperature, making it the optimum air temperature to deform the polycarbonate sheet to reach the target profile.

In **Figure** 5-7**c**, the profile of the deformed polycarbonate sheet is shown at different air temperatures, including 140°C, 160°C, and 180°C, alongside the CAD drawing. At 140°C, a significant profile variation is observed. However, when the temperature is increased to 160°C, a significant reduction in the profile variation becomes more apparent. This is due to the glass transition temperature of the polycarbonate, which is approximately 156.15°C. Beyond this temperature, the material becomes more pliable and gradually softens. At around 160°C, the material reaches a critical point where it can begin to flow and take on new shapes. This explains why the profile variation was at its minimum at this temperature [26, 27].

Furthermore, the storage modulus of the polycarbonate, which stores energy elastically and

resists deformation, is higher until it reaches 150°C and decreases to zero at around 160°C [28]. However, at higher temperatures, such as 180°C, the material becomes overly softened, resulting in an increase in deformation. At 160°C, the profile variation closely matches the CAD drawing, indicating that the profile is more uniform. Therefore, the optimum air temperature to deform the polycarbonate sheet and achieve the target profile was recorded around 160°C. In addition, the workpiece did not show any degradation after deformation. Furthermore, according to the literature, thermoplastic materials have the ability to be heated up to their melting point and cooled down to room temperature without significant degradation. [29].

Figure 5-7**d** illustrates the relationship between feed rate and profile variation. The results exhibit a clear trend of decreasing profile variation with increasing feed rate. Specifically, the highest feed rate produced the lowest profile variation value.

The reason for this effect can be explained by considering the exposure time of the localised hot air. A high feed rate reduces the exposure time, resulting in more uniform deformation. In other words, when the tool moves quickly, the hot air has less time to impact the material and cause uneven deformation. This observation aligns with previous research that has shown the critical role of exposure time in the deformation process [30]. Therefore, controlling the feed rate emerges as an important parameter to consider when optimising the deformation process and achieving a uniform profile.

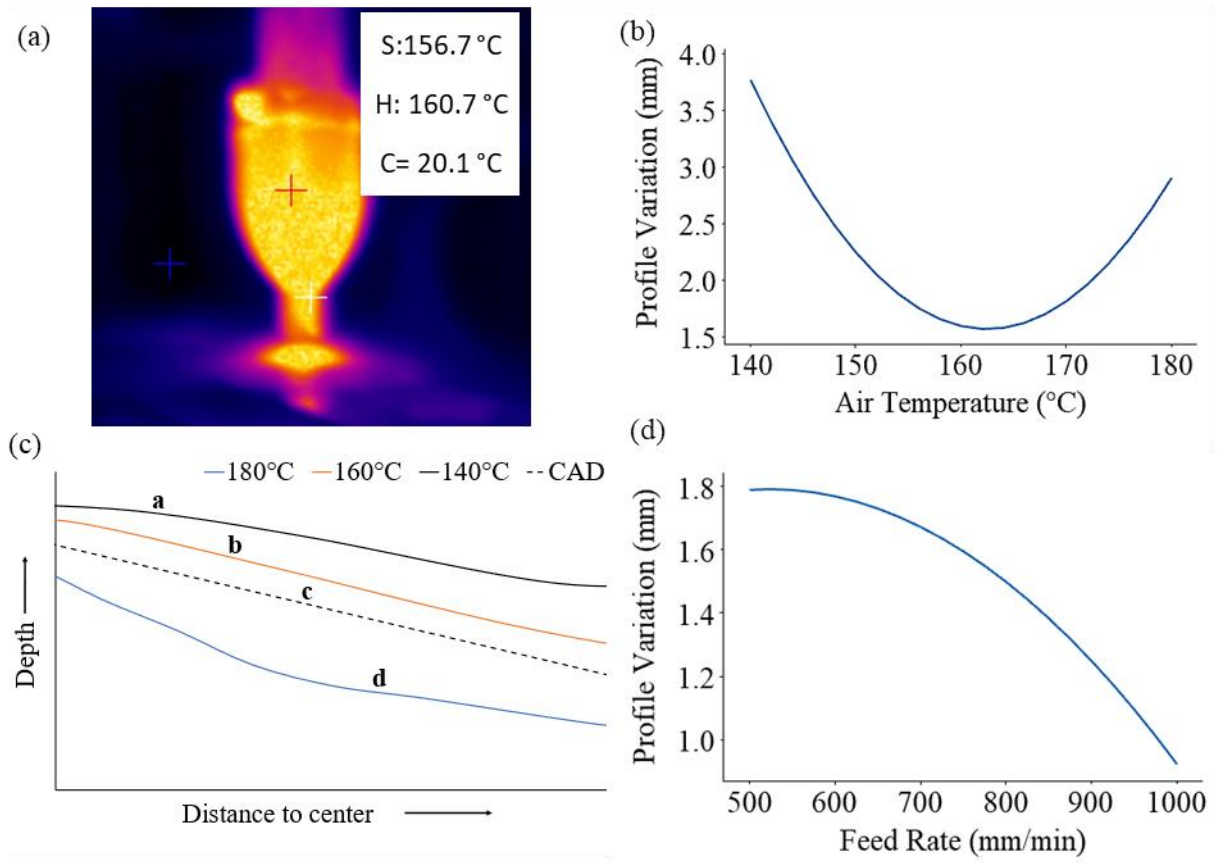

Figure 5-7 (a) one of the thermal camera snapshot showing temperature distribution (b) Effect of compressed air temperature on Profile variation using (a) DoE results, (c) measured profile, (d) effect of federate on the profile variation. Video of the thermal camera during forming.**https://cccumy.sharepoint.com/:v:/g/personal/hh36_canterbury_ac_uk/ESqLkdbfnK1Fj9mhJXSK970BoHP6xlsfXtzTbzaS7f1ARA?e=xvfDhX**

In **Figure** 5-8**a**, the impact of air temperature and pressure on the profile variation of a polycarbonate sheet is depicted. The two parabolic curves illustrate that both air temperature and pressure have a significant influence on the profile variation, exhibiting the same trend as in **Figure** 5-7**a**. The figure demonstrates that the profile variation initially decreases with increasing temperature up to a certain temperature point, beyond which it starts to increase due to the material becoming too malleable [31]. At low temperatures, the highest profile variation is recorded for both air pressures, while at high temperatures, the sheet is deformed more than

the target profile, resulting in over-deformation.

Additionally, the figure shows that air pressure plays a crucial role in achieving the desired profile variation of the sheet. At an air pressure of 0.75 bar, the parabolic curve has a minimum value at an air temperature of about 160°C. Conversely, at an air pressure of 1.25 bar, the bottom of the parabolic curve shifts to the right to around 165°C, producing the lowest profile variation of 2.4 mm. Pressures below 1 bar will not be sufficient to deform the sheet uniformly to the designed depth, while pressures above 1 bar will deform the sheet more than required. Therefore, controlling the air pressure within a specific range is essential for achieving the desired profile variation of the polycarbonate sheet.

Figure 5-8**b** demonstrates the effect of air temperature and feed rate interactions on profile variation. Similar to **Figure** 5-8**a** two parabolic curves illustrate that both air temperature and feed rate have a significant influence on the profile variation. As mentioned earlier, the highest feed rate results in the lowest profile variation due to its effect on the heating, depending on the heating time. Conversely, a low feed rate produces higher profile variations, as observed with a feed rate of 500 mm/min. Higher profile variation values for all different feed rates are noted at 140°C because the value of the storage modulus is too high to reach the softening temperature. On the other hand, the high temperature of 180°C leads to more deformation than the designed one due to rubbery flow, causing an increase in the profile variation for all different feed rates. Consequently, the lowest profile variation is observed at transition temperature and high feed rate.

Figure 5-8**c**. assesses the impact of the interaction between feed rate and step-down on profile variation. At a step-down of 1mm, the profile remains almost consistent, with only a slight change in profile variation (0.495mm ± 0.005) observed across a range of feed rates. More

uniform variation is recorded at high-speed movements. In contrast, at a step-down of 0.5mm, a sharp drop in profile variation is observed with increasing feed rate. The difference in profile between high feed rates of 1000 mm/min and low feed rates of 500 mm/min is attributed to different exposure times and surface heating, as illustrated in **Figure** 5-8**b**. At low feed rates, more heat is generated for all step downs, leading to an increase in the gap between the nozzle and the sheet surface. A higher surface temperature also results in more deformation. In contrast, a high feed rate generates less heat for all step downs, and a step-down of 1mm is the optimum value that maintains the gap similar to the end of the process and yields a more uniform profile result than a low feed rate due to exposure time. A step-down of 1mm provides a more homogeneous profile for different feed rates than a step-down of 0.5mm.

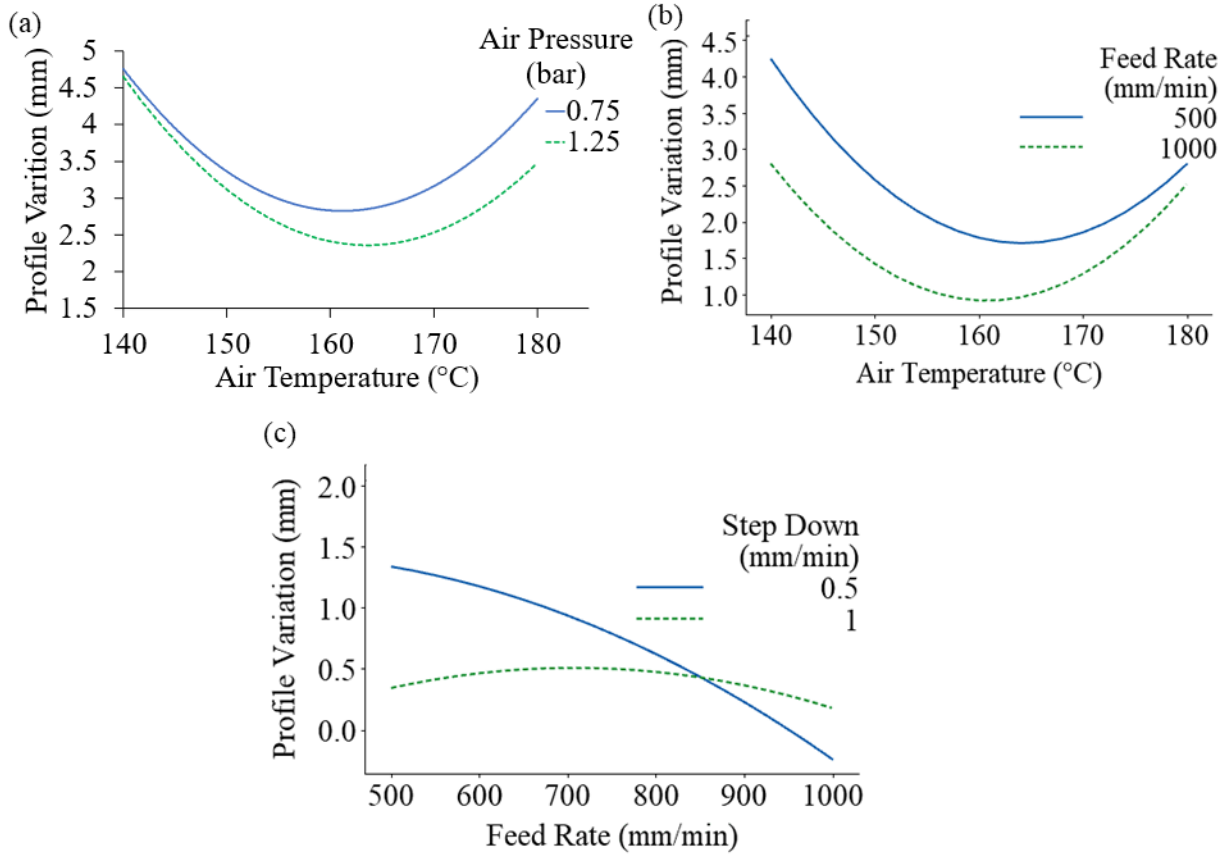

Figure 5-8 Effect on profile variation of interactions between (a) air pressure and air temperature (b) air temperature and feed rate (c) feed rate and step down.

5.4.3 Thickness Variation

In **Figure** 5-9**a**, it is evident that air pressure has a significant influence on thickness variation. The graph exhibits a parabolic shape, indicating the presence of an optimal air pressure range for achieving uniform thickness. At low air pressure levels, such as 0.75 bar, the sheet is not uniformly deformed, resulting in high thickness variation. As the air pressure increases from 0.75 bar to 1 bar, the thickness variation decreases significantly. However, further increasing the pressure to 1.1-1.25 bar leads to an increase in thickness variation again, as the sheet is excessively deformed. The optimum air pressure value for achieving uniform thickness is found to be 1.05 bar. This suggests that careful selection and adjustment of air pressure during the process can result in more consistent and accurate thickness of the polycarbonate sheet.

Figure 5-9**b** illustrates the effect of feed rate on thickness variation. Increasing the feed rate from 500 mm/min to 1000 mm/min results in a significant and uniform reduction in thickness variation. This is because a high feed rate (high moving speed) reduces the exposure time of localised hot air, leading to less material expansion and a decrease in thickness variation. On the other hand, a low moving speed for the nozzle provides more exposure time for heating the polycarbonate sheet, leading to an increase in thickness variation, as the amount of expansion is typically proportional to the temperature increase.

Figure 5-9**c** showcases the impact of air temperature and pressure interactions on thickness changes. At a pressure of 0.75 bar, lower thickness variation is observed at lower temperatures, and the variation increases with increasing temperature. At low air temperatures, the effect of the air pressure is completely diminished, as the material is difficult to deform regardless of the applied air pressure up to 1.25 bar. As the temperature increases, the effect of the air pressure becomes more notable, and differences in thickness variation grow. Conversely, the differences

in thickness at a pressure of 1.25 bar seem to be more consistent at lower and higher temperatures, but the best uniformity was observed at the storage modulus temperature, where the difference was less than 0.2 mm at temperature of around 160°C. These variations in thickness are caused by the interplay between the distributions of pressure and temperature on the polycarbonate sheet.

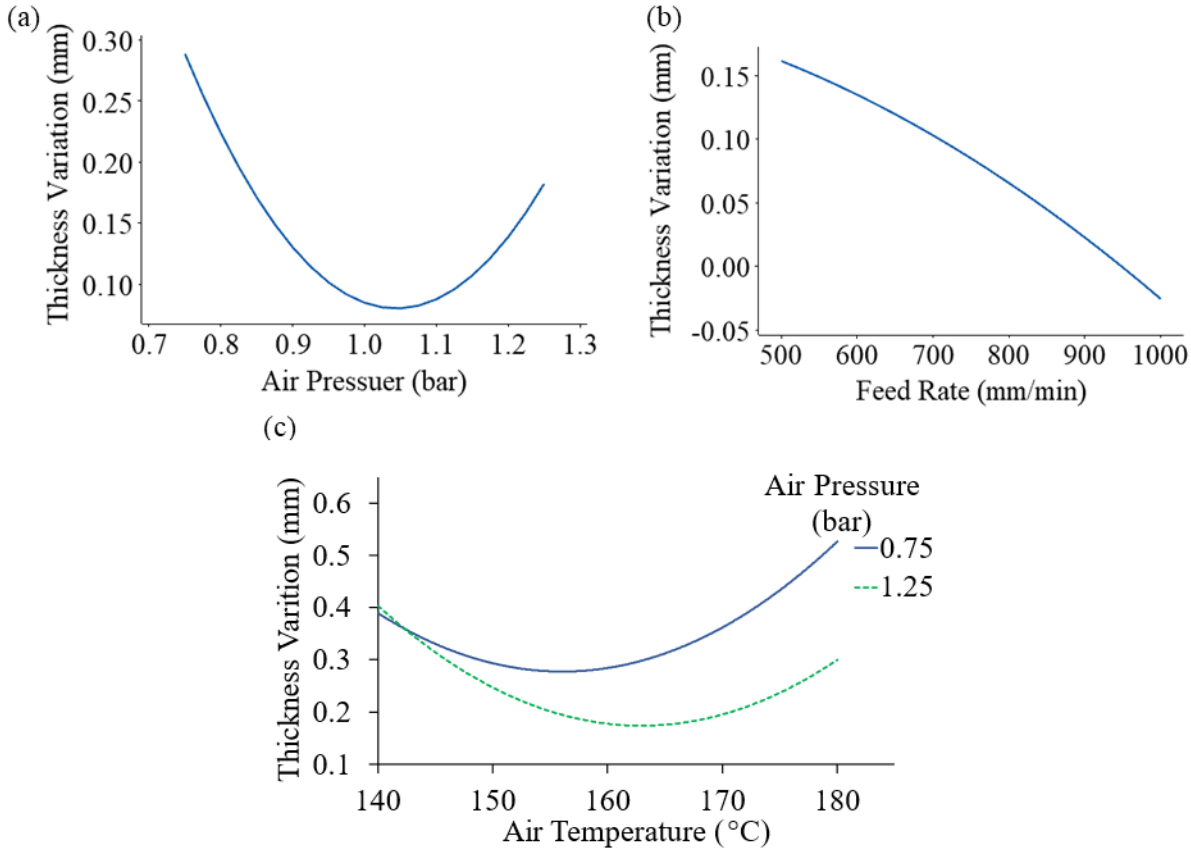

Figure 5-9 Effect of (a) air pressure and (b) feed rate on thickness variation, (c) interactions among air pressure and temperature on thickness variation.

The CFD results presented in **Figure** 5-10 demonstrate the impact of different air pressures on the pressurised hot air jet from the contactless SPIF nozzle to the polycarbonate sheet. The results reveal that the pressure and temperature affected areas are influenced differently by varying air pressures.

In **Figure** 5-10**a**, the pressure-affected area is observed to be smaller than the temperature affected area by approximately two times, and the maximum pressure value recorded is 7.448×10^4 pa. In contrast, the temperature-affected area appears irregular in shape, suggesting a non-uniform heating distribution across the sheet. When the air pressure is increased to 1 bar, as shown in **Figure** 5-10**b**, the pressure-affected area becomes larger, resulting in a more uniform temperature- affected area. However, it remains smaller than the temperature-affected area. This implies that increasing the air pressure can lead to a more uniform distribution of deformation on the material but does not necessarily result in a more uniform heating distribution.

Interestingly, the distribution of the pressure and temperature-affected areas becomes almost equal when the air pressure is increased to 1.25 bar, as shown in **Figure** 5-10**c**. This suggests that using an air pressure of 1.25 bar can result in a more uniform deformation of the material, leading to a more uniform thickness distribution, which aligns with the DOE results shown in **Figure** 5-9**c**.

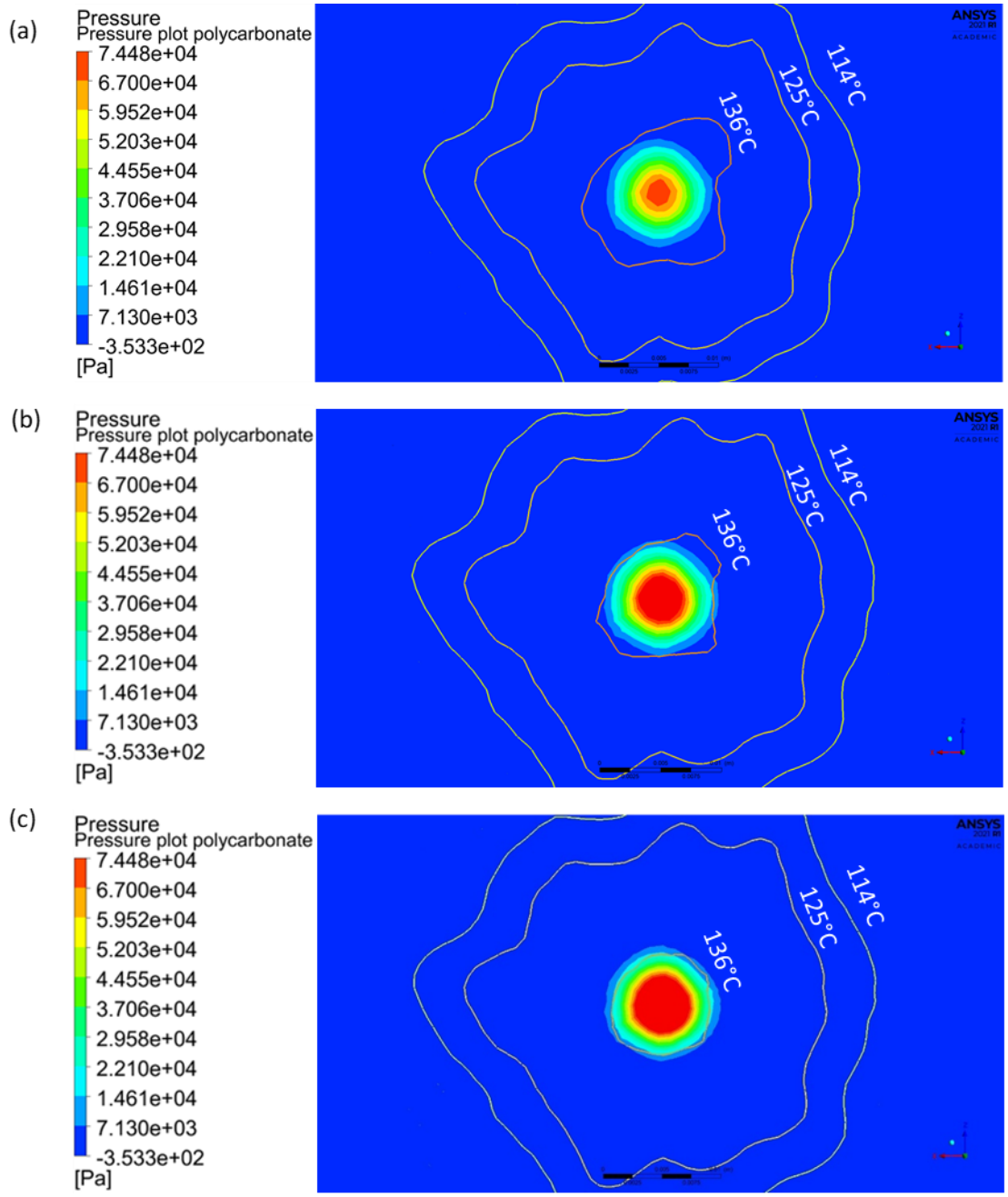

Figure 5-10 CFD results of the Pressure and temperature affected area when using air pressure of (a) 0.75 bar, (b) 1 bar, and (c) 1.25 bar.

5.4.4 Surface Roughness

In sheet forming processes such as in single point incremental forming, surface roughness is a

crucial factor that affects the quality of the formed part. **Figure** 5-11 demonstrates the effects of air pressure and feed rate on the surface roughness (Ra) of the formed polycarbonate sheet.

Figure 5-11**a** shows a clear relationship between air pressure and surface roughness. It is evident that the surface roughness value decreases linearly with an increase in air pressure. This finding is consistent with observations made in conventional SPIF, where an increase in the tool tip radius led to a decrease in surface roughness [32]. The reason behind this is that the area affected by air pressure in contactless SPIF behaves similarly to the tool tip area in conventional SPIF, and an increase in air pressure leads to a decrease in surface roughness. The smoothest surface is achieved at the highest air pressure (1.25 bar), with a surface roughness value of 0.12 µm. On the other hand, when the air pressure is low (0.75 bar), the surface roughness value is high (0.35 µm).

Figure 5-11**b** shows that increasing the feed rate results in a decrease in surface roughness. As the feed rate increases from 500 mm/min to 1000 mm/min, the surface roughness value decreases from 0.35 µm to 0.17 µm. The lowest surface roughness value is achieved at a feed rate of 1000 mm/min, while the highest surface roughness value is obtained at a lower feed rate (500 mm/min). The reason behind this is related to the effect of the heat spot generated by the nozzle on the material. At lower feed rates, the nozzle moves at a slower speed, allowing more exposure time for heating the material. This leads to deeper deformation for each path and, consequently, a higher surface roughness value. On the other hand, increasing the feed rate reduces the time of exposure to the heat spot, resulting in shallower deformation and, therefore, a lower surface roughness value.

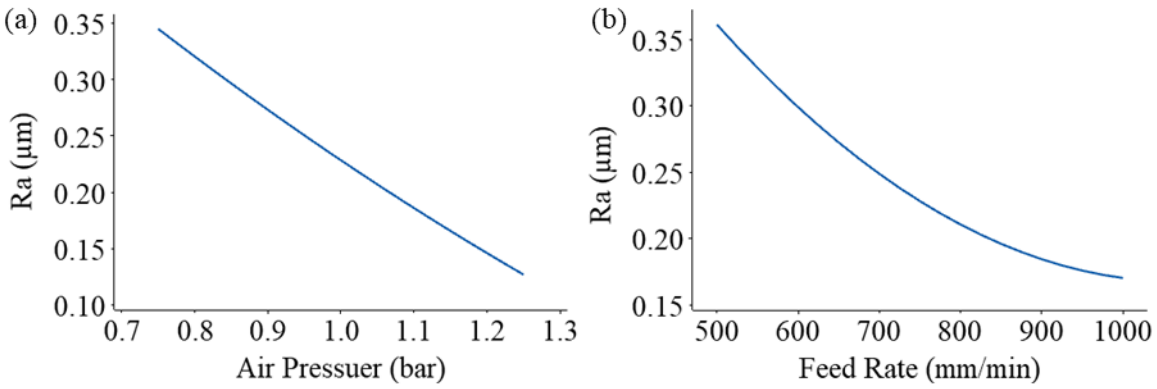

Figure 5-11 Effect of (a) air pressure and (b) feed rate on surface roughness.

5.4.5 Model Predictions and Process Optimisation

To achieve high-quality manufacturing processes, it is essential to have a reliable model that can accurately predict the quality criteria for various combinations of process parameters. An empirical model is particularly useful in this regard, as it offers several advantages. Firstly, it provides a comprehensive understanding of how each process parameter impacts the quality criteria. Secondly, it facilitates the identification of the optimal parameters that produce the desired quality criteria. Thirdly, it can be used to optimise the manufacturing process by predicting the quality criteria for any combination of parameters. Lastly, it can reduce the need for costly and time-consuming experimental trials.

In this study, data obtained from the Design of Experiments (DOE) was used to develop an empirical model capable to describing and predicting the quality criteria of deformed polycarbonate for any combination of process parameters. The model employed a general second-order polynomial equation that incorporated the critical parameters and their interactions. **Equation 5.2** illustrates that each process parameter and interaction is multiplied by a coefficient. The coefficients for each process parameter and interaction were determined from the data and are presented in

Table 5-5. The R-square value of the empirical model's exceeded 95% for all models, indicating a strong fit. Consequently, the empirical model can accurately predict the quality criteria of deformed polycarbonate for any combination of process parameters, reducing the need for expensive and time-consuming experimental trials while optimising the manufacturing process.

Prediction model =

X – X1A –X2B –X3C+X4D+X5E-X6AB+X7AC-X8AD+X9AE+X10BC+X11BD+X12BE-X13CD+X14CE+X15DE+X16A^2+X17B^2- X18C^2-X19D^2-X20E^2 (**5.2)**

Where A is the air pressure, B is the air temperature, C is the feed rate, D is the tool offset, E is the step-down, and x1 through x20 are the coefficients from Table 5 5.

Table 5-5 Corresponding coefficient values for the prediction model.

	Profile Variations	**Thickness Variations**	**Surface Roughness**
Constant (X)	122.2	10.61	20.11
X1	27.1	3.46	0.96
X2	1.429	0.1185	0.2435
X3	0.0090	0.00091	0.00133
X4	2.87	0.251	0.161

X5	14.2	1.46	1.56
X6	0.0455	0.01192	0.00286
X7	0.00135	0.000459	0.000768
X8	0.330	0.0228	0.0773
X9	1.26	0.177	0.394
X10	0.000058	0.000000	0.000003
X11	0.00101	0.000658	0.000199
X12	0.0137	0.00331	0.00362
X13	0.000303	0.000041	0.000011
X14	0.00564	0.000390	0.000215
X15	0.045	0.0755	0.0998
X16	16.8	2.40	0.12
X17	0.004355	0.000429	0.000748
X18	0.000004	0.000000	0.000001

X19	0.2153	0.0220	0.0119
X20	15.16	1.04	0.24

To achieve a final product with high precision and a desirable surface finish, it is crucial to identify the optimal operational parameters. This study aims to achieve minimal deviation in profile, thickness, and surface roughness while avoiding the formation of wrinkles or severe thin spots. All parameters are limited to pre-selected levels, and each quality attribute is given equal importance. To determine the optimal parameters satisfying all the objective functions, a Min-Max optimisation method is employed, as outlined in **Table** 5-6. This method concurrently solves the three empirical equations for profile, thickness variations, and surface roughness until the working variable values meet all objective functions. The optimisation process minimises the maximum deviation from the desired values for each quality attribute, ensuring that the final product adheres the required standards.

The process parameters used were an air pressure of 1.02 bar, an air temperature of 160.60°C, a feed rate of 1000 mm/min, a tool offset of 8 mm, and a stepdown of 1 mm. These parameters can be employed to ensure consistent and high-quality products in future manufacturing processes. Furthermore, the optimisation process aids in minimising waste and reducing costs by ensuring that the production process is optimised to achieve the desired quality standards while conserving resources.

To validate the effectiveness of the contactless SPIF technique, an experimental trial was conducted using the optimal working parameters identified during the development phase. The results demonstrated that the formed part exhibited minimal wrinkling or thinning, affirming the suitability of the process parameters for the intended application. **Table** 5-7 summarises the

quality characteristics that were tested and compares them to the predictions made using the DOE. The geometric accuracy between the design and experimental results was found to be in excellent agreement, with a profile variation of only 0.996 mm. **Figure** 5-12 illustrates this agreement, displaying the CAD profile of the manufactured workpiece alongside the experimentally measured profile under optimal operational conditions.

However, the comparison of thickness between the measured experimental results and the theoretical sine law values using the optimal parameters revealed a small but acceptable difference. This discrepancy can be attributed to the inherent complexities of the process and the uncertainties present in the actual manufacturing environment. Furthermore, the surface roughness (Ra) results for samples prepared using the optimised process parameters differed significantly from the predicted values. Subsequent analysis revealed that the waviness on the formed sheet was due to the step-down phenomenon of the process, leading to an increase in roughness. **Figure** 5-14 visually illustrates this phenomenon. In summary, the experimental trial confirmed the effectiveness of the contactless SPIF technique, highlighting its potential while also emphasising the need for further optimisation to achieve the desired surface finish.

Table 5-6 Optimum operational parameters.

	Air Pressure(bar)	**Air Temperature(°C)**	**Feed Rate (mm/min)**	**Tool Offset(mm)**	**Step Down(mm)**
Optimal Parameters	1.02273	160.606	1000	8	1

Table 5-7 Predicted and experimental results using the optimal conditions.

	Profile variation(mm)	Thickness variation (mm)	Surface Roughness (Ra)µm
Predicted	0.971	0.133	0.068
Optimised Experiment	0.996	0.14847	0.1310

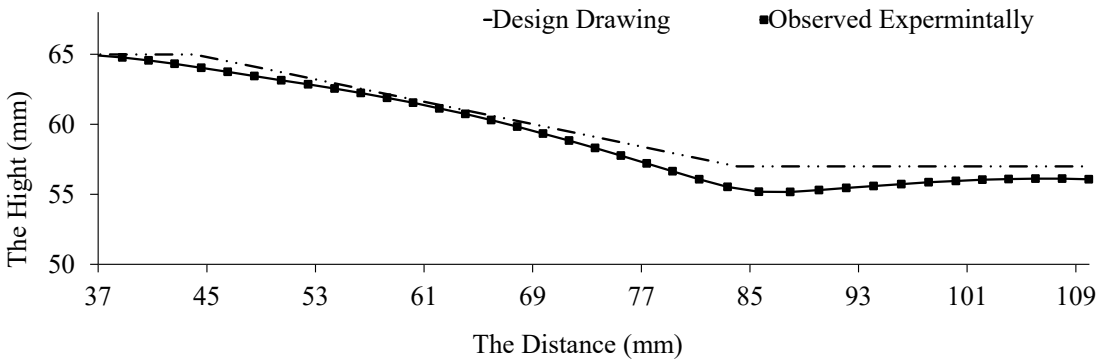

Figure 5-12 Comparison between CAD drawing and experimental profile.

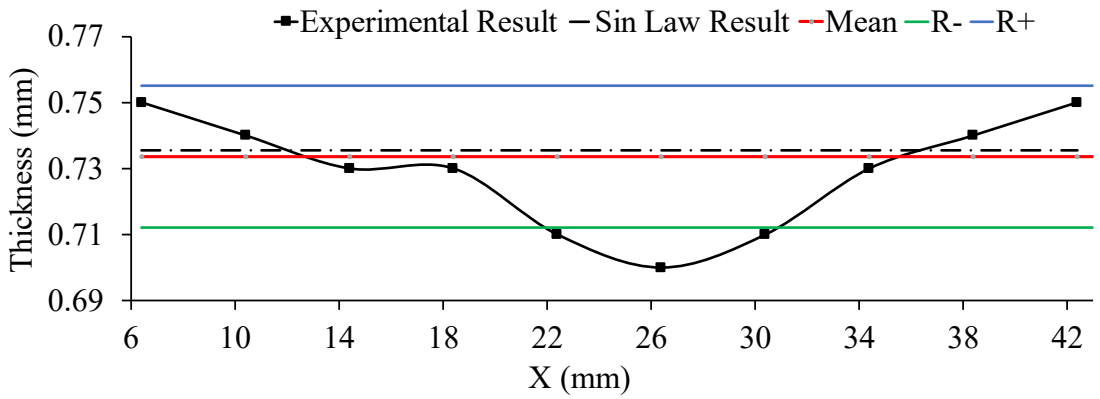

Figure 5-13 Comparison of thickness distribution obtained by the theoretical sine law, and

experiment.

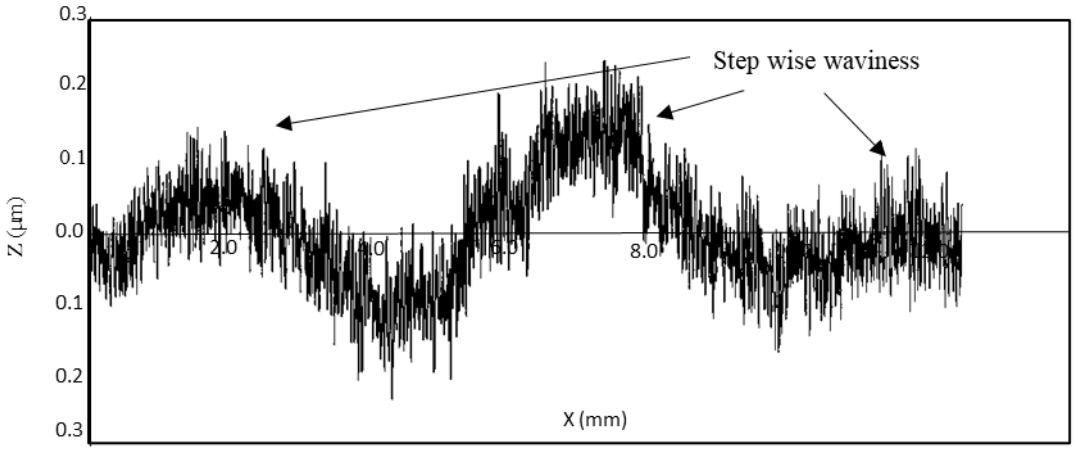

Figure 5-14 Surface Roughness (Ra) for samples using the optimised data.

5.5 Conclusion

This study introduces and optimises a highly flexible and adaptable contactless SPIF process utilising hot pressurised air as the forming tool to meet diverse manufacturing demands and customer requirements. By eliminating the interaction between the forming tool and the sample, the contactless SPIF process offers several benefits, including reduced tool wear, enhanced design flexibility, and improved dimensional accuracy.

To assess the process's effectiveness, 54 different forming conditions were tested and analysed using the Design of Experiments (DOE) methodology and a response surface method to pinpoint the most significant process variables. The study revealed that air pressure, air temperature, and feed rate were the most critical variables influencing the formability of the process, while the tool offset had no discernible effect. Significant parameter interactions were identified for profile variation, thickness variation, and surface roughness, and a mathematical model was developed to characterise the influence of the process components.

Researchers found that increasing the feed rate reduced profile variation, thickness variation, and surface roughness, while increasing air pressure had a opposite effect. By employing the min-max approach to optimisation, they pinpointed process parameters values that struck an optimal balance among conflicting quality characteristics. The optimised experiment in this study demonstrated that the contactless SPIF process can be tailored for a wide range of polymer materials. It produced a truncated pyramid polycarbonate shape with exceptional accuracy and consistency by identifying the key variables and optimising their settings. This finding is particularly significant considering the increasing demand for high-quality, complex-shaped plastic components in various of industries, including automotive, aerospace, and consumer goods.

5.6 References

1. Radu, C., Effects of process parameters on the quality of parts processed by single point incremental forming. Int. J. Mod. Manuf. Technol, 2011. 3(2): p. 91-96.

2. Petek, A., K. Kuzman, and J. Kopač, Deformations and forces analysis of single point incremental sheet metal forming. Archives of Materials science and Engineering, 2009. 35(3): p. 107-116.

3. Abaas, T.F. and A.S. Bedan, The Effect of Tool Path Strategy on Mechanical Properties of Brass (65-35) in Single Point Incremental Sheet Metal Forming (SPIF). Journal of Engineering, 2013. 19(5).

4. Kim, Y. and J. Park, Effect of process parameters on formability in incremental forming of sheet metal. Journal of materials processing technology, 2002. 130: p. 42-46.

5. Azevedo, N.G., et al., Lubrication aspects during single point incremental forming for steel and aluminum materials. International Journal of precision engineering and manufacturing, 2015. 16(3): p. 589-595.

6. Durante, M., A. Formisano, and F. Lambiase, Incremental forming of polycarbonate sheets. Journal of Materials Processing Technology, 2018. 253: p. 57-63.

7. Rosa-Sainz, A., et al., Experimental failure analysis in polycarbonate sheet deformed by spif. Journal of Manufacturing Processes, 2021. 64: p. 1153-1168.

8. Martins, P.A.F., et al., Single point incremental forming of polymers. CIRP Annals, 2009. 58(1): p. 229-232.

9. Le, V., A. Ghiotti, and G. Lucchetta, Preliminary studies on single point incremental forming for thermoplastic materials. International Journal of Material Forming, 2008. 1(1): p. 1179-1182.

10. Essa, K. and P. Hartley, Optimization of conventional spinning process parameters by means of numerical simulation and statistical analysis. Proceedings of the Institution of Mechanical Engineers, Part B: Journal of Engineering Manufacture, 2010. 224(11): p. 1691-1705.

11. Majagi, S.D. and G. Chandramohan. Optimization of incremental sheet metal forming parameters by design of experiments. in Applied Mechanics and Materials. 2014. Trans Tech Publ.

12. Le, V.S., A. Ghiotti, and G. Lucchetta, Preliminary Studies on Single Point Incremental Forming for Thermoplastic Materials. International Journal of Material Forming, 2008. 1(1): p. 1179-1182.

13. Jurisevic, B., K. Kuzman, and M. Junkar, Water jetting technology: an alternative in incremental sheet metal forming. The International Journal of Advanced Manufacturing Technology, 2006. 31(1-2): p. 18-23.

14. Jurisevic, B., et al. Incremental sheet metal forming process with a water jet and rigid tool. in Proc 17th International Conference on Water Jetting. 2004.

15. Yang, C., S. Sheu, and K. Yu, Optimal machining parameters in the cutting process of glass fibre using the reliability analysis based on the Taguchi method. Proceedings of the Institution of Mechanical Engineers, Part B: Journal of Engineering Manufacture,

2008. 222(9): p. 1075-1082.

16. Bacchewar, P., S. Singhal, and P. Pandey, Statistical modelling and optimization of surface roughness in the selective laser sintering process. Proceedings of the Institution of Mechanical Engineers, Part B: Journal of Engineering Manufacture, 2007. 221(1): p. 35-52.

17. Hussain, G., L. Gao, and N. Hayat, Empirical modelling of the influence of operating parameters on the spifability of a titanium sheet using response surface methodology.28Proceedings of the Institution of Mechanical Engineers, Part B: Journal of Engineering Manufacture, 2009. 223(1): p. 73-81.

18. Ham, M. and J. Jeswiet, Forming limit curves in single point incremental forming.CIRP annals, 2007. 56(1): p. 277-280.

19. Filice, L., G. Ambrogio, and F. Micari, On-line control of single point incremental forming operations through punch force monitoring. CIRP annals, 2006. 55(1): p. 245-248.

20. Ham, M. and J. Jeswiet, Single point incremental forming and the forming criteria for AA3003. CIRP annals, 2006. 55(1): p. 241-244.

21. Ambrogio, G., et al., An analytical model for improving precision in single point incremental forming. Journal of Materials Processing Technology, 2007. 191(1-3): p. 92-95.

22. Elghawail, A., et al., Prediction of springback in multi-point forming. Cogent Engineering, 2017. 4(1): p. 1400507.

23. Cao, K., Y. Wang, and Y. Wang, Experimental investigation and modeling of the tension behavior of polycarbonate with temperature effects from low to high strain rates. International Journal of Solids and Structures, 2014. 51(13): p. 2539-2548.

24. Li, Y., et al., Effects of process parameters on thickness thinning and mechanical properties of the formed parts in incremental sheet forming. The International Journal of Advanced Manufacturing Technology, 2018. 98: p. 3071-3080.

25. Abosaf, M., et al., Optimisation of multi-point forming process parameters. The International Journal of Advanced Manufacturing Technology, 2017. 92: p. 1849-1859.

26. Siviour, C., et al., Mechanical behaviour of polymers at high rates of strain.http://dx.doi.org/10.1051/jp4:2006134145, 2006. 134.

27. Sehrawat, M., et al., Glass Transition Temperature Measurement of Polycarbonate Specimen by Dynamic Mechanical Analyser Towards the Development of Reference Material. MAPAN, 2022. 37(3): p. 517-527.

28. Mulliken, A.D. and M.C. Boyce, Mechanics of the rate-dependent elastic–plastic deformation of glassy polymers from low to high strain rates. International journal of solids and structures, 2006. 43(5): p. 1331-1356.

29. Pelin, C.-E., et al., Recycling and reusing polyamide 6 extruded waste products to manufacture carbon fiber based composites. Annals of the Academy of Romanian Scientists Series on Physics and Chemistry Science, 2017. 2: p. 91-103.

30. Ayhan, Z. and Q. Zhang, Wall thickness distribution in thermoformed food containers produced by a Benco aseptic packaging machine. Polymer Engineering and Science -

POLYM ENG SCI, 2000. 40: p. 1-10.

31. Dunson, D., Characterization of polymers using dynamic mechanical analysis (DMA).EAG Appl Note, 2017.

32. Sabater, M., et al., Process parameter effects on biocompatible thermoplastic sheets produced by incremental forming. Materials, 2018. 11(8): p. 1377.

6 Chapter Six: Conclusion and Future work

6 Conclusion and Future Work

6.1 Conclusion

This doctoral research introduces a novel non-contact single incremental point forming technique assisted by hot compressed air, aiming to form high-quality polycarbonate sheets. The study demonstrates that this proposed forming method offers several improvements over the traditional SPIF process. Firstly, it enhances the surface quality of the sheets, eliminating the need for lubricants. Additionally, it effectively eliminates tearing or twisting defects that may occur during the forming process. The research not only focuses on improving the workpieces but also addresses issues related to the solid tool itself. Specifically, it tackles problems such as corrosion and wear caused by the forming process.

To evaluate the effectiveness of the technique, the study conducted experimental assessments of geometric precision, thickness distribution, and surface quality at different temperatures and parameters. A finite element model, combining computational fluid dynamics (CFD) and transient structural computations, was developed and implemented to predict the deformation of the sheet under specific localised air pressure and temperature conditions. Statistical methods were also employed to develop a non-contact tool, identifying the most critical working parameters and determining optimal settings for achieving high-quality characteristics and defect-free products.

The primary research contributions can be summarised as follows:

First research:

- The non-conventional SPIF was developed by substituting the traditional solid forming

tool of the conventional SPIF with a novel contactless heat-assisted incremental sheet forming tool that employs pressurised hot air. This novel SPIF setup provides localised hot compressed air as a tool to deform polymer workpieces without any physical contact.

- A polycarbonate (PC) sheet and a setup with a nozzle, heating tube, heater, temperature controller, air compressor, and a computer numerical control system with a clamped frame were successfully used. Experimental investigations were performed to study the new configuration and validate the obtained results using a design CAD drawing.

- The primary essential factors that significantly affect the performance of the new setup during the experiment (air pressure, air temperature, feed rate, initial gap, and step down) were determined.

- High accuracy in deforming the PC sheet with HASPIF was achieved by determining the precision and accuracy of the deformed workpiece using a coordinate measuring machine (CMM). The observations showed high accuracy with only modest springback and pillow effects.

- Deviation from the ideal profile was observed due to the bending effect at the starting point of the nozzle, highlighting the importance of properly considering fixture design, nozzle placement, and starting position to minimise deviation. The new approach outperforms the traditional SPIF process and addresses both the quality of the workpieces and the challenges faced by solid tools due to wear from the forming process.

- The sheet thinning demonstrated that it was proportional to pyramid depth and showed good agreement between the measured and theoretical thickness distributions. Additionally, the surface roughness of the sample was determined, which slightly but acceptably increases after

the incremental formation due to the stepwise nature of the air nozzle.

Second research:

- A new finite element model (FEM) was developed to analyse the impact of the contactless tool on the shaping process. The ANSYS software was used to simulate a truncated pyramid tool path with a total depth track of 7.5 mm divided into 10 steps.

- Two separate models were constructed and integrated to predict the final shape of the polycarbonate sheet. First, a computational fluid dynamics (CFD) model was built to calculate the pressure and temperature values of the air interacting with the sheet. Second, a transient structural model was employed to investigate the sheet deformation.

- The Parametric Design Language (APDL) was utilised to integrate and facilitate air movement, including heat and pressure, within the truck's pathway using the transient structural model.

- The model was validated against experimental data, comparing the predicted sheet deformation with the actual deformation observed in experiments. The comprehensive FE model developed in this work can accurately forecast the final parts of geometries and dimensions, as well as the normal strain progression. It also revealed that the primary deformation modes in SPIF were stretching, thinning, and bending.

- Based on the results, it can be concluded that the developed model accurately predicts sheet deformation generated by the newly proposed non-contact SPIF method.

Third research:

- This research focused on optimising critical operational parameters that influence the quality of the final product in polycarbonate sheet forming. The design of experiments (DOE) approach was employed to analyse the effect of the various operating parameters, including air pressure, air temperature, feed rate, tool offset, and step down. The quality of the formed sheets was evaluated by studying three criteria: profile variation, thickness variation, and surface roughness.

- The response surface experimental design was employed as a statistical method to determine the significance of these control factors. Air pressure, air temperature, and feed rate were found to have the most significant influence on the formability of the HASPIF process in terms of avoiding wrinkles or excessive thinning. While step-down also played a role, its impact was comparatively smaller. Tool offset did not appear to have a noticeable effect on the formability of the process.

- The min-max technique was employed for optimisation, and an optimal parameter setting that provides the best compromise between conflicting quality attributes was identified. This set includes an air pressure of 1.023 bar, an air temperature of 160.6 °C, a feed rate of 1000 mm/min, a tool offset of 8 mm, and a step down of 1mm.

6.2 Future work

The outcome of the preliminary investigation exceeded expectations and provided a clear roadmap for future development. The next step in such a setup will be to improve results using the essential factors of the new system. Such future advancements will make a strong impression on industrial sites, encouraging the implementation of this technique, which can

reduce costs while delivering excellent results. For future work, the following recommendations are suggested:

- Heat the clamp of the sheet during the process to eliminate any thermal torsional effects that may occur if the clamp is not heated. This will prevent defects or disorderly deformation after unclamping the plastic sheet, ensuring a high-quality outcome.

- Address the bending effect at the initial stage of the process by firmly holding the PC sheet with a specified force from the sides. This approach will prevent the sheet from bending during the initial stages, maintaining its flatness and stability throughout the process. Implementing this solution can save time and resources by avoiding the need for additional corrective measures later on. It will improve the overall quality of the final product and can be easily applied to various manufacturing processes where sheet bending is a common issue.

- Explore the application of the novel non-contact SPIF process on metal sheets. This would involve adjusting the air-compressed pressure and the heating capacity of the heater, depending on the softening temperature of the metal material. Investigating the forming limit, mechanical properties and microstructure of the produced parts using this novel technique will provide valuable insights for enhancing the final product's geometrical accuracy and surface quality.

- Enhance the model by applying an ellipsoidal heat source instead of a circular heat source, as it would yield more precise results. Additionally, it is recommended to incorporate a microstructure model for polymer materials. Further research on CPFEM (Crystal Plasticity Finite Element Method) and polymer investigations is advised to expand our understanding in these areas.

- Apply different tool paths and study their effects on the designs of forming shapes, geometric accuracy, and surface quality. Additionally, conducting research on tool path optimisation, including compensation techniques and machine learning models, is necessary to improve the process's overall performance.

- Investigate using different nozzle designs with various shapes and diameters. It is advised to optimise the nozzle geometry and study its effect on the process results.